Wave-Associated Seabed Behaviour near Submarine Buried Pipelines

Behnam Shabani

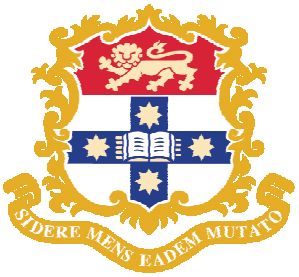

School of Civil Engineering
The University of Sydney

A thesis submitted in the fulfilment of requirements for the degree of Master of Engineering (Research) in Civil Engineering at the University of Sydney

March 2008

To my parents

ABSTRACT

Soil surrounding a submarine buried pipeline consolidates as ocean waves propagate over the seabed surface. Conventional models for the analysis of soil behaviour near the pipeline assume a two-dimensional interaction problem between waves, the seabed soil, and the structure. In other words, it is often considered that water waves travel normal to the orientation of pipeline. However, the real ocean environment is three-dimensional and waves approach the structure from various directions. It is therefore the key objective of the present research to study the seabed behaviour in the vicinity of marine pipelines from a three-dimensional point of view.

A three-dimensional numerical model is developed based on the Finite Element Method to analyse the so-called momentary behaviour of soil under the wave loading. In this model, the pipeline is assumed to be rigid and anchored within a rigid impervious trench. A non-slip condition is considered to exist between the pipe and the surrounding soil. Quasi-static soil consolidation equations are then solved with the aid of the proposed FE model. In this analysis, the seabed behaviour is assumed to be linear elastic with the soil strains remaining small. The influence of wave obliquity on seabed responses, i.e. the pore pressure and soil stresses, are then studied. It is revealed that three-dimensional characteristics systematically affect the distribution of soil response around the circumference of the underwater pipeline. Numerical results suggest that the effect of wave obliquity on soil responses can be explained through the following two mechanisms: (*i*) geometry-based three-dimensional influences, and (*ii*) the formation of inversion nodes. Further, a parametric study is carried out to investigate the influence of soil, wave and pipeline properties on wave-associated pore pressure as well as principal effective and shear stresses within the porous bed, with the aid of proposed three-dimensional model.

There is strong evidence in the literature that the failure of marine pipelines often stems from the instability of seabed soil close to this structure, rather than from construction deficiencies. The wave-induced seabed instability is either associated with the soil shear failure or the seabed liquefaction. Therefore, the developed three-dimensional FE model is used in this thesis to further investigate the instability of seabed soil in the presence of a pipeline. The widely-accepted criterion, which links the soil liquefaction to the wave-induced excess pressure is used herein to justify the seabed liquefaction. It should be pointed out that although the present analysis is only concerned with the momentary liquefaction of seabed soil, this study forms the basis for the three-dimensional analysis of liquefaction due to the residual mechanisms. The latter can be an important subject for future investigations. At the same time, a new concept is developed in this thesis to apply the dynamic component of soil stress angle to address the phenomenon of wave-associated

soil shear failure. At this point, the influence of three-dimensionality on the potentials for seabed liquefaction and shear failure around the pipeline is investigated. Numerical simulations reveal that the wave obliquity may not notably affect the risk of liquefaction near the underwater pipeline. But, it significantly influences the potential for soil shear failure. Finally, the thesis proceeds to a parametric study on effects of wave, soil and pipeline characteristics on excess pore pressure and stress angle in the vicinity of the structure.

Keywords: water waves; submarine buried pipelines; seabed consolidation; three-dimensional analysis; seabed instability; soil liquefaction; soil shear failure; Biot consolidation theory; Finite Element Method.

ACKNOWLEDGEMENTS

Writing up this thesis is the finishing point to a two-year journey, after which I feel deeply indebted to a great many people who have inspired, encouraged and supported my studies. In fact, it would not have been possible to complete this research, without their continuous support.

In the first place, I would like to thank Professor Dong-Sheng Jeng, formerly at the University of Sydney, Australia, currently at the University of Dundee, Scotland, for initiating and supervising this project between March 2006 and November 2007. His constructive comments on difficulties during this research, his encouragement, and his careful review of the manuscript of this thesis are greatly appreciated. I was particularly impressed by his broad contributions to the area of coastal geotechnical engineering. The financial support from the research assistantship offer to me by Professor Dong-Sheng Jeng is also appreciated. I am grateful to Professor John Small, at the University of Sydney, for his supervision on this study between November 2007 and March 2008. His gentle manner and kind support in providing me with the access to CGR computing facilities is also deeply acknowledged. The constructive comments by Dr. Jishan Liu, the University of Western Australia and by Professor Andrew Chan, the University of Birmingham, UK during their rigorous examination of this thesis are also highly appreciated.

It is my pleasure to express my thanks to Associate Professor Itai Einav and Dr. Tim Finnigan, at the University of Sydney, for providing me with teaching assistantship opportunities. Experiences that I have gained over this period will certainly remain priceless to me. I am also grateful for the financial support through the research assistantship offered to me by Dr. Tom Baldock and Associate Professor Peter Nielson, at the Division of Civil Engineering, the University of Queensland, Australia, while waiting for the outcome of the examination of this thesis.

It is also my duty to express my sincere gratitude to Dr. Abbas Yeganeh Bakhtiary, at the Department of Civil Engineering, Iran University of Science and Technology, for his constructive supervision during my undergraduate studies and the introduction of Professor Dong-Sheng Jeng to me. Without his training in fundamental research skills, I would not have been able to complete this project.

My appreciation also goes to my friends and colleagues, Mr. Arash Kanani, at Queen's University, Canada and Miss Sally Williams, at the University of Sydney, for their encouragements and generous help during the course of my studies. Their support is deeply acknowledged.

I would like to express my thanks to my partner Xingzhuo for her invaluable patience and endless support. Her encouragement is the main motivation for me to move on ahead. Last but not the least, my gratitude and respects goes to my parents. They sacrificed their lives for me and I always will feel indebted to them.

Behnam Shabani

March 2008

Sydney, Australia

TABLE OF CONTENTS

LIST OF FIGURES

LIST OF TABLES

NOMENCLATURE

B	pipeline burial depth
c	wave celerity
c_x	cross-trench component of wave celerity
C	minimum wave-induced stress angle required to trigger soil shear failure (also $\Delta\phi_{critical}$)
C_1 .. C_6	coefficients of the analytical solution by Hsu and Jeng (1994)
C_B	Bernoulli constant
d	trench depth
ds	dimension of an infinitesimal element of pipe circumference
dx, dy, dz	dimensions of an infinitesimal soil element
D	diameter of submarine pipeline
D_{ijkl}	coefficients of matrix describing the constitutive stress-strain relation in seabed soil
D_{Mohr}	diameter of greater Mohr circle
D_r	soil relative density
e	void ratio of seabed soil
g	gravitational acceleration (=9.81 m/s^2)
g_i	gravitational acceleration in i- direction
G	soil shear stiffness modulus
h	water depth
H	wave height
i	$=\sqrt{-1}$

I_1, I_2, I_3	stress invariants
k	permeability of seabed soil
k_{lower}	permeability of lower soil layer in a stratified porous seabed
k_{upper}	permeability of upper soil layer in a stratified porous seabed
K_o	coefficient of lateral earth pressure
K_w	true bulk modulus of elasticity of water (=2 GPa)
K'	bulk modulus of elasticity of pore fluid (=1/β)
l	length of computational domain in y- direction
L	wave length
m	an integer number
n	porosity of seabed soil
n_c	number of wave periods, after which finite element simulations reach to the steady state
n_l	number of finite element mesh divisions over one wave length along pipe centreline
n_p	number of finite element mesh divisions around pipeline perimeter
n_r	number of finite element mesh divisions in the radial direction on the pipe cross-section
$\vec{n}$	unit vector normal to the soil principal plane
p	wave-induced pore fluid pressure
p_{bed}	wave dynamic pressure on seabed surface
p_{cr}	critical excess pore pressure corresponding to soil liquefaction
p_{excess}	wave-induced excess pore pressure
p_o	amplitude of wave dynamic pressure on seabed surface
p_w	water pressure in the oscillatory flow under ocean waves
p_{wo}	absolute pore fluid pressure

r	a local axis normal to and positive outward from pipe and trench boundary surfaces
R	general notation for a wave-induced seabed response
R_{Mohr}	the radius of greater Mohr circle
S	degree of saturation of seabed soil
t	time
T	wave period
u	soil skeleton displacement in x- direction
u_{f}	average displacement of pore fluid in x- direction relative to that of soil skeleton
u_{i}	soil skeleton displacement in i- direction
$\ddot{u}_{\text{i}}$	soil skeleton acceleration in i- direction
$\tilde{u}_{\text{seepage}}$	horizontal seepage velocity within the porous bed as obtained from Darcy's law
u_{x}, u_{y}	velocities of fluid particles in x- and y-directions, in wave oscillatory flow field
v	soil skeleton displacement in y- direction
v_{f}	average displacement of pore fluid in y- direction relative to that of soil skeleton
w	soil skeleton displacement in z- direction
w	trench width
w_{f}	average displacement of pore fluid in z- direction relative to that of soil skeleton
x, y, z	coordinates in a Cartesian system
X, Y	a coordinate system generated by 90-α degrees clockwise rotation of xy system about z axis
X_p	position of pipe centre in Turcotte *et al*. (1984), relative to the left trench wall
α	wave angle of incidence
α_{cr}	wave direction that triggers the most critical stress angle around pipeline perimeter
α_{s}	a constant, which is dependent to local porosity, in "radiation-type" boundary condition

β compressibility of pore fluid

β_w compressibility of water

γ_s unit weight of soil mixture

γ_w unit weight of water

γ'_s submerged unit weight of soil mixture

δ vertical coordinate of free surface in ocean waves

δ_{ij} the ij^{th} element of Kronecker delta

Δt finite element time step

$\Delta\phi_{critical}$ critical wave-induced stress angle corresponding to soil shear failure

$\Delta\phi_{wave}$ wave-induced stress angle

ε volumetric soil strain

ε_{ij} elements of soil small strain tensor (= $\frac{1}{2}[u_{i,j} + u_{j,i}]$)

ε_{ij}^{0} elements of soil autogeneous strain tensor

ζ_i average displacement of pore fluid in *i*- direction relative to that of soil skeleton

$\dot{\zeta}_i$ average velocity of pore fluid in *i*- direction relative to that of soil skeleton

$\ddot{\zeta}_i$ average acceleration of pore fluid in *i*- direction relative to that of soil skeleton

η coefficient of critical excess pore pressure ($= \frac{-[1+2K_o][\gamma_s - \gamma_w]}{3p_o}$)

θ angular coordinates of points around pipeline circumference

κ wave number

κ_x, κ_y wave number projections in *x*- and *y*- directions

λ a parameter in the analytical solution by Hsu and Jeng (1994)

μ	Poisson's ratio
ρ_s	density of soil mixture
ρ_f	density of pore fluid
ρ_w	density of water
ς	a parameter in analytical solution by Hsu and Jeng (1994) (δ is used in original publication)
σ_{ij}	wave-induced total stress acting in *j*- direction in a plane normal to *i*- direction
σ_x, σ_y, σ_z	wave-induced total normal stresses
σ'_{11},σ'_{22},σ'_{33}	wave-induced major, intermediate and minor principal effective stresses (also σ_{11}, σ_{22}, σ_{33})
σ'_{ij}	wave-induced effective stress acting in *j*- direction in a plane normal to *i*- direction
σ'_n	wave-induced principal effective stress acting in $\vec{n}$ - direction
σ'_{ox},σ'_{oy},σ'_{oz}	geostatic effective normal stresses due to soil submerged self-weight
σ'_x, σ'_y, σ'_z	wave-induced effective normal stresses
$\overline{\sigma}'_{11}$,$\overline{\sigma}'_{22,}$ $\overline{\sigma}'_{33}$	absolute major, intermediate and minor principal effective stresses
$\overline{\sigma}'_x$, $\overline{\sigma}'_{y,}$ $\overline{\sigma}'_z$	absolute effective normal stresses
τ_{max}	wave-induced maximum soil shear stress, i.e. the radius of greater Mohr circle
τ_{xy}, τ_{xz}, τ_{yz}	wave-induced soil shear stresses
$\bar{\tau}$	absolute soil shear stress
$\bar{\tau}_f$	absolute soil shear stress corresponding to soil shear failure
φ	wave phase in radians (= κX - ωt)
φ_{lag}	phase lag between a wave-induced seabed response and wave dynamic loading at mudline
ϕ	absolute soil stress angle

ϕ_o	geostatic soil stress angle
ϕ_f	soil internal friction angle
ϕ_{max}	maximum stress angle around pipe perimeter
ϕ^0_{max}	maximum stress angle around pipe perimeter when waves are parallel with pipeline
ϕ^{90}_{max}	maximum stress angle around pipe perimeter when waves are normal to the pipeline
ϕ^{cr}_{max}	most critical stress angle that a wave of an arbitrary direction generates around pipeline
ϕ_w	velocity potential of flow field under ocean waves
ω	wave frequency
$\|...\|$	the *amplitude* operator, such that $\|R\|$ represents the amplitude of fluctuating parameter R

Chapter 1

INTRODUCTION

1.1 Background

About sixty percent of world energy is supplied from oil and natural gas resources, most of which are located offshore. The oil industry, therefore, substantially relies on the vital role of submarine pipelines to transport energy resources ashore. On the other hand, underwater pipelines are frequently used as ocean outfalls, extended several kilometres offshore, to discharge waste streams. Alternatively, offshore pipelines are sometimes exploited as the shortcut to transport water and other chemicals between two points.

Offshore pipelines are typically constructed as either *underwater-laid* or *submarine-buried* structures. From the design-engineering point of view, these two categories of marine pipelines are characterized by their different instability mechanisms and thus design procedures. Underwater-laid pipelines are mainly constructed in deep waters and laid on the seabed surface. In this category, the pipeline is subject to the instability due to the influence of presence of structure on its surrounding flow pattern, scouring near the pipeline, formation of free spans and the soil failure at span shoulders. This subject has been investigated by various researchers. Recently, the theory and literature of scouring around marine pipelines are outlined by Sumer and Fredsøe (2002). At the same time, underwater-laid pipelines are also found vulnerable to the liquefaction of underlying seabed soil layers. This issue, also, recently has attracted attention from researchers and pipeline engineers. Sumer *et al*. (1999) and Teh (2003) are the two recent contributions to the problem of the on-bottom stability of marine pipelines on liquefied seabeds.

In shallow waters, submarine pipelines are often buried within the seabed for the protection against human activities such as ship anchoring, dredging and fishing. In this region, ocean waves propagating over the seabed exert a significant dynamic pressure on the seabed soil and consequently wave-associated pore pressure and stresses are generated within the soil matrix. Such excessive pore pressure and the accompanied loss of soil effective stress will expose the seabed to the risk of liquefaction. At the same time, large wave-associated soil shear stresses will further impose the risk of seabed shear failure. The liquefied seabed near the pipeline provides the ground for the structure to sink or float within the bed due to its self-weight, while

the shear failure instigates large horizontal movements of pipeline. It is also possible for the pipeline in a mobilized seabed to displace under strong bottom currents. Regardless of its pattern, a large pipeline deformation is accompanied by considerable internal stresses within the structure; and thus may result in its failure. Therefore, it is crucial to gain a realistic understanding to wave-associated seabed behaviour near submarine buried pipelines, in order to enhance the safety of pipeline, reduce the risk of disruption in energy flow and prevent the economical and environmental hazards of pipe failure.

In general, the wave-induced response of the seabed around a pipeline is dominated by two main mechanisms, based on previous laboratory and field measurements (Nago *et al*., 1993; Zen and Yamazaki, 1990a). The first mechanism is characterized by the oscillatory nature of wave dynamic loading. As a result, the seabed responses are of harmonic nature, following the nature of wave loading. However, there may be attenuations of amplitudes of soil responses within the seabed, as well as, the phase lag between seabed responses and the wave loading. This type of soil response is often referred to as the wave-induced momentary seabed response (Yamamoto *et al.*, 1978). The second type of soil response is brought forward by the progressive nature of wave pressure on mudline. In this mechanism, soil cyclic *shear* stresses contribute to the generation of *normal* seabed strains and progressive build-up of pore pressure within the porous medium. The pore pressure build-up, nevertheless, is usually observed only in poorly permeable soils, where the pore fluid cannot be drained efficiently. This type of response is typically referred to as the wave-associated residual seabed response. Among the two mechanisms, the latter has been recently investigated in the LIMAS[1] research program and outlined in Sumer (2006) and Sumer (2007). The former is, however, the subject matter of the present study.

The importance of wave-associated seabed geomechanical responses near submarine pipelines has been well understood over the past five decades (after Brown, 1957). However, it is not more about than thirty years that excessive theoretical research has been carried out in this area (after MacPherson, 1978). This coincides with recent advancements in the area of coastal engineering and soil mechanics, and also the introduction of new measurement techniques to evaluate geomechanical properties of marine sediments, in the early 1980s. At the same time, breakthroughs in the computer technology and numerical modelling have also contributed to the expansion of this research field. The past thirty-years of research provides much literature on the momentary wave-seabed-pipeline interaction problem, which involves applications of various soil consolidation and wave theories to various types of marine soils. Yet, almost all of these studies have been conducted solely in two-dimensions. In reality, the ocean environment, porous seabed and pipeline, however, are three-dimensional. This research, therefore, focuses on the three-dimensional momentary behaviour of seabed soils around submarine buried pipelines.

[1] **LI**quefaction around **MA**rine **S**tructures

In forthcoming sections, the literature of wave interaction with submarine buried pipelines will be reviewed. The present knowledge of this area, however, is backboned by research on the wave-soil interaction problem. Therefore, it is essential to present an overview of current knowledge and techniques in wave-seabed soil interaction modelling. This will be further followed by a review of the wave-seabed-pipeline problem. In this regard, available theories, solution techniques, field and experimental investigations are addressed for both wave-soil and wave-soil-pipe interaction problems. Finally, the scope of present research and the thesis layout are outlined in the chapter closure.

1.2 General Theory of Soil Adaptation to a Loading

The seabed soil, like other soils, is a porous medium undergoing consolidation when exposed to a loading. Much of the present knowledge of this gradual adaptation of soil to the load variation is inarguably based on the pioneer work by Terzaghi (1925). Later, Biot (1941) generalised the Terzaghi's one-dimensional theory to develop a three-dimensional consolidation theory, which has been unanimously applied to various geotechnical engineering problems since then. Zienkiewicz *et al*. (1980), further, provided an alternative form of generalized consolidation theory of Biot (1941) and Biot (1962) to account for the most general situation of non-linear material behaviour. According to authors, this extended theory is applicable to soils but not rocks, which is however beyond the scope of present study.

The consolidation theory, despite being well-developed, is associated with significant complexities for applications in soil mechanics problems. Further, some simplified forms of this theory are also found sufficient for certain engineering applications. Much of the chronicle of wave-seabed interaction modelling, therefore, is in fact devoted to the transition from the use of simplified to the most general forms of consolidation theory. Hence, it is vital to provide a brief overview of consolidation theory before a more detailed review of the literature can be presented. As summarized by Zienkiewicz *et al*. (1980), general soil behaviour under loading is governed by following the five physical principals:

- The concept of soil effective stress:

$$\sigma'_{ij} = \sigma_{ij} + \delta_{ij} p \tag{1.1}$$

- The incremental form of constitutive relations of the soil skeleton:

$$d\sigma'_{ij} = D_{ijkl}(d\varepsilon_{kl} - d\varepsilon_{kl}{}^{0}) \tag{1.2}$$

- The equilibrium condition of the soil mixture:

$$\underbrace{\sigma_{ij,j}}_{\text{stress gradients}} + \underbrace{\rho_s g_i}_{\text{body forces}} = \underbrace{\rho_s \ddot{u}_i}_{\text{solid phase inertia}} + \underbrace{\rho_f \ddot{\zeta}_i}_{\text{fluid phase inertia}} \tag{1.3}$$

- The equilibrium condition of fluid phase (Darcy's law):

$$-p_{,i} + \rho_f g_i = \rho_f \ddot{u}_i + \frac{\rho_f}{n}\ddot{\zeta}_i + \frac{\rho_f g}{k}\dot{\zeta}_i \tag{1.4}$$

- The continuity of pore fluid flow:

$$\dot{\varepsilon}_{ii} + \dot{\zeta}_{i,i} = -n\beta\dot{p} \tag{1.5}$$

where, σ_{ij} and σ'_{ij} are components of tensors of total and effective soil stresses, respectively; δ_{ij} is the Kronecker delta; p represents the pore fluid pressure; D_{ijkl} stands for elements of constitutive matrix that describes the constitutive stress-strain relation; ε_{ij} is the *ij*-th element of soil strain tensor and is defined by $\varepsilon_{ij} = ½ (u_{i,j} + u_{j,i})$; similarly, ε_{ij}^0 accounts for soil autogeneous strains; ρ_s and ρ_f are the density of soil mixture and the pore fluid; g_i represents the acceleration in the *i*- direction corresponding to body forces; g is the gravitational acceleration (=9.81 m/sec^2); u_i stands for the soil skeleton displacement in the *i*- direction; similarly, ζ_i is the average displacement of fluid expressed relative to that of the soil skeleton; n and k are soil porosity and permeability; and β is the compressibility of pore fluid. A repetitive subscript denotes the algebraic summation, while an index preceded by (,) stands for the partial derivative with respect to the direction labelled by the index. Time derivates are also denoted by dot (.) superscripts.

1.3 Wave-Seabed Interaction

1.3.1 Uncoupled Consolidation Models

The seabed soil is a two-phase medium, where the pore fluid and the solid skeleton interact mutually to adapt to the external loading. Therefore, a general consolidation theory such as that in equations (1.1)-(1.5) reflects a coupled behaviour among solid and pore fluid phases. For many applications, the full set of coupled soil consolidation equations is extremely complicated to solve. The consolidation theory, however, may be reduced to an uncoupled system, through various simplifying assumptions. Uncoupled models, though only applicable in a very limited range of soil properties or under very specific circumstances, are relatively easy to use. Therefore, they had been often used by early researchers to study the seabed behaviour under wave loading. Uncoupled consolidation models, as will be seen later, are usually concerned with either the solid phase or the pore fluid phase. Thus, uncoupled soil models may also be referred to as single-phase consolidation models. In the following subsections, various uncoupled soil models along with relevant investigations on wave-seabed interaction problems are briefly reviewed.

1.3.1.1 Elasticity Theory for Impervious Solids

To simplify the consolidation theory to an uncoupled model, a possible assumption is to treat the soil as an impervious linear elastic continuum. Thus, neglecting the pore fluid pressure and pore fluid flow, the consolidation theory reduces to equations (1.2) and (1.3). Where, the effective stress in equation (1.2) will be replaced by the total stress, as the seabed material is assumed impermeable. At the same time, the fluid phase inertia term in relation (1.3) will also be neglected, following a similar reasoning. This reduced set of equations simply matches the theory of solid elasticity, formed by the solid dynamic equilibrium condition and a constitutive strain-stress relation. Further simplifications may also be made by neglecting body forces and the solid inertia term in the equilibrium equation of the solid. Using such simplified theory, Prevost *et al*. (1975) and Mallaid and Dalrymple (1977) provided solutions to the response of an elastic impervious seabed to the periodic wave loading. The latter also considered the effect of seabed bottom deformations to modify the wave speed. Later, Dawson (1978)'s analytical work extended this framework to demonstrate effects of the solid inertia term being taken into the account. Considering the soil as an elastic impervious medium, nevertheless, provides no information on the pore fluid pressure. To overcome this deficiency, Prevost *et al*. (1975) assumed that the pore fluid pressure is equal to the octahedral normal stresses within the elastic bed. The assumption of an elastic impermeable seabed, however, is physically inconsistent with the real nature of soil behaviour as a porous medium (Yamamoto *et al.*, 1978). This theory, therefore, is not appropriate for the prediction of wave-associated seabed responses.

1.3.1.2 Potential Flow Theory

A second-type simplification of general consolidation theory to an uncoupled model is possible via the assumption of a rigid (non-deformable) porous seabed. Neglecting the compressibility and accelerations of the solid phase, Darcy's law and the continuity of pore fluid flow, equations (1.4) and (1.5), become independent from the behaviour of solid matrix. The following set of reduced equations, therefore, can be used to express the pressure and velocity fields within the pore-fluid phase:

$$-p_{,i} + \rho_f g_i = \frac{\rho_f}{n}\ddot{\zeta}_i + \frac{\rho_f g}{k}\dot{\zeta}_i \tag{1.6}$$

$$\dot{\zeta}_{i,i} = -n\beta\dot{p} \tag{1.7}$$

Assuming a steady pore flow ($\ddot{\zeta}_i = 0$), an incompressible pore fluid ($\beta = 0$), and isotropic permeability, equations (1.6) and (1.7) may be further simplified. Substituting pore fluid velocities ($\dot{\zeta}_i$) from the relation (1.6) into (1.7), governing equations of fluid phase form the so-called Laplace equation:

$$\frac{\partial^2 p}{\partial x^2}+\frac{\partial^2 p}{\partial y^2}=0 \tag{1.8}$$

Early researchers, among them Putnam (1949) and Sleath (1970), followed this approach to analyse the damping of water waves propagating over a permeable seabed. Putnam (1949) provided an analytical solution for wave-induced pore pressure and velocity fields within a seabed of finite depth and uniform isotropic permeability. The solution then was used to obtain the dissipation of wave energy and damping of wave amplitude due to percolation currents. It should be noted that Putnam's solution is erroneous regarding the dissipation of wave energy, due to the mistake in using the wave height instead of the wave amplitude as pointed out by Reid and Kajiura (1957). Later, Sleath (1970) extended Putnam's work to study the case of a hydraulically anisotropic bed. Generally speaking, the potential theory provides no information on soil strains and stresses. Secondly, the pore pressure obtained from the Laplace equation is independent of soil properties, such as permeability. Thirdly, estimated pore pressures are essentially in the same phase as is the wave loading. The theory, as applied by the aforementioned researchers, is therefore incapable of providing an explanation of the existence of phase lag between pore pressures at various seabed depths. Meanwhile, it was later shown, in the state-of-art work by Yamamoto *et al*. (1978), that pore pressures evaluated from the Laplace theory may only be reliable in highly saturated loose/regular sands ($G\beta\rightarrow 0$). It should be pointed out that even such a conclusion is valid only for seabeds of infinite depth. Therefore, the Laplace theory may not be relied on when the thickness of a soil layer is finite. At the same time, even under the conditions of $G\beta\rightarrow 0$ and a seabed of infinite depth, Yamamoto *et al*. (1978) demonstrated that the pore pressure is still generated in association with soil deformations, the fact that is neglected when using the potential theory.

Inspired by and following some earlier studies such as Reid and Kajiura (1957), Hunt (1959) and Maurray (1965), Liu (1977) applied a boundary layer approach to develop a solution to the wave-induced potential flow. The model took into the account effects of rotational velocities of flow in the viscous boundary layer adjacent to the seabed surface. He assumed a stratified porous bed with an upper layer of finite thickness and a lower layer of infinite depth. Both layers were considered hydraulically isotropic, while each could be assigned a different permeability (k_{upper}, k_{lower}). The general solution then could be reduced to consider a seabed of infinite thickness ($k_{\text{upper}}=k_{\text{lower}}$), finite depth ($k_{\text{lower}}\approx 0$) and the wave propagation over a typical rigid impervious bed ($k_{\text{upper}}\approx 0$). The case of infinite depth, however, had been previously studied within the same framework by the author in Liu (1973).

Adding an extra set of boundary conditions at the seabed surface, i.e. matched pore fluid velocities with those in the viscous fluid boundary layer, Liu (1977) found the pore fluid pressure to be dependent on the permeability of the soil. Also, a small constant phase shift was theoretically demonstrated between the wave-induced pore pressure and the wave loading, while using the Laplace equation. However, it had been found

later that such characteristics are more realistically provable by using advanced consolidation models even when the effect of a viscous boundary layer is excluded (e.g. in Madsen (1978) and Jeng and Hsu (1996)). Therefore, the presence of a viscous boundary layer, though slightly influential, may not be the major concern prior to the application of a two-phase soil model.

Later, McClain *et al*. (1977) investigated the interaction between waves and a finite isotropic seabed by using a methodology similar to that of Liu (1977). However, they allowed the shear stress to be discontinuous across the wave-seabed interface. This involved the introduction of an additional viscous boundary layer within the porous medium near the mudline. The behaviour of such a layer was then assumed to be governed by the momentum equation of Brinkman (1947) for a field of closely packed spheres. A radiation-type boundary condition was further applied at the mudline, in addition to conditions of continuities of pressure and velocities. This extra condition, shown in equation (1.9), permitted the slippage of the horizontal velocity component.

$$\left.\frac{\partial u_x}{\partial z}\right|_{z=0} = \left.\frac{\alpha_s}{\sqrt{k}}(u_x - \tilde{u}_{seepage})\right|_{z=0} \tag{1.9}$$

These new implementations involved viscous effects being diffused a small distance into the porous seabed. In this viscid porous region, seepage velocities were also considered to consist of a potential and a viscous component with an analogy to those in the viscid fluid boundary layer. Finally, dynamic properties of wave motion and pore fluid flow as well as the expression for the bottom shear stress were analytically derived.

1.3.1.3 Diffusion Equation

As discussed in the foregoing section, governing equations of a solid-fluid mixture can be uncoupled by neglecting the compressibility and accelerations of the solid phase. This led to the governing equations of pore fluid phase being as shown in equations (1.6) and (1.7). The Darcy law and the continuity equation then may be combined, while further ignoring the unsteady pore-fluid velocity and keeping the compressibility of pore-fluid. This gives the so-called *diffusion equation*, traditionally applied in *heat conduction theory*. It is important to accentuate that the pore fluid is still considered to be compressible.

$$\frac{\partial^2 p}{\partial x^2} + \frac{\partial^2 p}{\partial y^2} = \left(\frac{\rho_f g n \beta}{k}\right)\frac{\partial p}{\partial t} \tag{1.10}$$

Nakamura *et al*. (1973) and Moshagen and Tørum (1975) applied this approach to the wave-seabed interaction problem. They confirmed the existence of two types of wave-induced pore pressure regimes. The first type occurs in highly permeable (coarse) soils such as sand, where it was concluded that the effect of

compressibility of pore-fluid and unsteady transmission of pressure can be neglected in the diffusion equation. Under such circumstances, therefore, the solution is essentially the same as that of potential pressure theory and thus is independent of permeability. Besides, in this range, the phase-shift in the pore pressure and its gradients are found to be small. The second mechanism takes place in less permeable soils such as fine sands and clays, in which the compressibility of pore fluid is found influential. This seabed response is therefore associated with a pronounced phase-shift and also larger pore-pressure gradients. In the meantime, the wave-induced pore pressure is also found to be dependent on the soil permeability. In this region, the use of the diffusion equation was recommended in order to obtain the seabed response. Yamamoto *et al*. (1978) later demonstrated that when the stiffness of sand becomes much larger than that of the pore fluid ($G\beta \to \infty$), such as in the unsaturated sandstone, the wave-induced pore pressure can be correctly obtained from the heat conduction theory.

1.3.2 Coupled Two-Phase Consolidation Models

Apart from a limited range of seabed soils, the skeleton deformations and pore fluid flow characteristics are interdependently linked to each other. Any form of an uncoupled model, therefore, is not capable of thoroughly expressing the soil behaviour under the wave loading. This necessitates taking advantage of two-phase consolidation models that allow the coupling of responses of solid and fluid phases. The use of coupled models, however, involves mathematical and computational complexities. Thus, their application to wave-seabed interaction problem was not initiated until late 1970s.

1.3.2.1 Quasi-Static Consolidation Theory

The general form of consolidation equations, presented in section 1.2, can be reduced to a linear quasi-static poroelastic model, if: (*i*) a linear elastic stress-strain relation represents the constitutive-law of soil skeleton in equation (1.2); (*ii*) unsteady transitions of both soil and fluid velocities ($\ddot{u}$ and $\ddot{\zeta}$) are neglected from equilibrium equations of soil mixture and the Darcy law. The reduced set of equations, the so called Biot (1941) consolidation equations and Verruijt (1969) storage equation, then will as:

$$G\nabla^2 u_i + \left(\frac{G}{1-2\mu}\right)\varepsilon_{jj,i} = p_{,i} \tag{1.11}$$

$$k\nabla^2 p - \left(\rho_f g n\beta\right)\dot{p} = \left(\rho_f g\right)\dot{\varepsilon}_{jj} \tag{1.12}$$

where, a repetitive subscript denotes the algebraic summation. The use of a quasi-static consolidation model avoids physical inconsistencies and shortcomings involved within uncoupled models. Despite neglecting inertia terms, the model provides yet a fairly well accuracy for both engineering and research purposes. It consequently became the dominant method of investigations in wave-seabed interaction problems over the

past thirty years. The numerousness of researches, which have applied Biot theory to obtain the wave-induced seabed response, provided a rich literature in this area. However the focus of present thesis is on the wave-seabed-pipeline interaction phenomenon. Therefore, a brief outline of major researches on wave-seabed problem is addressed here to track difficulties and advancements in the application of this method. A detailed review on the use of quasi-static models to analyse seabed behaviour near submarine pipelines will be presented in the due course.

The pioneering solution by Yamamoto (1977) was probably the first to apply the Biot theory to derive wave-induced seabed responses (pore pressure, displacement and stresses). He considered the response of a seabed of finite thickness and presented the solution in a semi-analytical form, cast in a 6 by 6 matrix (Jeng and Hsu, 1996). Considering the half space of an infinitely deep seabed, Yamamoto *et al.* (1978) later extended his previous work to provide an explicit analytical solution for the seabed response. However, the study, despite forming the backbone of present knowledge, only allowed for hydraulically and structurally homogeneous and isotropic soil properties; the sediment deposit was also considered to be in a one-layer form and infinitely thick; and finally, a two-dimensional set of consolidation equations was applied along with a two-dimensional progressive system of wave loading. Among these shortcomings, shortly after Yamamoto *et al.* (1978), the effect of hydraulic isotropy was addressed in an independent research by Madsen (1978).

The derivation of an explicit exact analytical solution for the case of a seabed of finite thickness involves considerable mathematical complexities. Therefore, Mei and Foda (1981) applied a boundary layer approximation to solve the Biot consolidation equations for a finite bed-thickness. Nevertheless, their solution was found to lose accuracy in unsaturated and also in coarse sands. Later, Yamamoto (1981) further extended the semi-analytical framework of Yamamoto (1977) to include cases of multi-layer seabeds. Considerations in regard to the thickness of seabed layer were also investigated numerically by Thomas (1989), Gatmiri (1990) and Thomas (1995) through applying the Finite Element Method. Among these, a two-layer seabed consisting of an upper layer of finite depth and a lower half-space of infinite thickness was examined in Thomas (1989) and Thomas (1995), while Gatmiri (1990) investigated influences of seabed thickness, multi-layered soil patterns, and sloping seabeds. However, a possible mistake in the lateral boundary conditions used by Gatmiri (1990) was reported in Jeng (1997b).

It was not until Hsu and Jeng (1994) and Jeng and Hsu (1996) that a closed-form analytical solution to wave-induced responses of a seabed of finite depth, using the quasi-static consolidation theory, was formulated. Moreover, they were the first to use the three-dimensional Biot consolidation equations in conjunction with a three-dimensional short-crested wave loading. Their solution, then, could be reduced to the two-dimensional simplified case of a seabed under actions of progressive and standing water waves. They, at the same time, included the hydraulic anisotropy of marine sediments in their models.

The implementation of anisotropic structural characteristics of a soil, such as the cross-anisotropy, in studying the wave-induced seabed behaviour was later considered and numerically examined by the finite element model of Gatmiri (1992). An analytical solution for the response of cross-anisotropic soils was also derived in Jeng (1997b) and Jeng (1997c). A simplified analytical solution for the case of cross-anisotropic soils was also derived in Yuhi and Ishida (2002). This model, however, was found inaccurate at distances far from the seabed surface (Jeng, 2003b). Another concern is the effect of inhomogeneous (spatially variable) seabed properties. Among others, Lin and Jeng (1997) and Lin and Jeng (2000) developed a Finite Element Model to numerically address the influence of variable permeability and shear modulus of marine sediments, respectively. At the same time, Jeng and Seymour (1997) and Kitano and Mase (2001) approached the case of a seabed of variable permeability analytically.

1.3.2.2 Semi- and Fully-Dynamic Consolidation Models

Although quasi-static models have been widely used to model the seabed behaviour under wave loading, there are still two other types of consolidation models that use the assumption of elastic soil behaviour. The first type is referred to herein as the semi-dynamic model of poroelasticity. This model, which is also called *u-p* consolidation model, is a simplification to the general consolidation theory for linear elastic materials. The key assumption in the *u-p* model is that the acceleration of pore fluid is negligible with respect to that of soil particles. Therefore, the inertia term of pore fluid motion, i.e. the unsteady pore fluid velocity, is crossed not used with the general soil model, while the inertia term of the solid phase is still included. This model was initially developed by Zienkiewicz *et al*. (1980). The coupled system of soil consolidation equations then can be written as:

$$-\rho_s \ddot{u}_i + G\nabla^2 u_i + \left(\frac{G}{1-2\mu}\right)\varepsilon_{jj,i} = p_{,i} \tag{1.13}$$

$$k\nabla^2 p - \left(\rho_f g n\beta\right)\dot{p} = \rho_f \left(g\dot{\varepsilon}_{jj} - k\ddot{\varepsilon}_{jj}\right) \tag{1.14}$$

To date, a few studies have contributed to the application of this theory to the problem of wave-induced seabed response. A review of these studies may be found in Jeng (2003a). On the other hand, there are also three studies in the literature to address the problem of wave-seabed-pipeline interaction using a semi-dynamic model. These studies will be reviewed, in due course, in section 1.4.2.2.

Finally, the fully-dynamic poroelastic model is in fact the full set of equations (1.1) to (1.5), but with the implementation of a linear elastic soil constitutive model to correlate stress and strains. Unsteady velocities of both pore fluid motion and soil displacements are considered in this type of model. The solution of fully-dynamic seabed response to the loading from ocean waves has been recently published by Jeng and Cha (2003).

1.4 Wave-Seabed-Pipeline Interaction

The propagation of waves over a porous bed corresponds to the formation of high and low pressure regions on the seabed surface under the wave crest and the wave trough respectively. The resultant pressure gradient is, therefore, accompanied by the seepage flow through the porous medium between these two regions. A pipeline being an impervious structure, when buried within the seabed, however, disrupts the seepage flow. Thus, the pattern of wave-induced seabed consolidation will be considerably influenced. On the other hand, soil displacements are also influenced by the behaviour of soil-pipe contacts, as well as deformations of a pipeline as a flexible free structure. Consequently, the seabed surrounding a buried pipeline will respond differently to the wave dynamic loading, in comparison with the seabed in the absence of such a structure.

In fact, the wave-induced pore pressure around a pipeline exerts a considerable seepage force on the structure. The upward seepage force in a severe storm can be significant enough to cause pipeline floatation. Meanwhile, the seabed near the pipe is also vulnerable to the liquefaction and soil shear failure. The latter is expected to be accompanied by sliding and large horizontal movements of the structure, while the former will cause pipe sinking/floatation, as well as allowing the structure to be dragged under sea bottom currents. Therefore, a realistic study on wave-induced seabed responses in the presence of a pipeline is crucial for design engineering purposes. Consequently, the wave-seabed-pipeline interaction problem has been the subject matter of many coastal geotechnical engineering investigations. Advancements in the modelling of submarine buried pipelines, however, are achieved in the light of developments in wave-seabed interaction models. Therefore, with an analogy to the previous section, investigations on submarine pipeline are classified here and presented according to the soil consolidation theory involved: i.e. uncoupled and coupled consolidation models.

1.4.1 Uncoupled Consolidation Models

Several cases of pipeline flotation due to the action of waves have been reported in the literature (Herbich, 1977). Among them, Brown (1957) and Christian *et al*. (1974) described cases of pipe flotation during storms at the Gulf of Mexico and Lake Ontario, respectively. Early investigations, such as *ASCE Pipeline Flotation Research Council* (1966) and Bonar and Ghazzaly (1973), approached this problem by concentrating on the provision of empirical data to facilitate the pipeline design. By this time, uncoupled consolidation models such as the potential theory[2] had already been applied to study the wave-seabed interaction such as in Sleath (1970). However, it was not until MacPherson (1978) that the application of those theories was theoretically extended to the problem of submarine buried pipelines.

It was first the Finite Element (FE) and the Finite Difference (FD) solutions of Lai *et al*. (1974) that used the potential theory to approach the problem of underwater buried pipelines. Later, MacPherson (1978)

[2] See section 1.3.1.

analytically solved the Laplace equation to obtain the wave-induced pore pressure field in a porous half-space with the presence of a fixed buried pipeline. Working in a bipolar coordinate system, he considered the pipe influence as a local disturbance superposed on the wave-induced pore pressure field derived by Putnam (1949). Finally, the expression for the wave-induced seepage force on the pipeline was also formulated. It was concluded that the magnitude of this force could reach 30 percent of the buoyant force and thus could be important in the occurrence of pipeline floatation. This solution, however, was only for the case of a seabed of infinite depth. Thus, it loses applicability when the distance between an impervious bed-rock and pipeline become less than half a wave length as is pointed out by Monkmeyer *et al*. (1983). Besides, it has been later revealed that MacPherson's (1978) solution also is not valid for shallow pipe-burial depths.

The Boundary Integral Equation Model (BIEM) of Liu and O'Donnell (1979) extended the range of wave-seabed-pipeline problems, which was previously analysed via potential theory, to the cases of multiple pipelines and seabeds of finite thickness. Nevertheless it was Monkmeyer *et al*. (1983) and Mantovani (1983), who derived an analytical solution to the potential pore pressure field and seepage forces on a pipeline buried in a seabed of finite depth. To satisfy mudline and bedrock boundary conditions, they used an *Image Superposition Scheme*, in which an infinite number of imaginary pipes were used as an aid to express the pore pressure local perturbation. They also obtained good agreement, in coarse sands, between their theoretical results and pore pressure measurements around the pipeline. However, it was found that there are some difficulties associated with the convergence of their solution, especially when the pipeline was located either close to the mudline or the bedrock.

A common deficiency, associated with all aforementioned studies was that a two-dimensional analytical or numerical model was applied. Therefore, the analysis could only be limited to cases where the orientation of the pipeline was parallel with the wave crests. Thus, Lennon (1983) and Lennon (1985) proposed a three-dimensional numerical model based on BIEM (Boundary Integral Equation Method) to examine influences of wave obliquity on pore pressure distribution and seepage forces on the pipeline. The model assumed that the seabed depth is finite and wave-associated pore pressure is a potential field. The numerical results concluded that amplitudes of pore pressures around the pipe increase when the wave orientation shifts from “being normal to” towards “being parallel with” the pipeline. Such an influence was reported to be more significant near the base of a pipe. Remaining among a few available three-dimensional studies in the literature of submarine buried pipelines, Lennon (1983) and Lennon (1985) did not provide any information on soil stresses as the result of potential theory being applied. However, Shabani and Jeng (2007a) and Shabani and Jeng (2007b) later found that the wave-induced soil stresses around a pipeline are significantly influenced by three-dimensional effects than the pore pressure.

Spierenburg (1986) developed analytical solutions to several configurations of potential pressure problems, using the technique of conformal mapping and the method of separation of variables. His work

included the derivation of expressions for the pore pressure distribution and seepage forces on both fully- and half-buried submarine pipelines in a seabed of infinite thickness. The former was found to fall within the solution of MacPherson (1978), while the latter was developed for the first time. McDougal *et al*. (1988) also followed a similar approach to address the identical problem of fully-buried pipelines, as in Spierenburg (1986). A similar convergence problem as in MacPherson (1978), Monkmeyer *et al*. (1983) and Mantovani (1983), was also associated with the solution of McDougal *et al*. (1988), while the pipeline was covered by a very thin layer of soil. However, they found their theoretical solution in the good agreement with a small-scale and in the fair agreement with their large-scale wave channel experimental data.

The common factor connected with all aforementioned studies is that an uncoupled soil consolidation model, namely the potential pressure theory, forms the core governing equation for the behaviour of a porous seabed. The simple mathematical layout of this theory, along with well-documented solution procedures, and geometrical complexities imposed by the presence of pipeline were possibly sufficient incentives for the application of potential theory in the first place. Pore pressures, obtained from the Laplace equation, however are valid in a limited range of seabed sediments: i.e. highly permeable or very stiff soils. The phase lag between the soil response and wave dynamic pressure will also not be predicted. At the same time, the theory unrealistically provides no connection between geotechnical seabed properties and its response to the wave loading. It is not also possible to evaluate soil stresses through the potential theory. Therefore, it is simply the pipeline instability, due to the dynamic seepage force, that can be roughly estimated by the Laplace equation. In other words, this theory is incapable of predicting soil instabilities such as shear failure and liquefaction near the structure, which are proven to be the source of many pipeline failure events. Hence, the problem of submarine buried pipelines has been addressed through two-phase coupled consolidation theories since early 1990. In such theories, the pressure transmission is also mutually associated with displacements of the soil skeleton. A review of relevant investigations is presented in the next section.

1.4.2 Coupled Two-Phase Consolidation Models

A review of formulation and applications of soil coupled consolidation models in the wave-seabed interaction problem has been presented in section 1.3.2. In the present section, the application of these theories to the wave-seabed-pipeline interaction problem will be reviewed.

1.4.2.1 Quasi-Static Soil Models

The first attempt to study the problem of undersea buried pipelines, by using a two-phase consolidation theory, probably was the Finite Element Analysis of Bobby *et al*. (1979). The study addressed concerns about the compressibility of seabed material. However, pipelines were unrealistically assumed to be buried as deep as 7.5 m below the seabed surface (Magda, 1996). Later, Matsui (1982) devised a hybrid numerical-analytical solution to wave-induced soil responses (pore pressure and soil stresses) near submarine buried

pipelines. He considered the seabed behaviour to be governed by the Biot (1941) consolidation equations. Further, he used a domain decomposition technique to break the seabed responses into the wave-induced seabed response in the absence of pipeline and a perturbation effect due to the pipeline presence. The author considered the two-dimensional solution of Yamamoto *et al*. (1978) to express the non-perturbed component of seabed response. Two components were then combined so the error in boundary conditions was minimized. However, Matsui (1982) did not provide the exact solution to the problem; rather, a numerical approach had to be aided to extract the seabed responses. Finally, the study only addressed a rigid fixed pipeline buried in a homogenous isotropic seabed of infinite thickness.

A similar set of governing equations has also been solved numerically by Cheng and Liu (1986) using a Boundary Integral Equation Method (BIEM). Two configurations, including pipes buried in a trench and also in an infinite seabed, were examined in Cheng and Liu (1986). Meanwhile, unlike Matsui (1982), it was assumed that the rigid pipeline is not anchored and thus is free to move. This included the introduction of an additional kinematic boundary condition at the pipe surface, as well as the dynamic equilibrium of the pipeline. The pore pressure distribution and seepage forces were investigated; and it was concluded that the magnitude of seepage force on the pipeline can reach up to 60 percent of the buoyant force. This was reported to be several times greater than the prediction by MacPherson (1978). Cheng and Liu (1986), however, did not present their numerical results on normal and shear stresses within the seabed soil.

Later, Magda (1996) formulated a 2-D Finite Element Model to approach the problem by using the quasi-static soil model. Although Magda (1996) assumed the submarine pipeline to be fitted within a trench, the boundary conditions in his model, nevertheless, may not be consistent with this assumption. In fact, the proposed boundary condition on the lateral trench walls was to restrict the soil displacement only normal to the wall. This condition is consistent with the trench walls being considered as fixed. However, the tangential soil displacement should also be zero, if the wall surface is assumed to be rough. Alternatively, it is also possible to implement appropriate controls to consider possible sliding between trench walls and seabed soil. Nonetheless, Magda (1996) did not seem to report either implementations. Therefore, the numerical results, which were later obtained based on his model, may be viewed as doubtful.

The Finite Element Model, formulated by Magda (1996), was later used in Magda (1997) and Magda (2000) to study the pore pressure and uplift seepage forces acting on a submarine pipeline. They also carried out a parametric study to determine influences of several soil, wave and pipe properties on wave-induced uplift forces on a pipeline. Among them, Magda (2000) focused on the determination of a ratio between scattered and non-perturbed wave-associated uplift forces, while Magda (1997) studied the total wave-induced uplift force. In addition to possible problematic lateral boundary conditions in these studies, only pore pressure and seepage forces were discussed, soil anisotropic and inhomogeneous behaviour was also not considered, and finally the model was developed in two-dimensions.

To overcome some shortcomings of the previous models, Jeng and Lin (1999a) proposed a Finite Element Model to consider the influence of non-homogenous seabed properties on the pore pressure distribution around a pipeline. Their model considered a Gibson soil, in which the shear modulus of the soil is assumed to vary either linearly or exponentially over the seabed depth. The paper, however, did not studied non-homogenous seabed properties due to the permeability. Hence, Jeng and Lin (1999b) extended the work to consider both variable shear modulus and permeability with soil depth. In this study, authors also included and studied the effect of cross-anisotropic soil structural properties such as the shear modulus. Nonetheless, it was only an exponential vertical variation of permeability being investigated. On the other hand, both Jeng and Lin (1999b) and Jeng and Lin (1999a), like their preceding counterparts, focused on the wave-induced pore pressure; and no information was provided on soil stresses near the structure. Therefore, Jeng and Lin (2000) later applied their FEM model to be among the first studies that addressed the soil normal and shear stresses around a pipeline. Their study also took into account the linear and exponential vertical variations of both permeability and shear modulus.

Jeng and Cheng (2000) addressed the subject of pipeline failure due to the seabed soil instability. They developed a Finite Difference Model in the curvilinear system to evaluate the pore pressure, soil displacements and seabed stresses in the presence of a pipeline. They further carried out an analysis on the maximum depth of shear failure. It was concluded that it is likely for this depth to be located below the pipeline and thus impose an instability risk on the structure. Nevertheless, only a limited number of pipe and soil properties (pipe burial depth, radius and soil saturation) were examined. Besides, the soil liquefaction, as another important mechanism of seabed instability, was not investigated in their instability analysis. These issues are addressed thoroughly as a part of the present study.

A series of studies conducted by Jeng and Postma (2001a), Jeng *et al*. (2001) and Jeng (2001) investigated internal stresses and deformations within a pipeline by using a Finite Element Method. Jeng (2001) also considered the non-homogenous seabed behaviour. Meanwhile, Wang *et al*. (2000), Postma and Jeng (2001) and Jeng and Postma (2001b) modified the same FEM model to study the effect of a cover-layer on the wave-induced pore pressure and pipeline internal stresses. They concluded that a protective cover layer of coarse sediments may significantly reduce the excess pore pressure and thus the potential of liquefaction near the pipeline. It was also found that the presence of such a layer, however, may not influence the internal stresses of a pipeline.

Gao *et al*. (2003) considered a wave-seabed-pipe interaction problem, in which the seabed was under a non-linear wave loading. In their Finite Element Analysis (FEA), for this purpose, the mudline pressure was expressed by the third-order approximation of non-linear wave pressures as in Hsu *et al*. (1979). Later, Gao and Wu (2006) followed the same framework to study the non-linear responses of seabed soil around a pipeline buried in a trapezoidal backfilled trench. In this study, the non-linear second-order approximation of

mudline pressure based on the Stokes wave theory was used. Both Gao *et al*. (2003) and Gao and Wu (2006) concluded that influences of wave non-linearity on soil responses are significant in shallow waters with steep waves. Thus, it was recommended not to neglect those effects.

Recently, Chen *et al*. (2005) extended the aforementioned Finite Element model to solve three-dimensional Biot consolidation equations in the seabed soil. Using their 3-D model, these authors examined the influence of wave direction on pore pressure distribution near the pipeline for one set of input data. Based on their numerical results, it was concluded that the wave direction does not affect the seabed response. However, such a conclusion is seriously questioned based on findings of Shabani and Jeng (2007a), as well as the present thesis, where the wave three-dimensionality is proven to systematically influence the pore pressure, stresses and potentials of seabed instabilities. Meanwhile, it is also important to note that Chen *et al*. (2005) also did not study 3-D effects on stresses or seabed instabilities.

1.4.2.2 Semi-Dynamic Soil Models

An overview of semi- and fully-dynamic soil consolidation models has been previously presented. As discussed, in a semi-dynamic model or a *u-p* consolidation model, unsteady pore fluid velocities are assumed negligible compared with those of a solid skeleton. However, the model accounts for the solid phase accelerations. On the other hand, a fully-dynamic model considers inertia terms in both pore fluid and solid phases, as formulated in equations (1.1) to (1.5). To date, only two studies have investigated the wave-seabed-pipeline interaction problem by using a semi-dynamic model.

In the first series of studies, Vun *et al*. (2005) and Dunn *et al*. (2006) used the Diana-Swandyne II computer Finite Element code of Chan (1995) to study the progressive pore pressure build up in a seabed with the presence of a buried pipeline. Their research primarily focuses on the phenomenon of pore pressure accumulation within the soil. However, the core soil theory, used to express the instantaneous seabed consolidation, is a *u-p* model. In their study, conditions of both fixed and movable pipelines, as well as slipping in soil-pipe and soil-impermeable bed boundaries were also implemented in the model.

Recently, Luan *et al*. (2008) applied the *u-p* soil consolidation model to study a similar problem. In their research the influence of inclusion of soil inertia terms on momentary seabed response is studied. As well, the authors considered the sliding boundary condition between soil and the elastic pipeline, while thoroughly addressing the soil-pipe contact problem. A simple study on the influence of three soil trench shapes, i.e. triangular, rectangular and trapezoidal, was also conducted. The numerical simulations in their study were carried with the aid of the Finite Element code ADINA (Bathe, 2004). It was concluded that the pipe internal stresses are significantly affected by allowing the sliding to take place between the seabed soil and the pipeline surface. It was also found that wave-induced pore pressures are fairly influenced by the inclusion of soil unsteady velocities, i.e. the use of a *u-p* model.

1.4.3 Experimental Studies

Along with theoretical approaches, including numerical and analytical techniques, to investigate the behaviour of undersea buried pipes, several experimental studies have also been conducted in this area. The experimental and field measurements are particularly important both for understanding dominant mechanisms involved in the wave-induced response of marine pipelines, as well as for the validation of theoretical solutions.

Among available experimental studies, Turcotte *et al*. (1984) carried out a series of tests in Joseph H. DeFrees Hydraulics Laboratory, Cornell University. This set of experiments were performed in a 17 m long, 0.76 m wide wave tank, where a 0.168m PVC pipe was buried in sand. Totally, 8 pore pressure transducers were places around the pipe circumference evenly at every 45 degrees. While the porous bed materials remained the same, seven cases of waves of different lengths (periods) were generated over the pipeline. Finally, pore pressure magnitudes, both around the pipeline and also far away from the structure, were measured. These sets of experimental results have been widely used by numerous researchers to verify theoretical results. The experimental data, though representing a two-dimensional case, still will be used in the present study to validate some simplified cases simulated by the present three-dimensional numerical model.

McDougal *et al*. (1988) also conducted a similar experiment in the wave channel in the Wave Research Laboratory of Oregon State University. The channel was 104 m long, 3.66 m wide and 4.57 m deep. An aluminium test pipeline with a diameter of 0.21 m was buried in fine sands in their experiments. Four pore pressure transducers and four stress cells were reported to be mounted at every 90 degrees around the pipeline. However, the stress measurements were scattered and thus not reported. Several pore pressure measurements were reported for various wave periods (lengths).

Sudhan *et al*. (2002) performed another experimental study on submarine buried pipelines. The wave flume in this study was 30 m long, 2 m wide and 1.7 m deep. The model aluminium pipeline was 0.20 m in diameter and totally 96 tests with variable wave properties and burial depths were conducted. Twelve (12) miniature pore pressure transducers were installed on the pipeline hoping to capture the pressure distribution on the structure with a higher resolution than measurements in the aforementioned studies. Horizontal and vertical forces, acting on the pipeline, were also reported.

Recently as a part of the LIMAS project, Sumer *et al.* (2006b) experimentally addressed the problem of submarine buried pipelines. They concentrated on the phenomenon of pore pressure accumulation in the seabed in the presence of pipelines. Pressure measurements were carried out in both close to the pipeline and in the far field to address the influence of the pipe on pressure built-up. Meanwhile, the LIMAS investigations also included several experimental studies on the stability of bottom-seated pipelines as well as

sinking/floatation of buried pipelines into/out of liquefied seabeds. This area, however, is beyond the scope of the present study. Details of these studies and others can be found in Sumer (2006), Sumer (2007), as well as in Sumer *et al.* (2006a).

1.5 Scope of Current Study and Outline of Presentation

Wave-induced seabed instabilities, as reviewed in the preceding sections, are recognized as the main source of many cases of submarine pipeline failure. In fact, it is revealed that in numerous instances, pipelines do not fail due to their construction deficiencies or hydrodynamic loads; rather the failure takes place when severe storms bring the soil near the structure into an unstable state. Under such circumstances, large internal stresses, triggered from large pipe displacements and deformations in an unstable soil, is known as responsible for the collapse of the structure. High costs of construction and maintenance of marine structures, in general, as well as environmental consequences of pipeline failure, in particular, necessitates comprehensive investigations on mechanisms of seabed soil instabilities near the structure.

Two known main mechanisms of soil instabilities are liquefaction and shear failure. The former is the loss of soil's ability to withstand any normal or shear stress, while acting like a liquid. The latter, is the soil loosing the ability to resist further shear stresses and thus, soil layers sliding on each other. To predict either phenomenon, wave-induced seabed responses, i.e. pore pressure, effective and normal stresses, should be evaluated and used in conjunction with appropriate soil instability criteria.

Numerous studies have concentrated on the evaluation of seabed responses under wave loading. However, the majority of them considered a two-dimensional wave-soil-pipeline interaction problem. These studies only deal with cases, in which the wave approaches normal to the orientation of pipeline. However, in the real ocean environment, waves may approach the pipeline from any direction. Therefore, it is necessary to establish a three-dimensional model to study these circumstances and gain a realistic understanding of soil behaviour under an oblique wave loading. The primary aim of this research is therefore to answer the question of "how significant are the three-dimensional effects on the wave-induced responses of seabed soil near a submarine buried pipeline?"

Among available investigations, only two studies have addressed this problem from a three-dimensional point of view. The first study was the BIEM model of Lennon (1983) and Lennon (1985), in which potential theory was applied to obtain the wave-induced pore pressure in the presence of a pipeline, while waves were considered to approach from multiple directions. As the primary concern, the potential theory, however, is associated with several deficiencies as described thoroughly in section 1.3.1.2. In fact, the potential theory is considered as being outdated, since it does not provide a realistic prediction of wave-induced seabed behaviour. Secondly, even if the potential theory could be considered as applicable in a very limited range of

soils, it does not provide any information on soil stresses. In other words, it is incapable of evaluating the potential of soil instability near the pipeline.

In another study, Chen *et al*. (2005) addressed a similar problem by using the consolidation equations of Biot (1941). Although Biot theory is accepted as suitable for describing the seabed behaviour under loading, Chen *et al*. (2005) questionably concluded that there is no difference between two-dimensional and three-dimensional cases. This conclusion is found to be incorrect in the present study. It is possible that such a conclusion is drawn based on the fact that Chen *et al*. (2005) only examined one set of wave/soil/pipe properties in their research. Meanwhile, similar to Lennon (1985), they also did not investigate soil stresses. The present study, however, reveals that the three-dimensional effects are significant particularly for soil normal and effective stresses. Therefore, the current research is intended to study both wave-induced pore pressure and stresses for a wide range of soil/pipe/wave properties, using a 3-D model.

A rare number of two-dimensional studies such as Jeng and Cheng (2000) investigated the potential of wave-induced seabed shear failure in the presence of a buried pipeline. However, to the author's knowledge, even among two-dimensional investigations, there is no study to systematically investigate both shear failure and liquefaction near submarine pipelines and over a wide range of wave/soil/pipe properties. At the same time, no three-dimensional model is also available in the literature to address three-dimensional effects on the potential of wave-induced shear failure and liquefaction around buried pipelines. Therefore, seabed instabilities will also be systematically investigated in the present study.

In summary, the present thesis consists of four chapters. In the first chapter a detailed review of the present knowledge of the wave-induced seabed behaviour is presented. This chapter consists of two major themes; first, available theories on soil consolidation modelling addressed with the emphasis on the problem of wave-seabed interaction. Secondly, a similar framework is followed to review available studies on the modelling of wave-induced seabed behaviour in the presence of a buried pipeline. In Chapter 2, the three-dimensional boundary value problem is formulated and the governing theories are introduced. Next, in the third chapter, details of numerical model setup, finite element mesh and convergence tests are presented. This will be followed by the extensive validation of numerical model versus both available experimental data and analytical solutions for more simplified cases. Numerical results are presented in Chapter 4, which consists of two major sections: a. wave-induced seabed responses and b. seabed soil instabilities – liquefaction and shear failure. Under each heading, a subsection is devoted to studying three-dimensional effects. This is then followed by a parametric study to investigate effects of a wide range of wave, soil, pipe and trench properties on seabed responses, and potentials of soil liquefaction and shear failure. It is worthwhile to point out that the parametric study will consider the case of water waves travelling along the pipeline, since this case has not been previously addressed in the literature. Finally, conclusive remarks

drawn from the present study as well as recommendations for future research will be outlined in the fifth chapter.

Chapter 2

THREE-DIMENSIONAL BOUNDARY VALUE PROBLEM

The propagation of ocean waves exerts significant dynamic loading on the seabed soil. The porous seabed, surrounding a buried pipeline, consequently responds to the wave loading and undergoes consolidation. This will result in the generation of pore pressure and stresses within marine sediments. The problem of determining wave-induced seabed responses in the presence of submarine buried pipelines can be viewed from two points. On one hand, the consolidation theory should be applied to analyse the behaviour of a seabed soil under the loading. For this, the three-dimensional Biot consolidation theory has been adopted in the present study. The theory and the formulation of the Biot consolidation model will be presented in section 2.1.1. Meanwhile, appropriate boundary conditions have to be applied in conjunction with the soil governing equations. Boundary conditions, constraining the behaviour of the porous seabed, will be introduced in section 2.1.2. On the other hand, the application of a proper wave theory is necessary to evaluate hydrodynamic loadings, triggered by the passage of water waves, on the porous bed. In this regard, the linear wave theory has been adopted in the present study. The theory will be applied to obtain the dynamic pressure exerted by water waves at the seabed surface. The linear wave theory and relevant formulations are briefly reviewed and presented in section 2.2. At this point, Chapter 2 provides the complete set of formulations associated with the three-dimensional boundary value problem (BVP) of wave-seabed-pipeline interaction.

2.1 Boundary Value Problem: Seabed Soil Consolidation

A submarine pipeline is considered to be buried within a trench as shown in the cross-sectional view in Figure 2.1. As illustrated, the x- direction is perpendicular to the trench lateral walls; the y direction is parallel to the pipeline; and the z axis is assumed to be positive upward from the mudline and located at the mid trench width. On the other hand, the plane view of the problem configuration is also plotted in Figure 2.2. Ocean waves are assumed to propagate in the positive X- direction. Therefore an incident wave angle of α is formed between the direction of wave progression (X- axis) and the pipe centreline (y- axis). For waves travelling parallel with the pipeline, thus, $\alpha=0°$, while for waves propagating normal to the pipeline, hence, $\alpha=90°$.

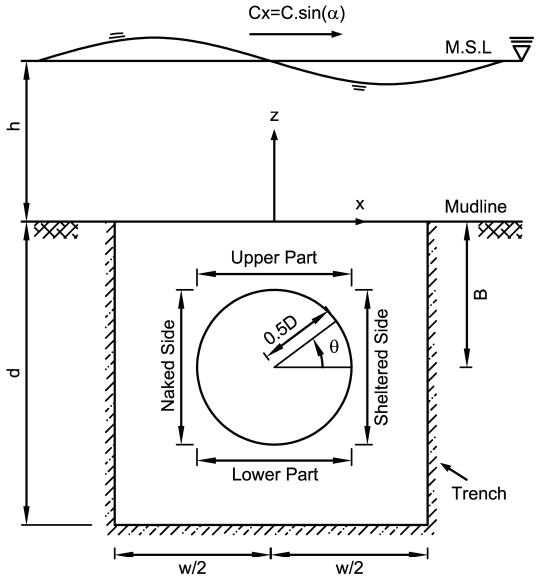

Figure 2.1. Definition Sketch: Cross-section of a trenched submarine buried pipeline.

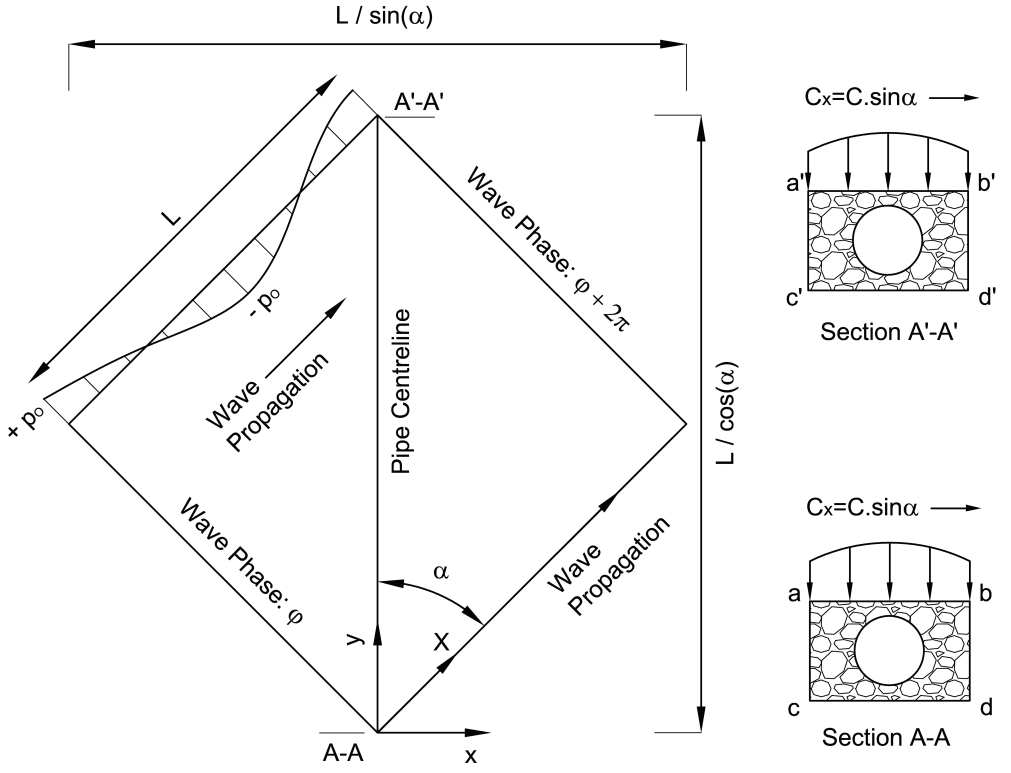

Figure 2.2. Definition Sketch: Plan of progressive waves approaching a trenched submarine buried pipeline.

2.1.1 Governing Equations

The seabed soil surrounding a submarine buried pipeline consolidates under the dynamic pressure from ocean waves. Full three-dimensional Biot consolidation theory (Biot, 1941) is applied in this study to evaluate the seabed response associated with the action of waves. The application of this theory is based upon the following assumptions of the seabed behaviour:

(1) The Darcy law dominates the pore fluid flow through seabed voids.

(2) The soil skeleton is a linear elastic material and its behaviour follows the Hooke's law.

(3) Both the pore fluid and soil skeleton are compressible materials.

(4) Unsteady velocities, i.e. accelerations, in both pore fluid flow and soil skeleton displacements are assumed to be small and therefore negligible.

(5) The pore fluid is a uniform material consisting of pore water and air bubbles; and its properties such as the air content and the compressibility do not change during and as the result of the consolidation process.

On the other hand, it is also assumed in the present study that the:

(6) The seabed soil is hydraulically and structurally isotropic.

(7) The seabed material is uniform and homogenous.

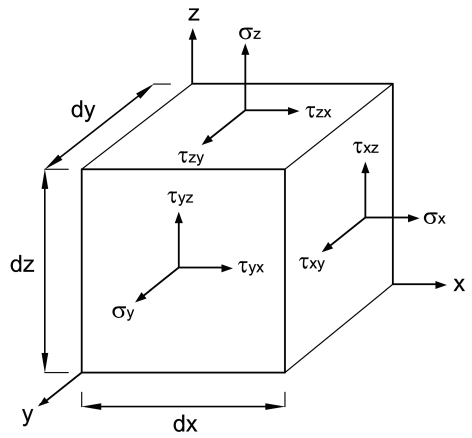

Figure 2.3. Definition Sketch: total stresses acting on a soil element.

Figure 2.3 shows a small cubic element of consolidating seabed soil with shear and normal total stresses acting on it. The element is considered large enough compared with the size of pores so that it may be treated

as homogenous, and at the same time small enough so it may be mathematically considered infinitesimal. The equilibrium state of stress, in the *x*-, *y*- and *z*- directions respectively, requires:

$$\frac{\partial \sigma_x}{\partial x} + \frac{\partial \tau_{yx}}{\partial y} + \frac{\partial \tau_{zx}}{\partial z} = 0 \tag{2.1}$$

$$\frac{\partial \tau_{xy}}{\partial x} + \frac{\partial \sigma_y}{\partial y} + \frac{\partial \tau_{zy}}{\partial z} = 0 \tag{2.2}$$

$$\frac{\partial \tau_{xz}}{\partial x} + \frac{\partial \tau_{yz}}{\partial y} + \frac{\partial \sigma_z}{\partial z} = 0 \tag{2.3}$$

in which, τ_{ij} is the soil shear stress acting in the *j*- direction and in the plane normal to the *i*- direction; σ_i represents total normal stress in the *i*- direction. On the other hand, the seabed material is reported to be highly saturated with the degree of saturation ranging from about 0.90 to 1.00 as pointed out in Esrig and Kirby (1977). In such nearly saturated condition, the relation between total and effective normal stresses of soil can be expressed, in any direction such as *i*-, as:

$$\sigma'_i = \sigma_i + p \tag{2.4}$$

where, σ'_i is the normal effective stress in *i*- direction. It is important to note that the relation (2.4) should be modified in partially saturated soils. Substituting equation (2.4) into equations (2.1)-(2.3), gives:

$$\frac{\partial \sigma'_x}{\partial x} + \frac{\partial \tau_{yx}}{\partial y} + \frac{\partial \tau_{zx}}{\partial z} = \frac{\partial p}{\partial x} \tag{2.5}$$

$$\frac{\partial \tau_{xy}}{\partial x} + \frac{\partial \sigma'_y}{\partial y} + \frac{\partial \tau_{zy}}{\partial z} = \frac{\partial p}{\partial y} \tag{2.6}$$

$$\frac{\partial \tau_{xz}}{\partial x} + \frac{\partial \tau_{yz}}{\partial y} + \frac{\partial \sigma'_z}{\partial z} = \frac{\partial p}{\partial z} \tag{2.7}$$

It is assumed that the soil skeleton is a linear elastic material. Therefore, stresses and strains in solid skeleton are related on the basis of Hooke's law. That is:

$$\tau_{xy} = \tau_{yx} = G\left(\frac{\partial u}{\partial y} + \frac{\partial v}{\partial x}\right) \tag{2.8}$$

$$\tau_{xz} = \tau_{zx} = G\left(\frac{\partial u}{\partial z} + \frac{\partial w}{\partial x}\right) \tag{2.9}$$

$$\tau_{yz} = \tau_{zy} = G\left(\frac{\partial v}{\partial z} + \frac{\partial w}{\partial y}\right) \tag{2.10}$$

$$\sigma'_x = 2G\left(\frac{\partial u}{\partial x} + \frac{\mu}{1-2\mu}\varepsilon\right) \tag{2.11}$$

$$\sigma'_y = 2G\left(\frac{\partial v}{\partial y} + \frac{\mu}{1-2\mu}\varepsilon\right) \tag{2.12}$$

$$\sigma'_z = 2G\left(\frac{\partial w}{\partial z} + \frac{\mu}{1-2\mu}\varepsilon\right) \tag{2.13}$$

in which, G is the shear modulus of soil; μ is the Poisson's ratio; u, v and w are soil displacements in x-, y- and z- directions, respectively; and ε is the volumetric soil strain defined as:

$$\varepsilon = \frac{\partial u}{\partial x} + \frac{\partial v}{\partial y} + \frac{\partial w}{\partial z} \tag{2.14}$$

Soil stresses, in relations (2.8) to (2.13), can be substituted into the equilibrium equations (2.5) to (2.7). This provides a system of partial differential equations for soil equilibrium in terms of soil displacements and the pore pressure:

$$G\left(\frac{\partial^2 u}{\partial x^2} + \frac{\partial^2 u}{\partial y^2} + \frac{\partial^2 u}{\partial z^2}\right) + \frac{G}{1-2\mu}\frac{\partial}{\partial x}\left(\frac{\partial u}{\partial x} + \frac{\partial v}{\partial y} + \frac{\partial w}{\partial z}\right) = \frac{\partial p}{\partial x} \tag{2.15}$$

$$G\left(\frac{\partial^2 v}{\partial x^2} + \frac{\partial^2 v}{\partial y^2} + \frac{\partial^2 v}{\partial z^2}\right) + \frac{G}{1-2\mu}\frac{\partial}{\partial y}\left(\frac{\partial u}{\partial x} + \frac{\partial v}{\partial y} + \frac{\partial w}{\partial z}\right) = \frac{\partial p}{\partial y} \tag{2.16}$$

$$G\left(\frac{\partial^2 w}{\partial x^2} + \frac{\partial^2 w}{\partial y^2} + \frac{\partial^2 w}{\partial z^2}\right) + \frac{G}{1-2\mu}\frac{\partial}{\partial z}\left(\frac{\partial u}{\partial x} + \frac{\partial v}{\partial y} + \frac{\partial w}{\partial z}\right) = \frac{\partial p}{\partial z} \tag{2.17}$$

It is also necessary to formulate the phenomenon of pore fluid flow through the seabed soil. Neglecting unsteady pore fluid motion and soil skeleton deformation, the Darcy's law can be used to describe the pore fluid flow:

$$-\frac{\partial p}{\partial x}=\frac{\rho_f g}{k}u_f \tag{2.18}$$

$$-\frac{\partial p}{\partial y}=\frac{\rho_f g}{k}v_f \tag{2.19}$$

$$-\frac{\partial p}{\partial z}+\rho_f g=\frac{\rho_f g}{k}w_f \tag{2.20}$$

where, ρ_f is the density of pore fluid; k is the permeability of the soil; and u_f, v_f and w_f are average relative velocities of pore fluid, in the x-, y- and z- directions, expressed relative to those of soil skeleton. Meanwhile, the equation of continuity of compressible pore fluid flow requires that:

$$\frac{\partial u_f}{\partial x}+\frac{\partial v_f}{\partial y}+\frac{\partial w_f}{\partial z}=-\frac{\partial \varepsilon}{\partial t}-n\beta\frac{\partial p}{\partial t} \tag{2.21}$$

in which, n is the porosity of the seabed soil and β is the compressibility of the pore fluid. The compressibility of pore fluid deviates from that of pure water based on the degree of saturation. In highly saturated soils (S>0.85), this is as:

$$\beta=\frac{1}{K_w}+\frac{1-S}{P_{wo}} \tag{2.22}$$

where, K_w (=2 GPa) is the true bulk modulus of elasticity of water; 1/ K_w thus represents the compressibility of pure (fully saturated) water; P_{wo} is the absolute water pressure. The term 1-S, in fact, represents the portion of air in the voids. Finally, pore fluid velocities, from equations (2.18)-(2.20) can be substituted into the equation of pore fluid continuity to obtain the so-called storage equation that describes the pore fluid flow:

$$k\left(\frac{\partial^2 p}{\partial x^2}+\frac{\partial^2 p}{\partial y^2}+\frac{\partial^2 p}{\partial z^2}\right)-\rho_f g n\beta\frac{\partial p}{\partial t}=\rho_f g\frac{\partial \varepsilon}{\partial t} \tag{2.23}$$

The system of equilibrium equations for the soil matrix in (2.15)-(2.17) and the storage equation in (2.23) is known as the quasi-static soil consolidation theory as well as the Biot consolidation equations. They are sufficient to analyse the seabed behaviour under the wave loading. However, appropriate boundary conditions should be introduced in conjunction with these equations in order to solve the problem of wave-seabed-pipeline interaction.

2.1.2 Boundary Conditions

Five sets of boundary conditions are required to solve the boundary value problem of wave-induced seabed responses in the presence of a pipeline. They are (*i*) Mudline Boundary Conditions (MBC), (*ii*) trench Bottom Boundary Conditions (BBC), (*iii*) Pipeline surface Boundary Conditions (PBC), (*iv*) Lateral Boundary Conditions in the *x*- direction (LBC_x), and (*v*) Lateral Boundary Conditions in the *y*- direction (LBC_y).

- *Mudline Boundary Condition (MBC)*:

At the interface between the water body and the porous seabed, a wave dynamic pressure is introduced to the soil. The continuity of pressure between the two media, i.e. soil and water body, therefore requires that the pore pressure within the seabed to be identical to the wave pressure. That is:

$$p = p_{bed} \tag{2.24}$$

in which, p_{bed} represents the spatial and temporal variations of wave pressure at the seabed surface (z=0). It will be shown in the next section that, based on the linear wave theory, the wave pressure at the mudline is:

$$p_{bed} = \frac{\rho_w g H}{2\cosh \kappa h}\cos(\kappa X - \omega t) \tag{2.25}$$

where, ρ_w is the sea water density; H is the wave height; h is water depth; and κ and ω are the wave number and frequency, respectively. Since the consolidation equations as presented in the previous section are proposed in the *xyz* coordinate system, the wave pressure in the relation (2.25) should be transformed to this system. For this purpose, the positive *X*- axis should be rotated (90-α)° clockwise about the *z*- axis to coincide with the positive *x*- axis. The rotational transformation matrix is:

$$\begin{bmatrix} X \\ Y \\ z \end{bmatrix} = \begin{bmatrix} \sin(\alpha) & \cos(\alpha) & 0 \\ -\cos(\alpha) & \sin(\alpha) & 0 \\ 0 & 0 & 1 \end{bmatrix} \begin{bmatrix} x \\ y \\ z \end{bmatrix} \tag{2.26}$$

Substituting *X* from (2.26) into (2.25), the mudline wave pressure will be:

$$p = p_{bed} = \frac{\rho_w g H}{2\cos \kappa h}\cos(\kappa_x x + \kappa_y y - \omega t) \tag{2.27}$$

in which, κ_x and κ_y are projections of wave number:

$$\kappa_x = \kappa \sin\alpha \qquad \text{and} \qquad \kappa_y = \kappa \cos\alpha \tag{2.28}$$

As previously stated total normal soil stresses in fact consist of effective normal stresses acting on soil skeleton and the pore pressure. On the seabed surface, the total vertical stress (σ_z) is generated by and identical to the wave pressure at the mudline. At the same time, at this point, the wave pressure is also identical to the pore pressure within the seabed due to the continuity of pressure between wave and seabed mediums. Therefore, the vertical effective stress (σ'_z) becomes zero at the seabed surface. In other words, the portion of vertical stresses carried by the *soil skeleton* vanishes at the water-soil interface. i.e.:

$$\sigma'_z\big|_{z=0} = 2G\left(\frac{\partial w}{\partial z} + \frac{\mu}{1-2\mu}\varepsilon\right)\Bigg|_{z=0} = 0 \tag{2.29}$$

Finally, there are two other requirements to be met on the seabed surface. They are that the shear stresses acting on seabed surface should be prescribed. These stresses are in fact generated by the action of viscous flow in the boundary layer adjacent to the mudline. The effect of shear stresses is well known as responsible for the sediment transport in a thin layer of porous seabed. However, considering the seabed domain as a whole, mudline shear stresses are found to have negligible contributions towards the consolidation process of a seabed soil, as examined by Sakai *et al*. (1991), Hittori *et al*. (1992) and Jeng (1997b). Therefore,

$$\tau_{zx}\big|_{z=0} = G\left(\frac{\partial u}{\partial z} + \frac{\partial w}{\partial x}\right)\Bigg|_{z=0} = 0 \tag{2.30}$$

$$\tau_{zy}\big|_{z=0} = G\left(\frac{\partial v}{\partial z} + \frac{\partial w}{\partial y}\right)\Bigg|_{z=0} = 0 \tag{2.31}$$

Equations (2.27), (2.29)-(2.31) form the mudline boundary conditions.

- *Boundary Conditions on Impermeable Fixed Rough Surfaces (BBC, PBC, LBC$_x$)*:

In this study, it is assumed that the surfaces of the trench walls, trench bottom and pipeline are impermeable. Such an assumption requires that pore fluid flow cannot penetrate into these surfaces. Therefore, the gradient of pore pressure normal to these surfaces should be zero. That is:

$$\frac{\partial p}{\partial r} = 0 \qquad \text{on,} \quad \left|\begin{array}{ll} \text{trench walls :} & x = \pm W/2 \\ \text{trench bottom :} & z = -d \\ \text{pipe surface :} & x^2 + z^2 = D^2/4 \end{array}\right. \tag{2.32}$$

in which, r is the direction normal to the boundary surface, specified as $r \equiv x$ on the trench lateral walls; $r \equiv z$ on the trench bottom. Also, w and d are the trench width and depth, respectively; and D is the pipe outer diameter. On the other hand, it is assumed that these surfaces are fixed, rigid and rough. Therefore, a no-slip condition between soil and boundary surfaces requires:

$$u = v = w = 0 \quad \text{on,} \quad \begin{cases} \text{trench walls :} & x = \pm w/2 \\ \text{trench bottom :} & z = -d \\ \text{pipe surface :} & x^2 + z^2 = D^2/4 \end{cases} \tag{2.33}$$

Assumptions, which are made on the boundary conditions at the pipe-soil interface, influence seabed responses. Among available studies, Cheng and Liu (1986) considered the case of an unanchored pipeline, Jeng *et al*. (2001) examined pipe internal stresses and deformations, and recently, Luan *et al*. (2008) studied the contact problem between the soil and the pipeline, where slipping was also allowed at the interface. In the present study, however, the concentration is on three-dimensional aspects of wave-seabed-pipeline interaction problem. Therefore, a simplified boundary condition, as in relation (2.33), is applied on pipe-soil interface. Besides, these conditions can also be justified as reasonable in cases such as anchored pipelines with a concrete coating.

- *Lateral Boundary Conditions in y- direction (LBC_y)*:

An examination of Figure 2.2 reveals that a periodic-type lateral boundary condition is required in the y-direction. Before proceeding to this issue, however, it is necessary to introduce conditions upon which the response of the seabed soil at two locations can be considered as being identical to each other. In fact, the soil elements at any two points respond identically to the wave loading, only if these two points are:

(a) located at the same depth (z) beneath the mudline (z_1=z_2).

(b) located at the same position (x) measured from the pipe centreline (x_1=x_2).

(c) exposed to similar wave loadings on the seabed surface above them (wave phase$_1$= wave phase$_2$+2$m\pi$).

where, m is an integer. As shown in Figure 2.2, these conditions are satisfied among sections A-A and A'- A', on which the wave loadings are 2π distant from each other. Therefore, a periodic boundary condition in the y-direction can be proposed between any two such sections, provided that they are $\Delta y = \dfrac{L}{\cos\alpha}$ distant from each other. This issue can also be mathematically confirmed by an inspection of equations (2.27) and (2.28).

$$\text{Seabed Response}\big|_{abcd} = \text{Seabed Response}\big|_{a'b'c'd'} \tag{2.34}$$

That is,

$$u(x,y,z) = u(x, y + \frac{L}{\cos\alpha}, z) \tag{2.35}$$

$$v(x,y,z) = v(x, y + \frac{L}{\cos\alpha}, z) \tag{2.36}$$

$$w(x,y,z) = w(x, y + \frac{L}{\cos\alpha}, z) \tag{2.37}$$

$$p(x,y,z) = p(x, y + \frac{L}{\cos\alpha}, z) \tag{2.38}$$

It is worthy to note that for the special case of waves that are propagating normal to the pipeline (α=90°), the periodic lateral boundary condition in the *y*- direction can be applied between any two sections with an arbitrary distance Δ*y*. Nonetheless, for numerical simulation purposes, a minimum length of computational domain in the y- direction is considered. This will be discussed in the next chapter.

2.2 Boundary Value Problem: Small-Amplitude Progressive Water Waves

Neglecting the effect of a thin viscous boundary layer near the mudline, it is reasonable to consider that the incompressible fluid flow of ocean waves is irrotational. Therefore, a velocity potential $\phi_w(x,z,t)$ can be defined so that:

$$u_x = \frac{\partial \phi_w}{\partial x},\ u_z = \frac{\partial \phi_w}{\partial z} \tag{2.39}$$

in which, u_x and u_z are velocities of fluid particles in the *x*- and *z*- directions, respectively. Substituting these velocities into the equation of continuity of fluid flow leads to the potential theory that governs the fluid flow throughout the water body:

$$\frac{\partial^2 \phi_w}{\partial x^2} + \frac{\partial^2 \phi_w}{\partial z^2} = 0 \tag{2.40}$$

A solution to the Laplace equation may be specified in conjunction with appropriate flow conditions on the boundaries, as indicated in the Figure 2.4. On the mudline, it is assumed that the seabed surface is rigid and impermeable. Hence, a Kinematic Bottom Boundary Condition (KBBC) requires the vertical component of water particle velocities to remain zero at the mudline.

$$\left.\frac{\partial \phi_w}{\partial z}\right|_{z=-h} = 0 \tag{2.41}$$

where, h is water depth. It should be noted that it is the wave pressure, obtained from the solution of the water wave problem, which dominates the wave-induced soil responses in the porous seabed. Therefore, any simplifying assumption in the problem of water waves will lead to some extent of approximation in the problem of wave-seabed interaction. However, although the assumption of a rigid impermeable bottom introduces an approximation to the water wave problem, the follow-on wave pressure field is still reasonably acceptable for the evaluation of wave-induced seabed responses in most practical engineering applications. It should be pointed-out that under these circumstances, however, the mechanics of water waves is in fact decoupled from that of the porous seabed. Similar explanations are also applicable to justify the use of linear wave theory in this problem, in general.

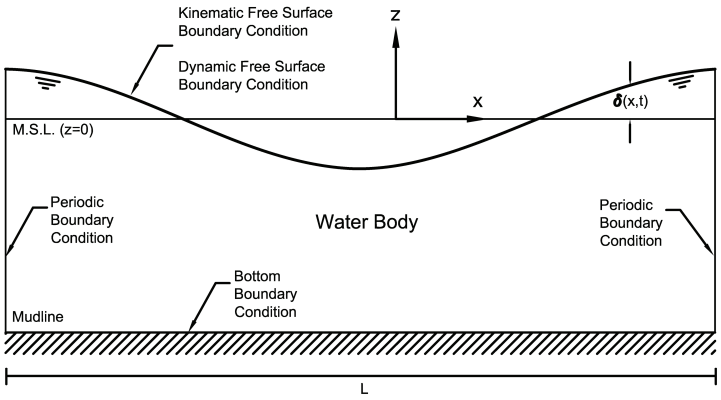

Figure 2.4. Definition sketch: Boundary value problem of water waves (Dean and Dalrymple, 1984).

Along the free surface, two other boundary conditions should also be satisfied: a Kinematic Free Surface Boundary Condition (KFSBC) and a Dynamic Free Surface Boundary Condition (DFSBC). The former requires the fluid particle vertical velocity at free surface to be confined to:

$$\left.\frac{\partial \phi_w}{\partial z}\right|_{z=\delta(x,t)} = \left.\left(\frac{\partial \delta}{\partial t} + \frac{\partial \phi_w}{\partial x}\frac{\partial \delta}{\partial x}\right)\right|_{z=\delta(x,t)} \tag{2.42}$$

in which, $\delta(x, t)$ indicates vertical coordinates of points located on the free surface, as illustrated in Figure 2.4. The introduction of KFSBC, in fact, guarantees fluid velocities being in conformity with temporal and spatial evolutions of free surface. On the other hand, the fluid pressure across the free surface can be considered to be uniformly distributed and equal to the atmospheric pressure. The pressure distribution at free surface can be used in conjunction with the unsteady Bernoulli equation on the free surface to express DFSBC:

$$\left(-\frac{\partial \phi_w}{\partial t} + \frac{1}{2}\left(\frac{\partial \phi_w}{\partial x}\right)^2 + \frac{1}{2}\left(\frac{\partial \phi_w}{\partial z}\right)^2 + \frac{\overbrace{p_w}^{=0}}{\rho_w} + gz \right)\Bigg|_{z=\delta(x,t)} = C_B(t) \tag{2.43}$$

where, C_B is the Bernoulli constant and a function of time (t) only; g is the gravitational acceleration and ρ_w is the water density. For convenience, a solution to the Laplace equation along with the aforementioned boundary conditions can be derived via the assumption of wave amplitudes, as well as fluid particle velocities at the free surface, being small. These assumptions result in KFSBC and DFSBC being linearised and thus the water wave problem to be simplified to a large extent. Details of the solution procedure can be found in Dean and Dalrymple (1984) and therefore is not repeated herein. The evaluated field of velocity potential for the case of a small amplitude progressive wave, finally, is as:

$$\phi_w(x,z,t) = \frac{H}{2}\frac{g}{\omega}\frac{\cosh \kappa(h+z)}{\cosh \kappa h}\sin\left(\kappa x - \omega t\right) \tag{2.44}$$

in which, H is the wave height; ω is the wave frequency; and κ is the wave number. Among engineering properties of progressive waves, its dynamic pressure on the seabed surface is of particular interest for the evaluation of wave-induced seabed responses around a submarine buried pipeline. The pressure field associated with a progressive wave can be determined from the linearised Bernoulli equation, in which squared terms of fluid velocities are neglected based on the assumption of wave amplitude being small:

$$\frac{p_w}{\rho_w} = gz + \frac{\partial \phi_w}{\partial t} \tag{2.45}$$

Further substituting equation (2.44) into equation (2.45) and performing the partial differentiation, the fluid pressure field is obtained as:

$$p_w = \rho_w gz + \frac{\rho_w gH}{2}\frac{\cosh \kappa(h+z)}{\cosh \kappa h}\cos(\kappa x - \omega t) \tag{2.46}$$

The pressure field consists of a hydrostatic pressure distribution and a dynamic component due to the wave action. The dynamic component is of both spatially and temporally periodic nature. It is the pressure at the seabed surface, z=-h, that exerts the consolidating load on the seabed soil. The dynamic component of wave pressure at the mudline can be formulated as:

$$p_{bed} = p_0 \cos(\kappa x - \omega t) \tag{2.47}$$

where, the amplitude of wave dynamic pressure at mudline (p_0) is:

$$p_0 = \frac{\rho_w g H}{2\cos\kappa h} \tag{2.48}$$

The wave pressure at the seabed surface is applied as the mudline boundary condition in equation (2.25) for the boundary value problem of the consolidation of seabed soil.

2.3 Summary

In the foregoing chapter, the three-dimensional boundary value problem (BVP) of wave-seabed-pipeline interaction is formulated. The three-dimensional Biot consolidation equations are considered to express the behaviour of a seabed soil under the wave loading. At the same time, the linear wave theory is applied to evaluate wave loadings on the porous seabed. The system of soil governing equations includes the equilibrium of soil matrix in (2.15)-(2.17) along with the storage equation of (2.23), which describes the pore fluid flow within the seabed soil. Such a system is complete in conjunction with five sets of boundary conditions given respectively as MBC in equations (2.27)-(2.31); BBC, PBC, LBC_x in equations (2.32)-(2.33); and LBC_y in equations (2.35)-(2.38). The wave pressure on the seabed surface is also formulated by the assumption of small amplitude ocean waves as in equation (2.47). The established boundary value problem is ready to be numerically simulated to evaluate wave-induced seabed responses in the vicinity of a submarine buried pipeline. More details on the numerical model will be subsequently presented in the next chapter.

Chapter 3

THREE-DIMENSIONAL FINITE ELEMENT MODEL

The three-dimensional boundary value problem, presented in the previous chapter, will be solved numerically. For this purpose, the Finite Element Method is adopted to develop a numerical model. The proposed model, WSPI-3D (*Wave-Soil-Pipe Interaction simulator in 3-D*), is constructed with the aid of the PDE module of Comsol Multiphysics, a Finite Element Analysis software. The flexibility of Comsol Multiphysics, as it works in conjunction with MATLAB, further allows the implementation of a well-organized post-processing module within WSPI-3D. For more details on Comsol Multiphysics, the reader is referred to COMSOL (2006). In this chapter, general characteristics of the developed FE model, as well as details of spatial and temporal discretization in the FE system will be presented. Furthermore, the new 3-D numerical model will be rigorously examined and validated against an available analytical solution, experimental data, as well as, a previous two-dimensional numerical model.

3.1 Finite Element Model

In the present model, *Quadratic (2nd order) Lagrange* elements have been used to ensure the second order of accuracy in evaluating seabed responses. The three-dimensional finite elements are considered to be *Hexahedral*. Details of the FE mesh pattern are also presented in Section 3.1.1. Meanwhile, numerical integrations are approximated by using the *Quadrature formula*, which computes the integral over a mesh element by taking a weighted sum of the integrand - evaluated in a finite number of points in the mesh element. The order of Quadrature formula, as a rule of thumb, is taken to be twice the order of the adopted finite element. Thus, the 4^{th} order Quadrature formula is used. The time-dependant consolidation problem is solved by using the *GMRES linear system solver* along with an *Incomplete LU* preconditioner scheme. The problem is solved to obtain the pore pressure and soil displacement fields. These were then used to extract soil stresses by using equations (2.8) to (2.13). Post-processing subroutines are then applied to transfer the stress tensors into the desired coordinate system, as well as, to extract amplitudes and phase lags of seabed responses. Numerical simulations were carried out on a 2.4 GHz dual processor machine with 8 GB of RAM at the Centre for Geotechnical Research (CGR), the University of Sydney.

3.1.1 Spatial Discretization: Finite Element Mesh

The occurrence of soil instability in the vicinity of a pipeline leads to the instability of the structure itself and therefore to its failure. Consequently, it is the interest of this study to evaluate seabed responses near to and in particular around the pipeline. On the other hand, the presence of a structure such as a pipeline is expected to trigger a stress concentration in the region close to the structure. Therefore, it is necessary to refine the Finite Element Mesh near the pipeline. The cylindrical geometry of the structure also suggests that a far-field mesh has to be modified in conformity to this geometry, when it gets closer to the structure. In the region near the pipeline, hence, a specific mesh pattern is considered herein as illustrated in Figure 3.1. Some preliminary numerical results also suggest that it is sufficient for such a specific pattern to spread to twice the pipe diameter, as is shown. In fact, this is because of the concentration of stress, due to the presence of the structure, being likely to vanish beyond this distance. On the other hand, the adopted pattern allows the mesh to refine as it moves towards the structure.

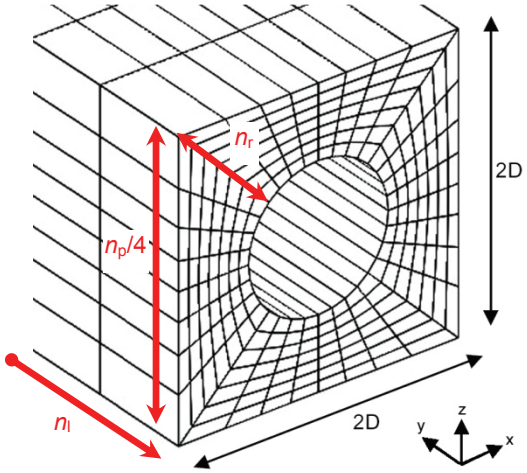

Figure 3.1. Definition Sketch: 3-D Finite Element Mesh in the vicinity of pipeline.

Numerical experiments were carried out in this study to determine the minimum required mesh resolution near the pipeline that provides a desired accuracy for the evaluation of wave-induced seabed responses. In the present study, such a desired accuracy is defined as when numerical results contain less than 1% of error in comparison with the exact solution. However, no exact solution is yet available for the response of seabed soil in the presence of a pipeline. In this regard, it is possible to consider a benchmark numerical solution to act as the exact solution. For this purpose, benchmark numerical results should be obtained based on using an extremely fine mesh. The refinement of the introduced mesh pattern can be controlled by a set of three parameters. They are: n_p showing the number of mesh divisions around the pipeline perimeter; n_r representing the number of mesh divisions in the radial direction on the pipe cross-section; n_l standing for the number of mesh divisions over one wave length along the pipe centreline, which

coincides to the *y*- direction in Figure 3.1. Now, let us assume that the numerical results would fall on the exact solution, when an extremely fine mesh, which is generated by adopting $n_p = 64$, $n_r = 12$ and $n_l = 40$, is used. This mesh refinement, therefore, corresponds to the benchmark numerical solution. It is worthy to note that this assumption will be automatically confirmed upon the convergence of coarse-mesh numerical results to the benchmark solution. It is also assumed that the benchmark solution may be achieved when FE Analysis is continued for up to five wave periods (that is $n_c = 5$) to ensure a fully stable numerical scheme. The benchmark FE time step (Δt) is also considered as small as 1/90 of the wave period.

Hereafter, results from a set of numerical tests will be presented. Tests are aimed at identifying the minimum mesh refinement that permits soil responses to fall within 1% of deviation from the defined benchmark solution. Properties of wave, soil and pipeline, which are used in numerical tests, are listed in Table 3.1, unless otherwise stated. It should be pointed out that Table 3.1 represents data for a typical wave-seabed-pipeline interaction problem. Nevertheless, similar numerical tests were also carried out for a wide range of soil, pipe and wave properties and led to the same degree of required mesh refinement. In this section, $\Delta t = T/36$ and $n_c = 2$ are adopted to perform the FE analysis[3].

Table 3.1. Properties of wave, soil and pipe used in numerical tests to determine required mesh refinement.

Wave Properties		Soil Properties		Trench / Pipeline Properties	
Water depth (h)	10 m	Shear stiffness (G)	5 MPa	Trench width (w)	4 m
Wave period (T)	10 sec	Poisson's ratio (μ)	0.33	Trench depth (d)	4 m
Wave length (L)	92.32 m	Porosity (n)	0.40	Pipe diameter (D)	2 m
Wave angle (α)	0° and 90°	Saturation (S)	98.5%	Pipe burial depth (B)	2 m
Wave height (H)	2 m	Permeability (k)	10^{-3} ms^{-1}		

It is essential for FEM modelling to examine the influence of mesh resolution on both the pore pressure and soil stresses around the pipeline. For this purpose and as a measure of seabed responses around the structure, integrals of pore pressure and soil stresses over the perimeter of pipe cross-section will be studied. These are as $\oint_s \frac{p}{p_o} ds$, $\oint_s \frac{\sigma'_x}{p_o} ds$, $\oint_s \frac{\sigma'_y}{p_o} ds$ and $\oint_s \frac{\sigma'_z}{p_o} ds$ in which s indicates the circumference of pipe cross-section. In fact, it was also possible to individually study the effect of mesh resolution on a number of points around the structure. However, using the integrated form provides a general view of accuracy of the model in evaluating the seabed behaviour around the pipeline as a whole. The wave dynamic pressure on seabed

[3] It will be shown in the next section that $\Delta t = T/36$ and $n_c = 2$ correspond to an error of no more than one percent in numerical results and thus are sufficient for the present study.

surface oscillates periodically over a wave period and therefore so does the integral of a seabed response. But, the amplitude of this oscillation is used herein to justify the required mesh refinement.

It is convenient to consider the case of ocean waves propagating normal to the pipeline (α=90°) to investigate the effect of mesh refinements in the *xz* plane, i.e. n_p and n_r. The boundary value problem will be reduced to a two-dimensional soil consolidation problem under these circumstances. Results of numerical simulations, presented in Table 3.2 and Table 3.3, suggest that by the use of n_p = 32 and n_r = 8 the deviation of integrated soil responses from the benchmark solution will be reduced to less than 1%. Therefore, it is sufficient to consider a finite element mesh, which divides the pipeline circumference into 32 sections, while it splits the radial direction into 8 segments. It is worthy to mention that some investigations such as Magda (1996) also used a simplified two-dimensional version of mesh pattern that is depicted in Figure 3.1. However, Magda (1996) only examined the influence of mesh resolution on wave-induced uplift forces acting on the pipeline. The uplift force is in fact a measure of pore pressure around the circumference of structure, as a whole. Nevertheless, the present tabulated numerical results reveal that soil stresses would suffer from much more significant errors, if a coarse mesh is inappropriately used. Thus, the effect of mesh resolution on soil stresses also has to be investigated.

Table 3.2. Seabed responses around pipeline for various mesh refinements (n_p) while α=90°; n_r = 12; n_l = n./a.

n_p	$\left\lvert\oint_s \frac{p}{p_o} ds\right\rvert$	Deviation from Benchmark Solution	$\left\lvert\oint_s \frac{\sigma'_x}{p_o} ds\right\rvert$	Deviation from Benchmark Solution	$\left\lvert\oint_s \frac{\sigma'_z}{p_o} ds\right\rvert$	Deviation from Benchmark Solution
8	3.641	% 2.65	0.096	% 49.47	0.161	% 78.53
16	3.703	% 0.99	0.192	% 1.05	0.774	% 3.20
32	3.740	% 0.00	0.190	% 0.00	0.750	% 0.00
64	3.736	% 0.11	0.190	% 0.00	0.748	% 0.27

Table 3.3. Seabed responses around pipeline for various mesh refinements (n_r) while α=90°; n_p = 32; n_l = n./a.

n_r	$\left\lvert\oint_s \frac{p}{p_o} ds\right\rvert$	Deviation from Benchmark Solution	$\left\lvert\oint_s \frac{\sigma'_x}{p_o} ds\right\rvert$	Deviation from Benchmark Solution	$\left\lvert\oint_s \frac{\sigma'_z}{p_o} ds\right\rvert$	Deviation from Benchmark Solution
4	3.729	% 0.29	0.198	% 4.21	0.743	% 0.93
6	3.737	% 0.08	0.193	% 1.58	0.747	% 0.40
8	3.744	% 0.11	0.192	% 1.05	0.751	% 0.13
10	3.711	% 0.78	0.190	% 0.00	0.750	% 0.00
12	3.740	% 0.00	0.190	% 0.00	0.750	% 0.00

To study the mesh refinement along the pipeline, i.e. n_l, an ocean wave propagating parallel with the pipe orientation (α=0°) is considered. This is because under these circumstances, the wave loading varies along the pipeline. Therefore, the number of mesh divisions along the structure is expected to influence the accuracy of numerical simulations. Table 3.4 clearly indicates that a refinement of n_l = 20 per wave length is sufficient, for this dimension. It is, however, worthy to note that although n_l = 20 keeps the deviation from the benchmark solution below 1%, a simulation time of 16 hours is required to complete the numerical analysis. However, the case of n_l = 10 despite slightly larger errors (maximum 1.60 %), requires only 1.6 hours to complete. Therefore, n_l = 10 is recommended to be used when computing facilities are limited.

Table 3.4. Seabed responses around pipeline for various mesh refinements (n_l) while α=0°; n_p = 32; n_r = 8.

n_l	$\left\|\oint_S \frac{p}{p_o} ds\right\|$	Deviation from Benchmark Solution	$\left\|\oint_S \frac{\sigma'_x}{p_o} ds\right\|$	Deviation from Benchmark Solution	$\left\|\oint_S \frac{\sigma'_y}{p_o} ds\right\|$	Deviation from Benchmark Solution	$\left\|\oint_S \frac{\sigma'_z}{p_o} ds\right\|$	Deviation from Benchmark Solution	Simulation Time (hour)
10	3.721	% 0.32	0.191	% 1.60	0.309	% 1.31	0.746	% 1.36	1.6
20	3.707	% 0.05	0.187	% 0.53	0.304	% 0.33	0.735	% 0.14	16.0
40	3.709	% 0.00	0.188	% 0.00	0.305	% 0.00	0.736	% 0.00	52.0

3.1.2 Temporal Discretization

The finite element model developed in this study is time dependent. Therefore, it is essential to determine the maximum allowed FE time step (Δt). As mentioned previously, it is assumed that an exact solution may be achieved while Δt is adopted as low as 1/90 of a wave period. The objective of this section is to determine the FE time step so numerical errors are kept below 1% deviation from the exact solution. For this purpose, various time steps ranging from 1/9 to 1/90 of a wave period is examined hereafter. Simulation results are shown in Table 3.5. They demonstrate that a time step of Δt = T/36 provides sufficient numerical accuracy.

Table 3.5. Seabed responses around pipeline for various Δt while α=90°; n_p = 64; n_r = 12; n_l = n./a.; n_c = 5.

$T/\Delta t$	$\left\|\oint_S \frac{p}{p_o} ds\right\|$	Deviation from Benchmark Solution	$\left\|\oint_S \frac{\sigma'_x}{p_o} ds\right\|$	Deviation from Benchmark Solution	$\left\|\oint_S \frac{\sigma'_z}{p_o} ds\right\|$	Deviation from Benchmark Solution
9	3.621	% 3.18	0.189	% 0.53	0.749	% 0.13
18	3.700	% 1.07	0.190	% 0.00	0.749	% 0.13
36	3.739	% 0.03	0.190	% 0.00	0.749	% 0.13
54	3.741	% 0.03	0.190	% 0.00	0.749	% 0.13
72	3.737	% 0.08	0.190	% 0.00	0.748	% 0.27
90	3.740	% 0.00	0.190	% 0.00	0.750	% 0.00

In general, the numerical analysis has to be continued for several wave periods (cycles) to converge. The number of such cycles herein is represented by n_c. While n_c = 5 is considered as the benchmark solution, Table 3.6 lists a series of experiments, in which values of n_c between 1 to 5 have been tested. It is found that although in the first cycle of calculations the transient solution has not yet died out, from the second cycle onward a steady state solution with an error of no more than 1% will be reached. Therefore, numerical results throughout this thesis are extracted from the second cycle of the FE analysis.

Table 3.6. Seabed responses around pipeline for n_c while α=90°; n_p = 32; n_r = 8; n_l = n./a.; $\Delta t = T/36$.

n_c	$\left\|\oint_s \frac{p}{p_o} ds\right\|$	Deviation from Benchmark Solution	$\left\|\oint_s \frac{\sigma'_x}{p_o} ds\right\|$	Deviation from Benchmark Solution	$\left\|\oint_s \frac{\sigma'_z}{p_o} ds\right\|$	Deviation from Benchmark Solution
1	3.846	% 2.83	0.276	% 45.26	1.240	% 65.33
2	3.736	% 0.11	0.190	% 0.00	0.748	% 0.27
3	3.733	% 0.19	0.190	% 0.00	0.750	% 0.00
4	3.737	% 0.08	0.190	% 0.00	0.749	% 0.13
5	3.739	% 0.03	0.190	% 0.00	0.749	% 0.13

3.2 Validation of Numerical Model

3.2.1 Verification against an Analytical Solution

Since the three-dimensional Finite Element model developed in the present study is new, it is necessary to validate the present model before proceeding to apply it to the 3-D wave-soil-pipeline interaction problem. For this purpose, a possible option is to consider the simplified case of the wave-induced response of a seabed in the absence of a structure. The exact solution for the interaction between a progressive wave and the naked seabed has been proposed by Hsu and Jeng (1994). In their solution, the wave-associated pore pressure, effective and shear stresses in the seabed soil are expressed by:

$$\frac{p}{p_0} = \frac{1}{1-2\mu}\left\{(1-\lambda-2\mu)\left(C_2 e^{\kappa z} - C_4 e^{-\kappa z}\right) + (1-\mu)\left(\varsigma^2-\kappa^2\right)\left(C_5 e^{\varsigma z} + C_6 e^{-\varsigma z}\right)\right\} e^{i(\kappa x-\omega t)} \tag{3.1}$$

$$\begin{aligned}\frac{\sigma'_x}{p_0} = -\Bigg\{&\left[\left(C_1 + C_2\kappa z\right) + \frac{2\mu\lambda}{1-2\mu}C_2\right]e^{\kappa z} + \left[\left(C_3 + C_4\kappa z\right) - \frac{2\mu\lambda}{1-2\mu}C_4\right]e^{-\kappa z} \\ &+ \left[\kappa^2 - \frac{\left(\varsigma^2-\kappa^2\right)\mu}{1-2\mu}\right]\left(C_5 e^{\varsigma z} + C_6 e^{-\varsigma z}\right)\Bigg\} e^{i(\kappa x-\omega t)}\end{aligned} \tag{3.2}$$

$$\frac{\sigma'_z}{p_0}=\left\{\left[\left(C_1+C_2\kappa z\right)-\frac{2\lambda\left(1-\mu\right)}{1-2\mu}C_2\right]e^{\kappa z}+\left[\left(C_3+C_4\kappa z\right)+\frac{2\lambda\left(1-\mu\right)}{1-2\mu}C_4\right]e^{-\kappa z}+\frac{1}{1-2\mu}\left[\varsigma^2\left(1-\mu\right)-\kappa^2\mu\right]\left(C_5e^{\varsigma z}+C_6e^{-\varsigma z}\right)\right\}e^{i(\kappa x-\omega t)} \tag{3.3}$$

$$\frac{\tau_{xz}}{p_0}=i\left\{\left[C_1+\left(\kappa z-\lambda\right)C_2\right]e^{\kappa z}-\left[C_3+\left(\kappa z+\lambda\right)C_4\right]e^{-\kappa z}+\kappa\varsigma\left(C_5e^{\varsigma z}-C_6e^{-\varsigma z}\right)\right\}e^{i(\kappa x-\omega t)} \tag{3.4}$$

where, ς[4], λ and coefficients C_1 to C_6 can be obtained as functions of seabed and wave properties, as detailed in Hsu and Jeng (1994); and i^2=-1. It should be noted that the presented solution is for the case in which the seabed soil is not confined within a trench. Therefore, the numerical model should be modified so that the lateral trench wall boundary conditions in the x- direction presented in section 2.1.2 would be replaced by a periodic boundary condition, while the length of computational domain (w) is considered as one wave length. Variations of amplitudes of soil responses over the seabed depth (z), obtained from the present numerical model as well as the exact solution, are plotted in Figure 3.2 for a set of soil and wave properties. It is apparent that numerical results excellently coincide with those evaluated by equations (3.1)-(3.4).

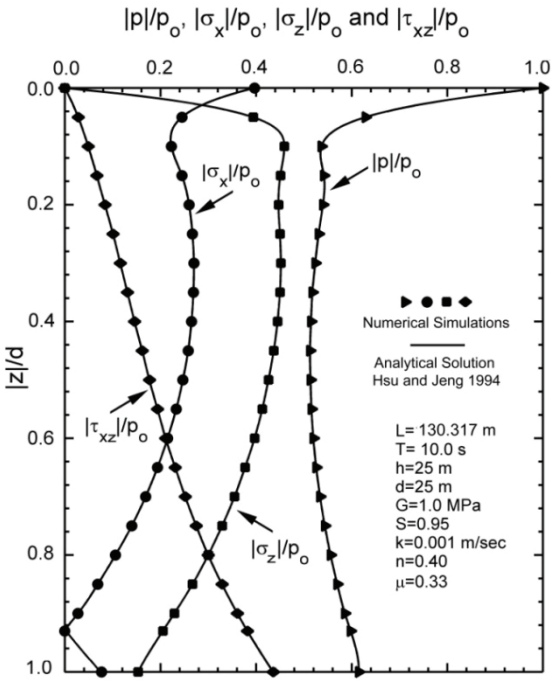

Figure 3.2. Verification of numerical simulations from the present model against the analytical solution of Hsu and Jeng (1994) for the wave-induced response of a seabed without a structure.

[4] The symbol ς is used instead of δ in the original publication.

3.2.2 Verification against Experimental Data

This is the numerical model developed to investigate the influence of wave angle of incidence on seabed responses near a submarine buried pipeline. Hence, it is essential to examine the performance of this model in a seabed with the presence of a pipeline. Although numerous investigations have applied the potential theory to derive an analytical solution for the problem of wave-seabed-pipe interaction, no exact solution using Biot consolidation theory is yet available in the literature even for a simplified two-dimensional case. On the other hand, to the author's knowledge no experimental investigation has been carried out to consider three-dimensional influences. Therefore, it may be beneficial to verify numerical results against experimental data for the seabed response around a pipeline under the action of waves propagating normal to the structure. Such a simplified two-dimensional case has been experimentally studied in Turcotte *et al*. (1984) and Sudhan *et al*. (2002), among others. Results presented in Sudhan *et al*. (2002) appear to be extremely scattered. Therefore, experimental data from Turcotte *et al*. (1984) is used herein to validate the numerical model.

Turcotte *et al*. (1984) carried out a series of seven tests in Joseph H. DeFrees Hydraulics Laboratory, Cornell University. Experiments covered a range of short to long waves with a constant water depth. Seabed bed materials also remained unchanged over tests. Experiments were performed in a 17 m long, 0.76 m wide wave tank, where a 0.168m PVC pipe was buried in trenched sand. Eight pore pressure transducers were instrumented around pipe circumference at every 45 degrees. The authors reported contours of pore pressure amplitudes in the vicinity of pipeline. Among the tested wave lengths, three cases representing short, intermediate and long waves have been adopted herein for the comparison between numerical and experimental data. Figures 3.3 to 3.5 show pore pressure amplitudes, corresponding to these three wave lengths, around the pipeline circumference. Soil, pipe and wave properties are also indicated on these figures.

It can be seen in Figures 3.3 to 3.5 that a very good agreement is obtained between numerical simulations and experimental data. Such an agreement becomes more significant, when waves are longer. However, experimental results from the pore pressure probe instrumented at $\theta = 135°$ around the pipe perimeter is found not to comply with the general trend of data in Figures 3.4 and 3.5. However, no information on possible deficiencies of this pore pressure transducer was reported in Turcotte *et al*. (1984). Figure 3.3 also presents a comparison between numerical results obtained from the present study and those from the Finite Element model of Lin and Jeng (2000). The present model outperforms the FEM analysis of Lin and Jeng (2000) specially in the lower half of the pipeline, that is $\theta = 180°$-$360°$. It is worthy to note that the work by Lin and Jeng (2000), however, considered the case of a submarine pipeline being buried in the seabed without the presence of a trench.

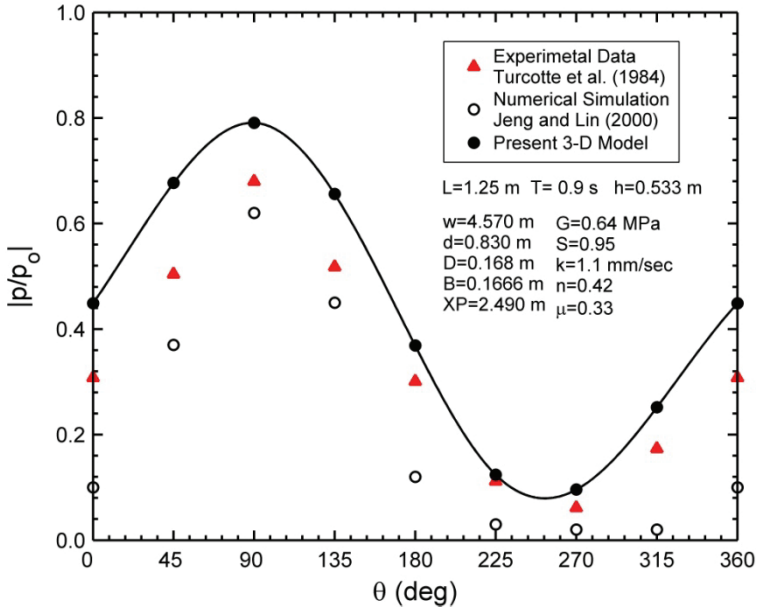

Figure 3.3. Verification of numerical simulations from the present model against experimental data in Turcotte *et al*. (1984) for short wave lengths.

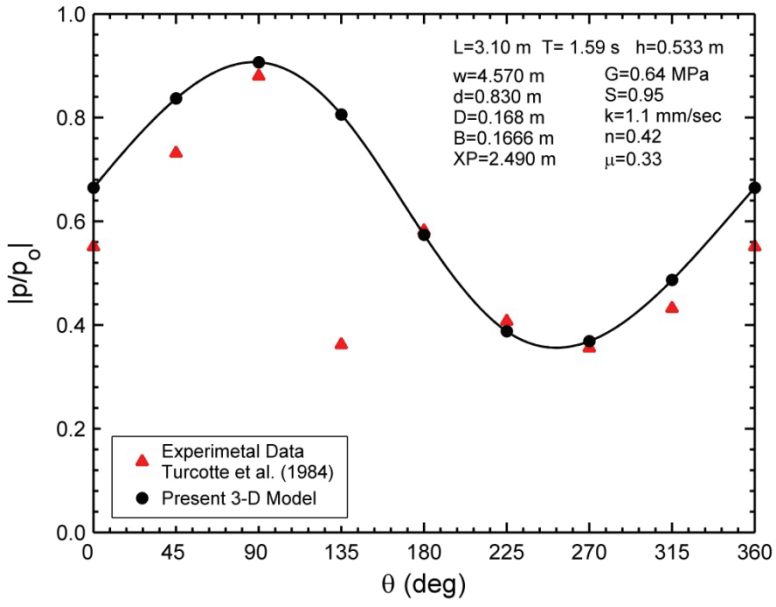

Figure 3.4. Verification of numerical simulations from the present model against experimental data in Turcotte *et al*. (1984) for intermediate wave lengths.

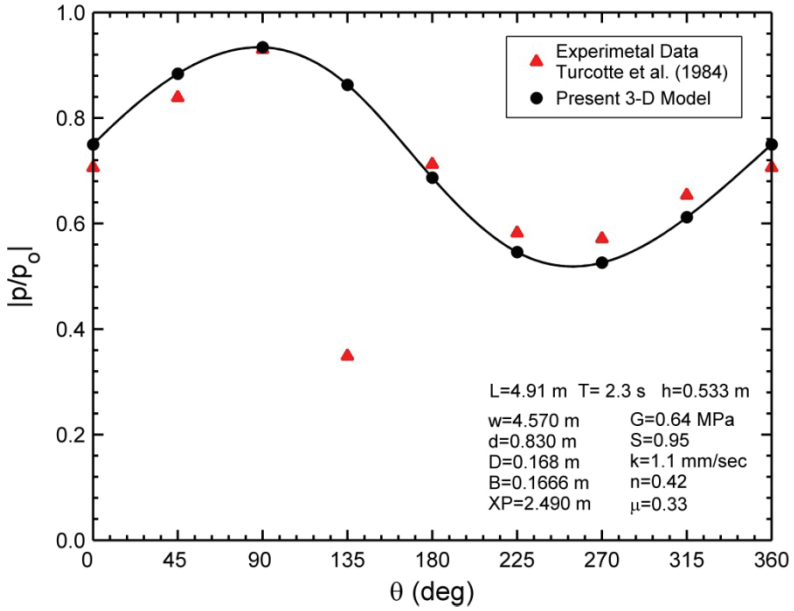

Figure 3.5. Verification of numerical simulations from the present model against experimental data in Turcotte *et al*. (1984) for long wave lengths.

3.3 Summary

Details of the Finite Element Model applied to simulate wave-soil-pipe interaction are presented in this chapter. Numerical experiments to justify the minimum required mesh resolution are performed. Further, the desired temporal discretization of time dependant FEA is examined. This was followed by a series of tests to validate the proposed numerical model. This included the verification of numerical results against an available analytical solution for the case of wave-induced seabed responses in the absence of a structure, as well as the comparison between numerical results and data from wave tank experiments of Cornell University. The latter covers the two-dimensional case of wave-seabed-pipeline interaction with waves approaching normal to the pipeline orientation. In both cases, excellent agreement was achieved. It was also found that the numerical model matches the experimental data better, when water waves are longer. The present three-dimensional model was also compared with an existing two-dimensional model. The 2-D model was found to be outperformed by the current model. In the next chapter, the proposed model will be used for a thorough parametric study on wave-induced seabed behaviour around pipelines, including the three-dimensional effects.

Chapter 4

WAVE-INDUCED SEABED BEHAVIOUR AROUND A TRENCHED PIPELINE

The three-dimensional numerical model, previously developed in the third chapter, is used in this chapter to study the wave-associated seabed behaviour in the presence of a submarine pipeline. The investigation, in this regard, is conducted under two major subheadings: a. seabed responses and b. seabed instabilities around the pipeline circumference. Under the former, the significance of three-dimensional effects on wave-induced seabed responses, i.e. pore pressure and soil stresses, will be determined. Of particular importance, it will be revealed that the wave direction, despite the traditional belief, considerably affects seabed stresses. This will be then followed by a detailed parametric study to address influences of soil, wave and geometrical properties on soil responses. Such parametric investigation also provides grounds for the next section, over which the wave-associated seabed liquefaction and soil shear failure will be discussed.

It is also crucial to investigate the mechanisms involved in the failure of marine pipelines, as environmental, economical, and even political consequences of such a catastrophe are significant. At the same time, it has been well understood that the failure of many coastal structures, including submarine buried pipelines, mainly stems back into seabed soil instabilities, rather than into construction deficiencies (Jeng, 1997b). Therefore, it is essential to use the present three-dimensional numerical model to also study potentials of soil instabilities in the vicinity of a pipeline. There are two modes of soil instability: liquefaction and shear failure, which are respectively linked to the wave-induced excess pore pressure and the soil stress angle. The second main heading in this chapter, therefore, is devoted to studying the aforementioned mechanisms. This will be started by a review of available theories on two soil-instability mechanisms. Further, a thorough parametric study will be carried out on the influences of three-dimensionalities, soil properties, trench/pipe geometries, and wave characteristics on the potential of such instabilities near the pipeline. The parametric study will be conducted in the same manner as that on studying wave-associated seabed responses.

4.1 Wave-Associated Seabed Responses

4.1.1 Principal Effective Stresses and the Maximum Shear Stress

It is the interest of coastal geotechnical engineers to study soil stresses around a submarine buried pipeline. The fact that soil stresses are dependant to the coordinate system, in which they are expressed, however, necessitates an agreement on the desired coordinate system for the expression of soil stresses prior to any parametric study. At the same time, it is worthy to note that a part of the parametric study in this chapter is to investigate effects of wave direction on soil stresses. Now, let us consider a coordinate system such as *xyz*, which is fixed with respect to the seabed domain and was introduced in the second chapter. Clearly, it is not suitable to express soil stresses in the *xyz* system for the purpose of studying the influence of wave direction. To clarify this, let us consider a naked seabed without the presence of a pipeline. It is easy to recognize that a comparison between *xyz* stresses at various wave directions is in fact the basic problem of rotation of a stress tensor, whose solution may be found in any classic textbook of mechanics of materials. In the presence of a pipeline, therefore, the expression of stresses in a system such as *xyz* will not reveal the pure nature of how the wave direction affects seabed stresses. Instead, it becomes a confusing mixture of rotation of stress tensors and other possible influences of wave direction. As an alternative, it is beneficial to take advantage of studying wave-induced soil principal stresses instead of stresses in the *xyz* system. Meanwhile, the fact that a major principal stress is the maximum normal stress that the soil undergoes in a specific state of stress makes the use of principal stresses more appealing to design engineers.

The mathematical expression for the extraction of principal stresses out of those expressed in the *xyz* system can be found in textbooks of mechanics of materials, such as in Solecki and Conant (2003). Hereafter, a brief description on the issue is presented, for the sake of complicity. Meanwhile, this introductory note may become useful in the next sections, where seabed instabilities due to the soil shear failure are addressed. A subroutine also has been implemented within WSPI-3D to extract principal stresses out of raw numerical results. The concept of rotation of a stress tensor and the definition that a principal stress is a normal stress in a plane, on which shear stresses are zero, leads to:

$$\begin{bmatrix} \sigma'_x - \sigma'_n & \tau_{xy} & \tau_{xz} \\ \tau_{xy} & \sigma'_y - \sigma'_n & \tau_{yz} \\ \tau_{xz} & \tau_{yz} & \sigma'_z - \sigma'_n \end{bmatrix} \vec{n} = \begin{bmatrix} 0 \\ 0 \\ 0 \end{bmatrix} \tag{4.1}$$

in which, $\vec{n}$ is the unit vector normal to the principal plane; and σ'_n is the principal effective stress acting along the $\vec{n}$ direction and on the plane normal to $\vec{n}$. This system of linear algebraic equations possesses a nonzero solution, i.e. $\vec{n}$, only if the determinant of the matrix formed from coefficients of unknowns is zero. Applying this concept leads to the so-called *characteristic equation* of stresses:

$$\sigma'^{3}_n - I_1 \sigma'^{2}_n + I_2 \sigma'_n - I_3 = 0 \tag{4.2}$$

where, I_1, I_2 and I_3 are *stress invariants*, being independent of the orientation of coordinate system, and are as:

$$I_1 = \sigma'_x + \sigma'_y + \sigma'_z \tag{4.3}$$

$$I_2 = -\tau^2_{xy} - \tau^2_{yz} - \tau^2_{xz} + \sigma'_x\sigma'_y + \sigma'_y\sigma'_z + \sigma'_x\sigma'_z \tag{4.4}$$

$$I_3 = \sigma'_x\sigma'_y\sigma'_z - \sigma'_x\tau^2_{yz} - \sigma'_y\tau^2_{xz} - \sigma'_z\tau^2_{xy} + 2\tau_{xy}\tau_{yz}\tau_{xz} \tag{4.5}$$

Obtaining *xyz* stresses from equations (3.1)-(3.4) and consequently stress invariants from relations (4.3)-(4.5), principal stresses can be extracted by evaluating three roots of the cubic characteristic equation of stresses in (4.2). Let us sort the three principal effective stresses in a descending fashion and designate them by σ_{11}, σ_{22} and σ_{33}. The superscript (') has been omitted for the sake of simplicity. It should be mentioned that principal effective stresses act on the faces of a soil element, over which all shear stresses are zero.

For a given state of stress at a point located within the seabed, the maximum shear stress (τ_{max}) is another important type of soil response to be investigated. It is possible to get assistance from three-dimensional Mohr circles, in Figure 4.1, to obtain τ_{max}. In fact, the state of soil stresses for any arbitrary plane within a soil element (σ', τ) would fall at a point located within the shaded area confined by Mohr circles. Therefore, the radius of the greater Mohr circle represents the maximum shear stress that the soil undergoes at the specific location and moment corresponding to that state of stress. Knowing numerical values of soil principal stresses, the radius of the greater Mohr circle is as:

$$\tau_{\max} = R_{Mohr} = \frac{\sigma_{11} - \sigma_{33}}{2} \tag{4.6}$$

On the other hand, among principal stresses, it is the major principal effective stress (σ_{11}) that is of particular interest, since it will be the maximum normal effective stress that a soil element experiences, as is illustrated.

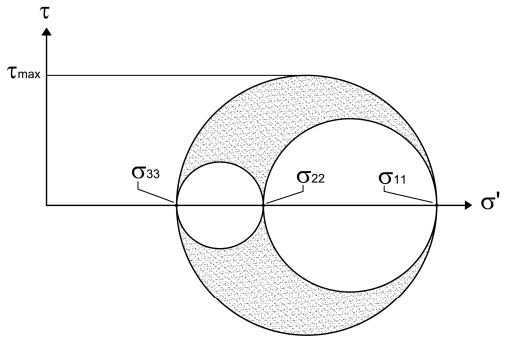

Figure 4.1. Definition sketch: three-dimensional Mohr circles.

4.1.1 Parametric Study

A parametric study is carried out in this section to investigate the influence of various parameters on the wave-induced soil responses, including pore pressure, major principal effective stress, and maximum shear stress around the pipeline circumference. The parametric study reveals effects of wave angle of incidence, soil properties, wave characteristics, and trench/pipe geometries on wave-associated seabed behaviour. It should be pointed out that this is for the first time that influences of wave direction are investigated. On the other hand, some early investigations had already studied the effects of soil and pipe properties. However, they had used a two-dimensional consolidation model. Consequently, it was only possible to study those effects while ocean waves were assumed to propagate normal to the orientation of the pipeline. In this study, however, influences of soil and pipe properties are addressed while waves are considered parallel with the pipeline. This approach, in conjunction with studying three-dimensional effects, provides a useful guide for practical engineering purposes.

Since the wave loading on any point of the seabed surface varies periodically with time, the soil responses also change over a wave period. However, it is the peak value of a soil response that is of importance in engineering applications. Therefore, the present parametric study will be concerned with amplitudes of wave-induced soil responses. In this regards, it is worthy to note that although fluctuations of not all soil responses are sinusoidal over a wave period as will be demonstrated later, the term *amplitude* is used in this text to refer to the peak value of a seabed response over a wave period. Hereafter, the amplitude of a fluctuating parameter such as R is denoted by $|R|$.

4.1.1.1 Influences of Ocean Wave Properties

Wave Obliquity

Inspired by the importance of studying the behaviour of submarine buried pipelines, numerous researches have been carried out in this area over the past thirty years. Almost all previous investigations, however, have been concerned about the interaction between pipe, soil and wave for a special case of ocean waves propagating normal to the pipeline. Nevertheless, waves in the real ocean environment approach the pipeline from any direction, forming an angle of incidence (α) with the orientation of pipeline. Furthermore, it is in shallow waters that the pipeline is buried within the seabed for protection against human activities. In this region, ocean waves also change direction due to the occurrence of wave refraction. Therefore, it is essential to investigate possible effects of wave direction on the seabed behaviour by using a three-dimensional model.

To date, two sets of studies may be found in the literature concerning the three-dimensional simulation of the response of a sandy bed around an underwater buried pipeline. In the first set of investigations, Lennon (1983) and Lennon (1985) applied a 3-D Boundary Integral Equation Method (BIEM) to evaluate the pore pressure distribution and seepage forces on the pipeline. His numerical results confirmed that the wave-

induced pore pressure on the bottom and sides of the pipeline are slightly affected by varying the wave angle of incidence. Consequently, it was concluded that for practical engineering problems, the use of a two-dimensional model is sufficient. Appling the potential pressure theory, however, this set of studies did not provide any information on the influence of wave direction on stresses within the seabed soil. Besides, the potential theory has now been found far away from realistically expressing the wave-induced seabed behaviour for most types of marine sediments. Finally, the author did not make an attempt to investigate seabed instabilities by using his three-dimensional BIEM model.

In a second study, Chen *et al*. (2005) recently simulated the three-dimensional consolidation of a seabed soil by using a Finite Element Model. Though applying Biot's consolidation theory, the authors surprisingly concluded that the wave direction does not affect the soil responses around the pipeline. In their study, however, only one set of soil/wave/pipe data have been used. At the same time, neither seabed liquefaction nor the soil shear failure was investigated. In the present section, a comprehensive study on the effects of wave direction and three-dimensionalities on the seabed response near the pipeline is carried out. Confirming the existence of three-dimensional effects, it will then proceed to the next sections, where the potential of seabed instabilities are also investigated. Meanwhile, since there is no available study in the literature, focusing on the special case of waves propagating parallel to the pipeline, such configuration has been adopted to be constantly used throughout the entire parametric study in this thesis.

Influences of wave obliquity on the seabed behaviour can be generally summarized within two frameworks:

A. Three-dimensional geometry-based influences

The schematic plan view of a 3-D wave-soil-pipe problem is sketched in Figure 4.2[5]. As depicted, oceans waves propagate along the positive X direction with an angle of α with pipeline orientation that is the y- axis. Using the linear wave theory, as in chapter 2, the temporal and spatial distribution of wave dynamic pressure on the seabed surface is expressed as:

$$p_{bed} = p_o \cos(\kappa X - \omega t) \tag{4.7}$$

in which, by applying the rotational transformation between X- and x- axis, i.e. $X = x\sin\alpha + y\cos\alpha$, one will have:

$$p_{bed} = p_o \cos(\kappa_x x + \kappa_y y - \omega t) \tag{4.8}$$

$$\kappa_x = \kappa\sin\alpha \quad \text{and} \quad \kappa_y = \kappa\cos\alpha \tag{4.9}$$

[5] This illustration is duplicated from the second chapter for easy reference.

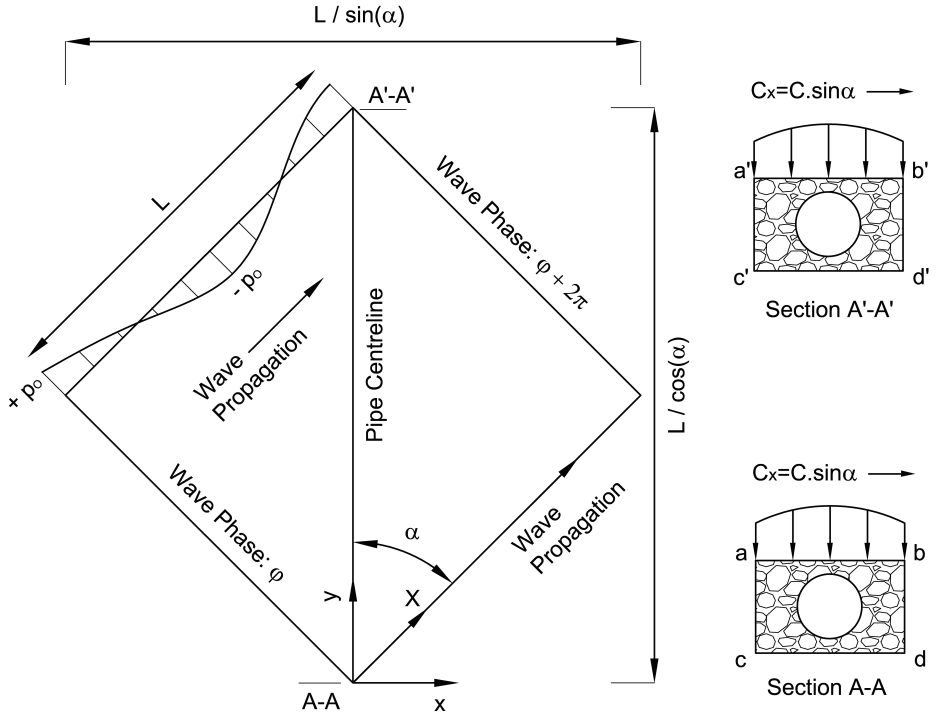

Figure 4.2. Definition sketch: Three-dimensional wave-seabed-pipeline interaction.

Under the dynamic pressure loading, expressed by equation (4.8), any two seabed soil elements respond identically to the wave loading, only if they are: (a) Located at the same depth; (b) Located at the same normal distance -*x*- from the pipe centreline (including the sign of *x*); and (c) Exposed to the same phase of dynamic wave pressure acting on the seabed surface above those elements. Consequently, seabed responses (*R*) in sections *A*-*A* and *A*′-*A*′ in Figure 4.2 are identical, provided that two sections are chosen *L*/cos α distant form each along the pipe centreline. That is:

$$R_{abcd} = R_{a'b'c'd'} \qquad \text{while} \qquad R = |R|\cos(\kappa_x x + \kappa_y y - \omega t + \varphi_{lag}) \tag{4.10}$$

The distribution of seabed response between sections *A*-*A* and *A*′-*A*′, along the *y* axis, therefore is periodic. To illustrate this, variations of pore pressure (p) and vertical normal effective stress (σ_z) over the pipeline span between *A*-*A* and *A*′-*A*′, are plotted in Figure 4.3 for a sample point on pipe perimeter (θ=135°). Note that the upper horizontal axis in Figure 4.3 shows the *y*- axis; the section *A*-*A* is represented by $\kappa_y y = 0$, while section *A*′-*A*′ is indicated by $\kappa_y y = 2\pi$ rad. At the same time, Figure 4.3, illustrates variations of p and σ_z for the same point on the pipe perimeter at the section *A*-*A*, but over a wave period, when the lower horizontal axis is considered. Such coincidence was evident beforehand, since the time required by the wave frontier to travel along *X* direction from *A*-*A* to *A*′-*A*′ is equal to the wave period (*T*).

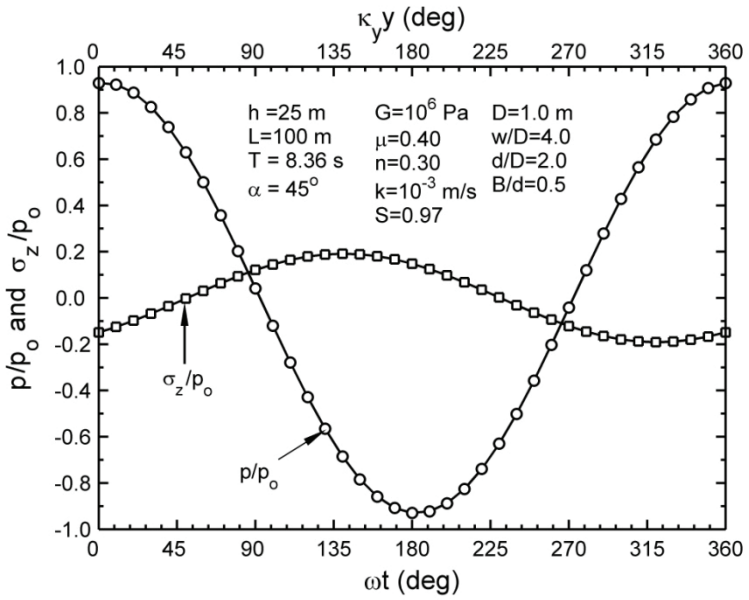

Figure 4.3. Variations of p and σ_z for a point located on the pipe circumference at θ=135° (a) over a pipeline span between *A*-*A* and *A'*-*A'*, when $t=T$ (see upper horizontal axis: $\kappa_y y$), (b) in section *A*-*A*, over a wave period (see lower horizontal axis: ωt).

With an analogy to the previous discussion, variations of wave-induced principal effective soil stresses both over the pipeline span along the *y*- axis, as well as over a wave period, are plotted in Figure 4.4. Similarly, it is evident that principal stresses will also show a periodic behaviour temporally and spatially. However, contrary to those of p, σ_x, σ_y and σ_z, such a periodic manner does not follow a linear sinusoidal pattern for principal stresses. This seemingly irregular behaviour stems back to the fact that principal stresses at different locations or at different times will occur on different planes of a soil element. Consequently, these stresses are not constrained to follow a harmonic sinusoidal pattern, as is shown in Figure 4.4. Snapshots of three-dimensional Mohr circles are also illustrated on the figure. The radius of greater Mohr circle at any point indicates the maximum wave-induced shear stress (τ_{max}). It is interesting to note how the radius of the greater Mohr circle varies over t or y. It is important to note that that the periodic distribution of shear stress is also not sinusoidal, as for instance a Mohr's circle with a radius of zero is not observed at any point/time, for the presented case.

B. Influences of three-dimensionalities on amplitudes of soil responses

In this study, the maximum positive value of wave-induced major principal stress (σ_{11}) is referred to as the *Amplitude of major principal stress* $|\sigma_{11}|$. The idea behind this is that the non-cohesive seabed soil is vulnerable to tensile (positive normal) stresses. The use of term *Amplitude*, however, is misleading, since neither temporal nor spatial variations of principal stresses are sinusoidal. Nevertheless, using this term is inspired by an analogy to sinusoidal behaviour of the x, y and z stresses. A similar idea is used to define the

term *Amplitude* for the maximum shear stress. On the other hand, the immediate *geometry-based influence of wave direction* – as demonstrated in the previous section – is that by varying α from 0° (waves parallel with the pipeline) to 90° (waves normal to the pipeline), the long-trench wave length[6] ($L/\cos\alpha$) changes from L to infinity. It is, therefore, evident that any change in the wave direction shortens or lengthens the pipeline span, over which seabed responses vary periodically. The influence of wave direction, however, does not remain limited to this change in the distribution pattern of soil responses. In fact, the variation in the length of long-trench pipeline spans results in the long-trench gradient of both wave-loading and seabed responses to be monotonically decreasing towards zero, when waves tend to propagate normal to the pipeline ($\alpha \rightarrow 90°$). This, in turn, could further change the soil behaviour under loading and influence amplitudes of seabed responses.

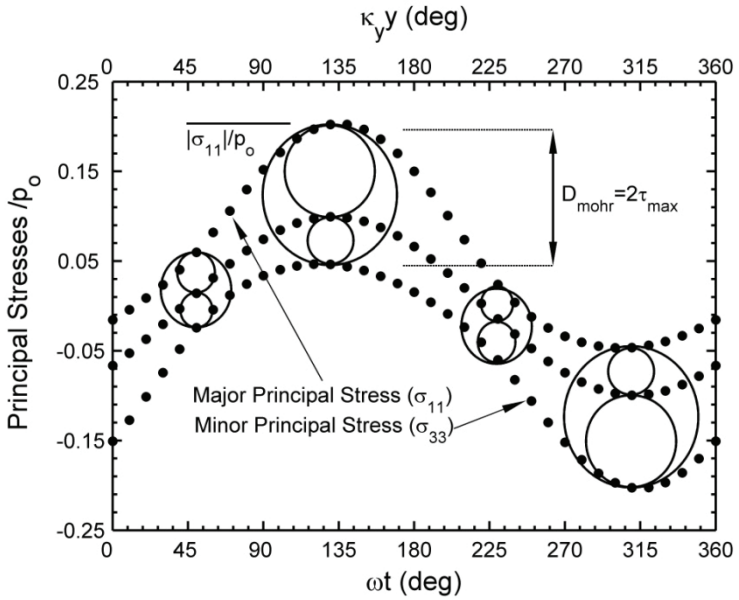

Figure 4.4. Variations of wave-induced principal effective stresses for a point located on the pipe circumference at θ=135° (a) over a pipeline span between *A*-*A* and *A'*-*A'*, when *t*=*T* (see upper horizontal axis: $\kappa_y y$), (b) in section *A*-*A*, over a wave period (see lower horizontal axis: ωt).

Variations of pore pressure, principal stress and shear stress in a three-dimensional wave-soil-pipe system were discussed in detail in the preceding section. Such patterns can be readily concluded based on the geometry of wave loading, without the need to perform numerical simulations. An investigation on the effect of wave direction on the amplitudes of a soil response, however, requires using the outcome of numerical simulations. Before proceeding to this issue, nevertheless, it is essential to introduce some basic definitions. As depicted in Figure 4.5, the circumference of the pipeline is divided into four regions: (a) Upper Part, $0° < \theta < 180°$, (b) Lower Part, $180° < \theta < 360°$, (c) Naked Side, $90° < \theta < 270°$ and (d) Sheltered Side, $270° < \theta <$

[6] See Figure 4.2

(360°) + 90°. Among these, the naked and sheltered sides are characterized based on the direction of the cross-trench component of wave celerity (C_x). According to the definition, the sheltered and naked sides of the pipe circumference are exchangeable when waves are propagating parallel to the length of the pipeline (α=0), since C_x=0.

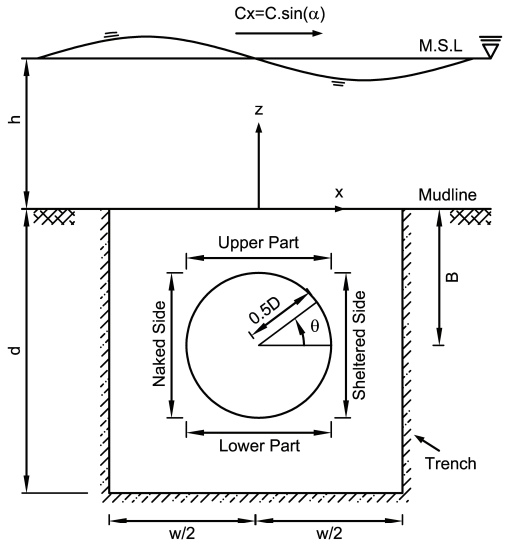

Figure 4.5. Cross-section of the pipeline: definition sketch of different regions around the pipe circumference.

To investigate the effect of wave direction, five wave angles of incidence α = 0°, 22.5°, 45°, 67.5° and 90° are adopted in this study. Such a combination has been considered and examined over a wide range of the soil, wave and pipe properties. However, the three-dimensional behaviour was found to be of similar nature for much of soil, wave and pipe properties, investigated here. Therefore, the numerical results solely corresponding to one set of soil/wave/trench data are presented in this section. Meanwhile, for the sake of legibility of the plots, only seabed responses corresponding to α = 0°, 45° and 90° are plotted hereafter, as results that are extracted from α = 22.5° and 67.5° are found to fall well between those of their corresponding upper and lower limits.

Figure 4.6 illustrates the effect of wave direction on the distribution of the amplitude of major principal stress around the pipeline. It is evident that for ocean waves propagating along the pipeline (α=0°), the distribution of seabed response is symmetric between the sheltered and naked sides. In other words, θ = 90° for the upper part and θ = 270° for the lower part of pipe circumference are the two axes of symmetry in the presented graph. Such a pattern is the direct result of the sheltered and naked sides being exchangeable with respect to the wave setup. The symmetry, however, does not hold when α deviates from zero. At the same time, the principal stress monotonically varies by increasing such deviation, i.e. the stress uniformly increases

or decreases as α increases. This asymmetric monotonic behaviour gives birth to a number of nodes, about which the direction of such monotonic trend is inverted. These so-called *inversion nodes* are marked by numbers 1 to 6 on the figure. Although the number and locations of these nodes may not be directly linked to the four previously-defined regions around the pipeline, the existence of such points stems from the asymmetry between the sheltered and naked sides. Besides, the monotonic nature of stress variations against α may be linked to the monotonic increase of the cross-trench component of wave celerity (C_x) as α increases. It is interesting to know that the asymmetry in distribution of soil response around the pipeline was indirectly reported in the two-dimensional numerical results of Cheng and Liu (1986), which considered the simple case of α=90. However, the occurrence of inversion nodes is for the first time being reported in the literature. Finally, it may be of interest to design engineers that the maximum principal stress, ever experienced around a pipeline for α = 90° is only about 4.5% larger than that for α = 0°, as illustrated.

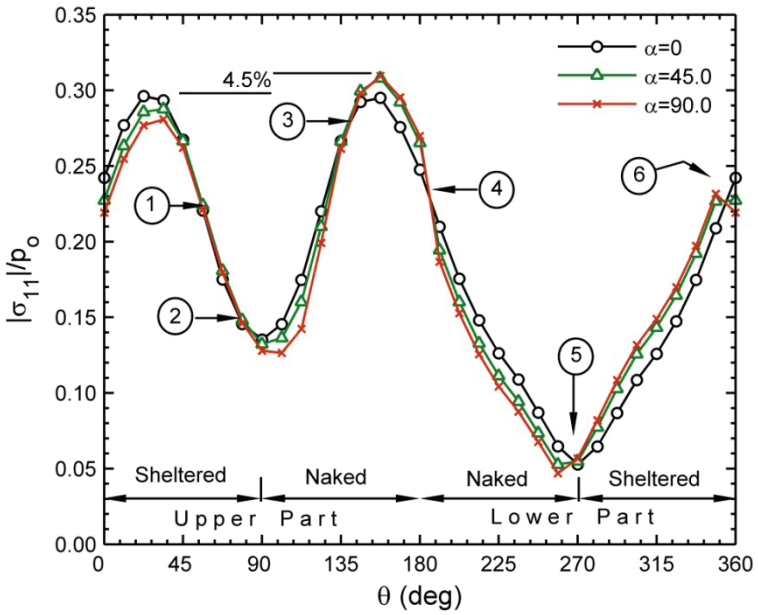

Figure 4.6. The distribution of amplitude of wave-induced major principal stress ($|\sigma_{11}|/p_o$) around pipe circumference for various wave angles of incidence (soil/wave/pipe properties are: h=12.07 m, T=10 s, L=100 m, G=10^6 Pa, μ=0.4, n=0.3, k=10^{-3} m/s, S=0.97, D=1.0 m, w/D=4.0, d/D=2.0 and B/d=0.5).

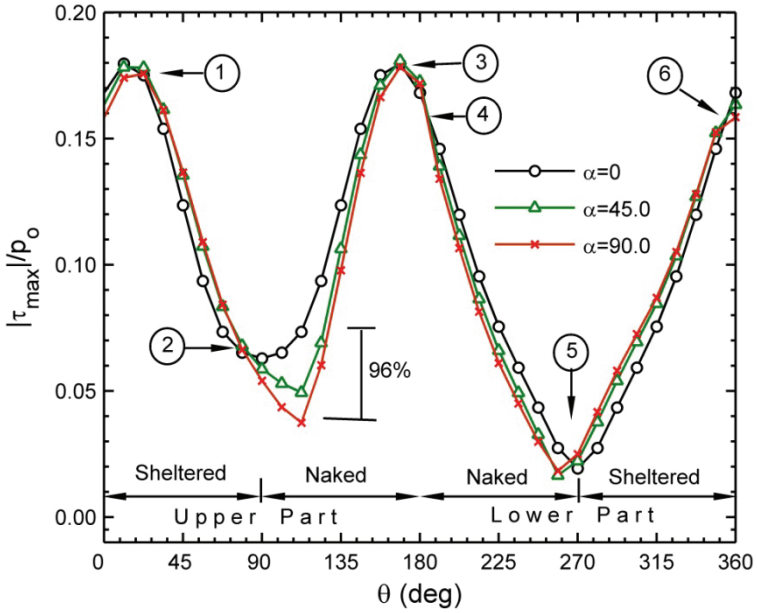

Figure 4.7. The distribution of amplitude of wave-induced maximum shear stress ($|\tau_{max}|/p_o$) around pipe circumference for various wave angles of incidence (see input data in Figure 4.6).

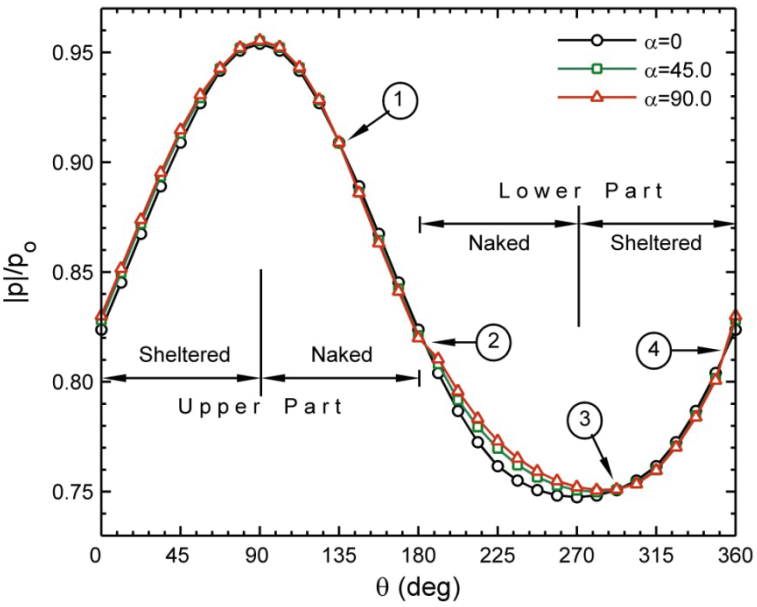

Figure 4.8. The distribution of amplitude of wave-induced pore pressure ($|p|/p_o$) around pipe circumference for various wave angles of incidence (see input data in Figure 4.6).

Similarly, the influence of wave angle of incidence on the amplitude of maximum shear stress, $|\tau_{max}|/p_o$, is plotted in Figure 4.7. The shear stress follows the same trend as does the major principal stress, with 6 inversion nodes being observed and the shear stress varying monotonically with the wave angle of incidence. Herein, however, the influence of wave direction is more significant in this case, so the shear stress varies up to 96% as α changes from 0° to 90°. The peak $|\tau_{max}|/p_o$ ever experienced around a pipeline remains almost unchanged for all wave directions. Nevertheless, it is extremely important to note that this issue is of little value for design engineering purposes. This is because the potential for shear failure is linked to the *ratio* of total shear stress to the normal effective stress, according to the Mohr-Coulomb failure criterion. Thus, a change in the shear or normal stress, due to the effect of wave direction, at any point around a pipeline would affect the potential of pipeline instability. Influences of α on soil instabilities will be thoroughly studied in coming sections.

As Figure 4.8 shows, four inversion nodes are observed in the pore pressure distribution around a pipeline. However, influences of three-dimensionalities on the distribution of pore pressure may be considered as negligible. Regarding the pore pressure, it is observed in all cases examined in this study that the naked bottom region of the pipe circumference, $180° < \theta < 270°$ is more likely to be affected by the wave direction.

Wave Period

Real fluctuations of the ocean surface usually have irregular and complex spatial and temporal distribution patterns. The seabed response to this irregular water surface and thus the pressure fluctuations, however, can be expressed by the superposition of seabed responses to multiple sinusoidal waves as in Liu and Jeng (2007) and Jeng (2008). The period of such a sinusoidal pattern is one of the most important mechanical properties of a wave event. Among waves of the same length, low frequency waves (longer periods) will correspond to wave events of shallower water depths, according to the linear wave theory:

$$L = \frac{gT^2}{2\pi}\tanh(\frac{2\pi h}{L}) \tag{4.11}$$

Therefore, while keeping the wave length constant, the amplitude of mudline dynamic pressure generated by a low frequency wave is larger than that produced by a high frequency one, since:

$$p_\circ = \frac{\gamma_w H}{2\cos(\kappa h)} \text{ and } p_{bed} = p_\circ \cos(\kappa x - \omega t) \tag{4.12}$$

A change in p_o will influence seabed responses, as the amplitude of wave loading is directly proportional to responses of the seabed soil. However, this effect could be excluded, when studying the

influence of wave period, through normalizing seabed responses by the amplitude of mudline pressure (as $|p|/p_o$, $|\sigma|/p_o$, $|\tau|/p_o$). At this point, it may be mistakenly argued that a change in the wave period may only influence the period of seabed responses, but not their normalized amplitude. However, such an argument is valid only for an impermeable elastic bed, which represents a classic solid mechanics problem. In a porous seabed, however, the wave pressure on the mudline may not completely penetrate into the seabed if the loading is very "quick" Zen and Yamazaki (1990a). Therefore, a high frequency wave or the so-called "quick" loading is expected to generate a different seabed response compared with a low-frequency loading. To demonstrate this concept, Zen and Yamazaki (1990b) carried out a one-dimensional experimental study, where a column of sandy deposit was exposed to a periodically varying water pressure. The oscillation-induced pore pressure ratio (p/p_o) was measured in the deposit (filled circles in Figure 4.9) and was reported along with some other experimental data. An inspection into experimental results, shown below, demonstrates that the wave period significantly affects normalized amplitudes of oscillatory pore pressure within the bed. In the meanwhile, when the wave period is increased, its influences on the response of the deposit gradually fades away, seemingly because the wave loading is no longer "quick" compared to the time required by the sand to adapt to the loading.

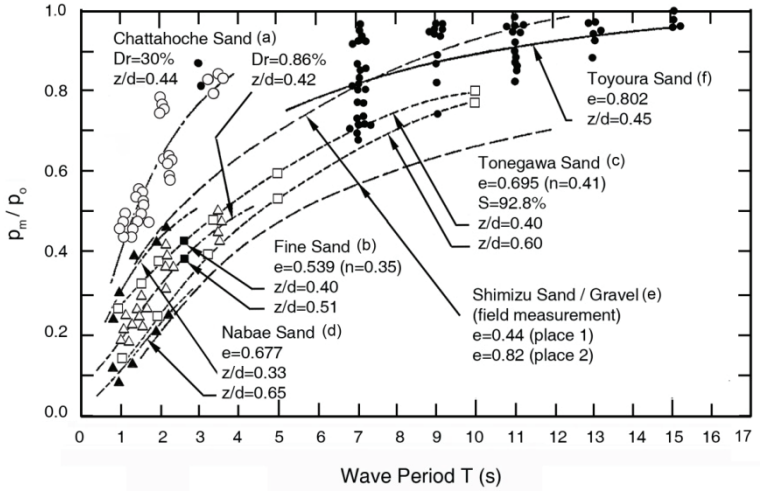

Figure 4.9. Pore pressure ratio against the period and oscillatory loading, after: (a) Tsui and Helfrich (1983), (b) Yamamoto (1977), (c) Inoue (1975), (d) Maeno and Hasegawa (1985), (e) Okusa *et al*. (1984) and (f) Zen and Yamazaki (1990b); and reproduced from Zen and Yamazaki (1990b).

A similar conclusion is drawn here by using the exact three-dimensional solution of wave-seabed interaction formulated by Hsu and Jeng (1994). As depicted in Figure 4.10, the non-dimensional wave-induced pore pressure amplitude ($|p|/p_o$) for various wave periods deviates from each other, when seabed depth is increased. This is perhaps because the deeper soil elements require a longer time to adapt to the loading. Thus, they are more likely to be affected by the influence of a "quick" loading. At the same time, the effect of so-called "quick" wave loading vanishes when longer wave periods are used, as the pressure profiles

from longer wave periods become closer to each other. This phenomenon is similar to what was observed in the experimental results of Zen and Yamazaki (1990b).

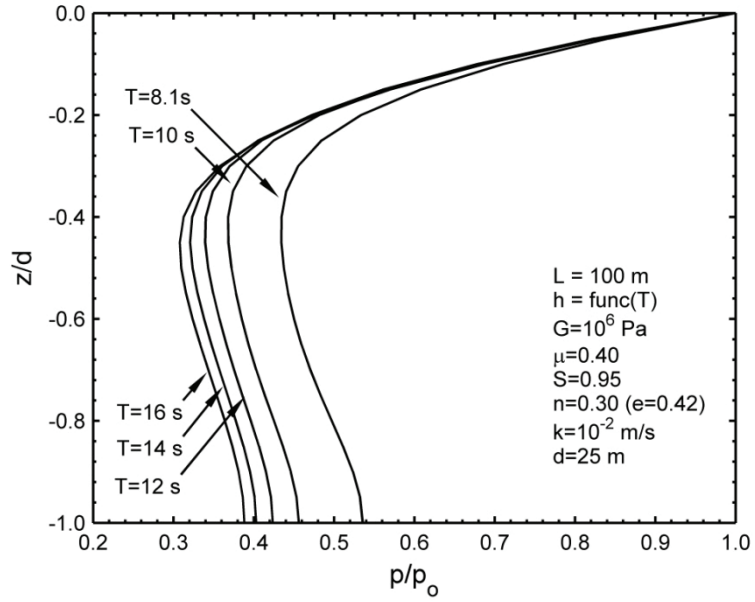

Figure 4.10. The distribution of normalized amplitude of pore pressure over the seabed depth based on the three-dimensional analytical solution of Hsu and Jeng (1994).

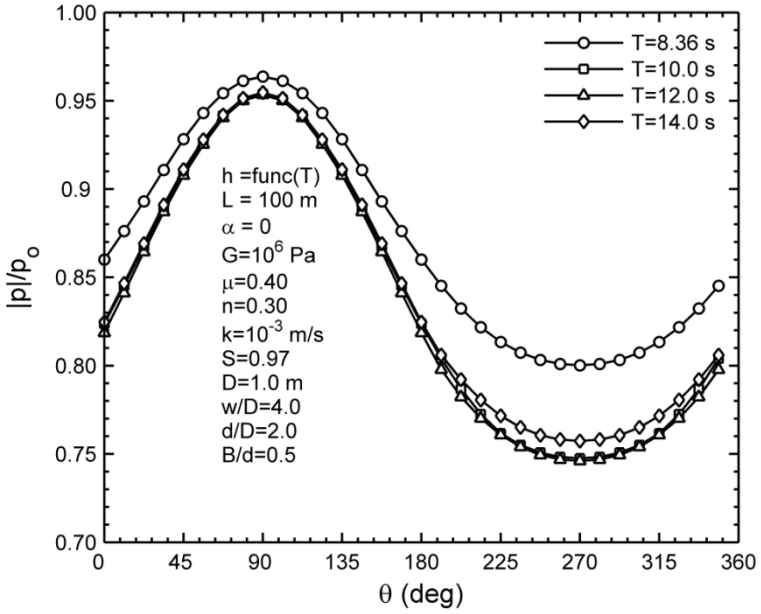

Figure 4.11. The distribution of $|p|/p_o$ around pipeline circumference for various wave periods.

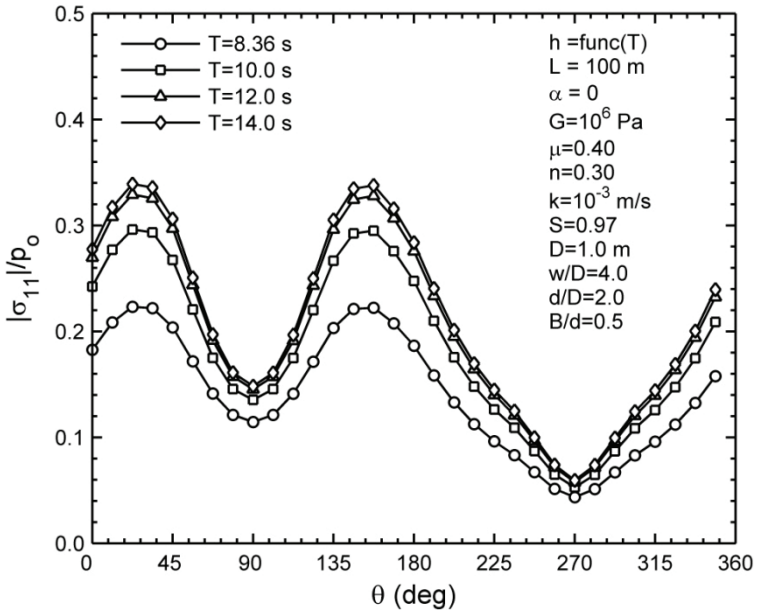

Figure 4.12. The distribution of $|\sigma_{11}|/p_o$ around pipeline circumference for wave periods.

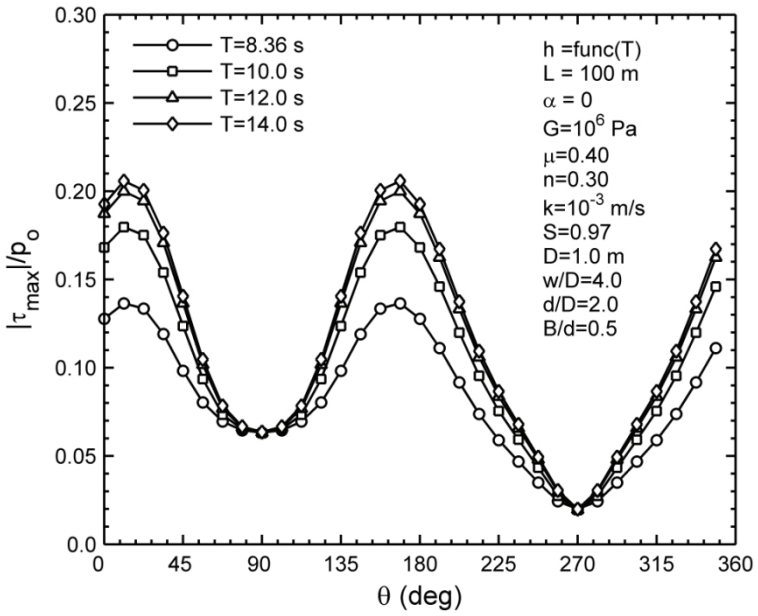

Figure 4.13. The distribution of $|\tau_{max}|/p_o$ around pipeline circumference for various wave periods.

Based on such strong indications of the importance of wave period, it is therefore beneficial to examine this effect on seabed responses around a pipeline circumference. Wave periods of T = 8.36s to 14s are chosen in this study to investigate the influence of wave period on seabed response. The normalized pore pressure amplitude, shown in Figure 4.11, stays less attenuated when T = 8.36 seconds, while the other periods show relatively close behaviour. However, the pore pressure around the pipeline is not found to vary monotonically with the wave period. Normalized principal effective and shear stresses increase monotonically while increasing T, as in Figure 4.12 and Figure 4.13. The increment of such an increase becomes smaller in longer wave periods. With the analogy to the earlier discussion, this phenomenon can be linked to the effect of so-called quick loading gradually fading away, as the wave period increases.

Water Depth

As a wave travels ashore, its mechanical properties change due to the wave dispersion. At the same time, according to the linear wave theory and while the wave period remains unchanged, the mudline dynamic pressure increases in shallower waters. The influence of water depth on the amplitude of wave loading, however, can be excluded from the parametric study through normalizing the wave-induced seabed responses by the amplitude of mudline pressure. However, as the wave enters shallower waters, the wave length also becomes shorter. This may consequently contribute to changes even in normalized seabed responses. To examine these effects, non-dimensional soil responses around the pipeline circumference were evaluated and plotted in Figure 4.14 to Figure 4.16 for a common range of water depths. Corresponding wave lengths are also indicated within the figures. It can be seen that the water depth does not influence the distribution pattern of normalized pore pressure and stresses near the structure. However, the non-dimensional amplitude of pore pressure increases unanimously when the water is deeper. Meanwhile, amplitudes of major principal and shear stresses act in a contrary manner to the behaviour of pore pressures. These responses will drop down monotonically as the water gets deeper. Influences of water depth, in fact, could be attributed to changes in wave length (L) that in turn results in the geometry of the mudline loading being affected. In other words, the horizontal pressure gradient ($\frac{1}{p_o}\frac{\partial p}{\partial X}$) between the wave trough and its crest increases as the wave length becomes shorter (i.e. in shallow waters). According to Darcy's law, the pressure gradient is responsible for the pore fluid flow though the porous bed from the region under the wave crest towards the region under its trough. Therefore, such pore fluid flow will be enhanced under the action of shorter waves (in shallow waters).

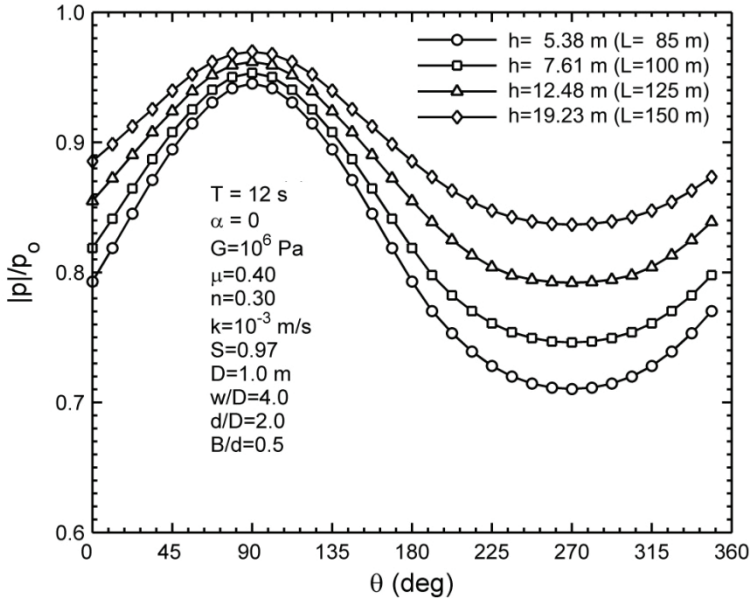

Figure 4.14. The distribution of $|p|/p_o$ around pipeline circumference for various water depths.

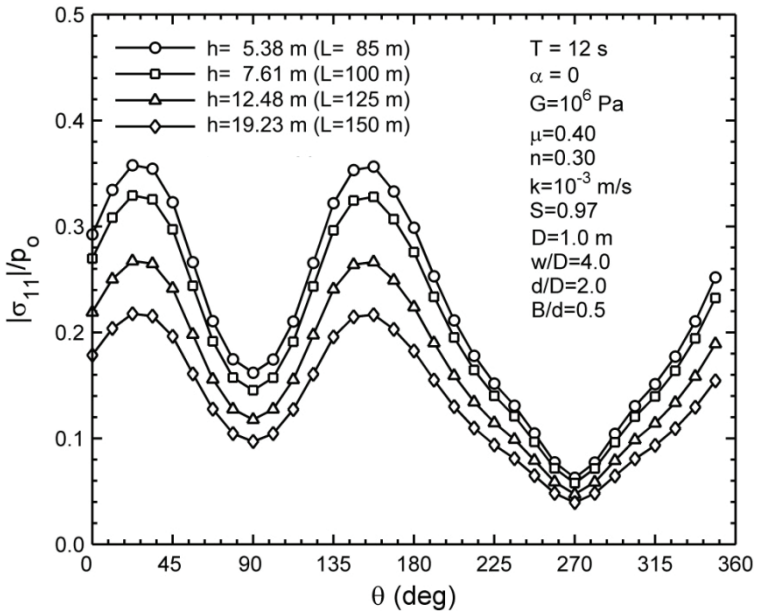

Figure 4.15. The distribution of $|\sigma_{11}|/p_o$ around pipeline circumference for water depths.

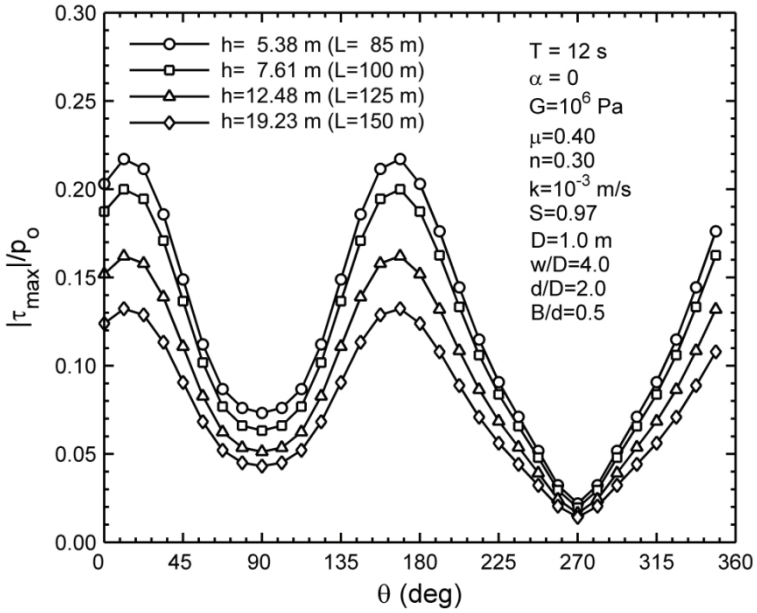

Figure 4.16. The distribution of $|\tau_{max}|/p_o$ around pipeline circumference for various water depths.

4.1.1.2 Influences of Seabed Soil Properties

Soil Shear Modulus

In general, the shear modulus (G) characterizes the stiffness of a sandy seabed. The influence of this parameter on seabed responses, however, had been absent from the early literature on wave-seabed-structure interaction, since the seabed behaviour was often expressed by the potential theory. As described in the first chapter, the use of the Laplace equation results in the behaviour of the pore fluid and solid soil phases decoupling from each other. Consequently, the wave-associated pore pressure obtained from the potential theory becomes independent of soil mechanical properties such as shear stiffness. Later, however, the pioneering work of Yamamoto *et al*. (1978), who applied a quasi-static soil consolidation model, revealed that the assumption of the independency of seabed responses from G may be acceptable only when the sandy bed is of fully-saturated loosely-packed nature so that $G/K' \rightarrow 0$. Nevertheless, even such conclusion has also been proven to be incorrect for seabeds of finite depth. In fact, the analytical solution of Jeng (1997b) revealed that the response of a finite-thickness seabed is always influenced by the shear stiffness, regardless of the degree of saturation. Jeng and Hsu (1996) reported that the extent of influence of G, however, is variable and depends on the degree of saturation and the permeability of seabed material. A similar conclusion as that in Jeng (1997b) is true for the present problem of wave-seabed-pipeline interaction. This is because the seabed is considered to be buried within a trench, in which both bottom and lateral walls are impermeable. It is believed that even in the absence of a trench, the existence of the pipeline itself would play the same role in letting the soil response be influenced by G even when the seabed soil is fully-saturated

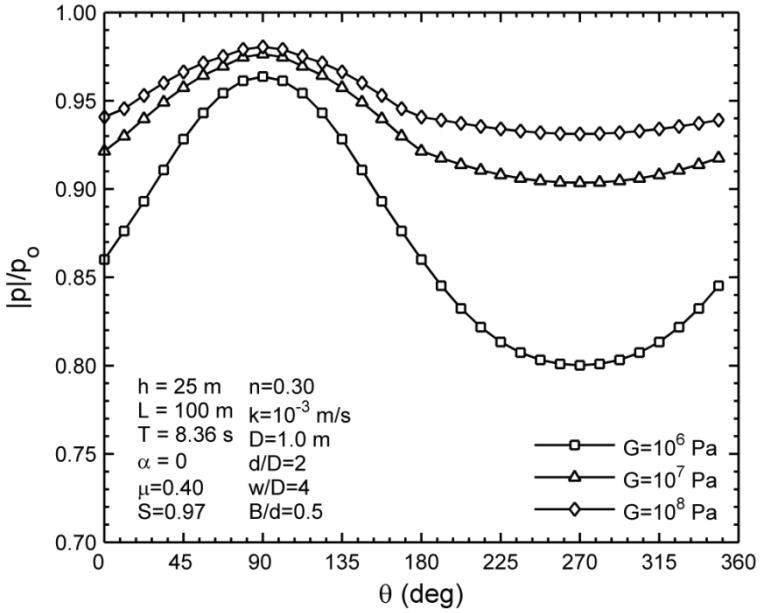

Figure 4.17. The distribution of $|p|/p_o$ around pipeline circumference for various G.

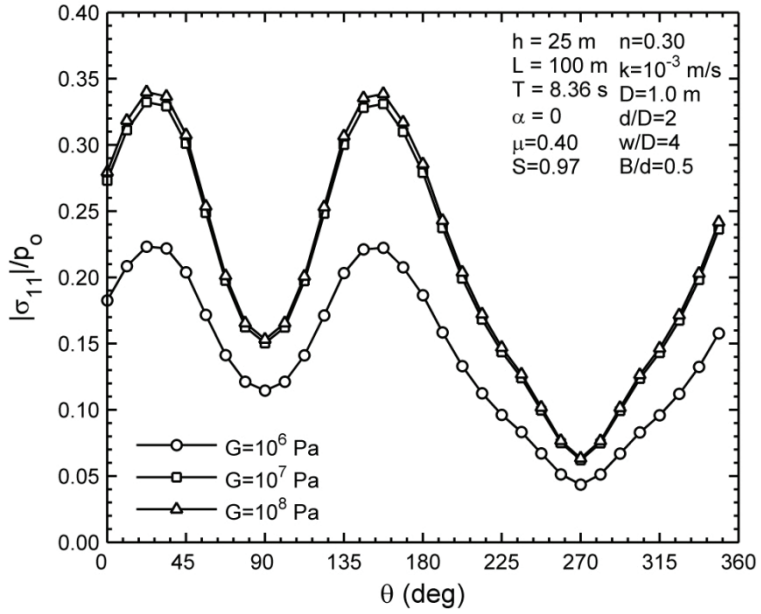

Figure 4.18. The distribution of $|\sigma_{11}|/p_o$ around pipeline circumference for various G.

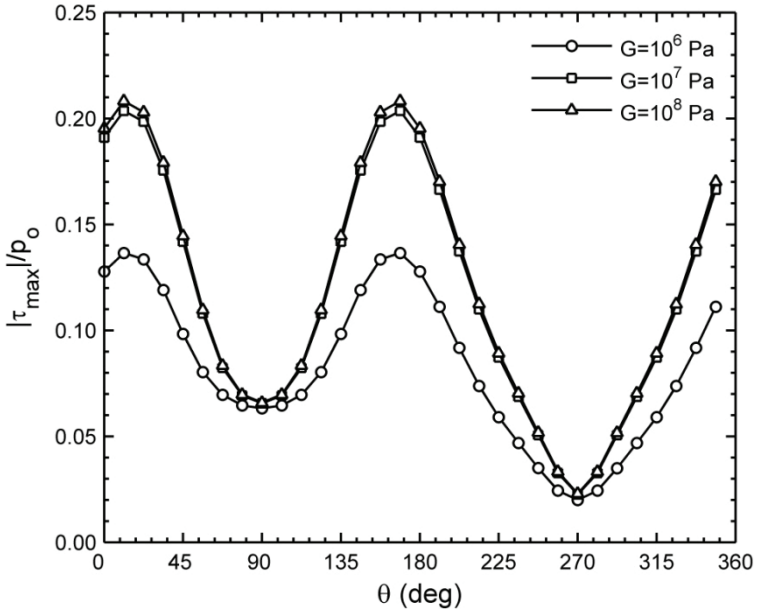

Figure 4.19. The distribution of $|\tau_{max}|/p_o$ around pipeline for various G (input data are as in Figure 4.18)

Most marine sediments are found to have a shear modulus ranging from 4.8×10^5 Pa to 4.8×10^8 Pa. The lower limit corresponds to silty and clayey sediments, while the upper one belongs to very dense sands such as sandstone. Wave-associated seabed responses around a pipeline are evaluated for several values of G over this range and are shown in Figure 4.17 to Figure 4.19. The pattern of distribution of responses around the pipeline, again, is found to be independent of soil stiffness. However, amplitudes of pore pressure, principal effective and shear stresses are found to be larger in dense soils. Soil stresses, at the same time, are almost identical for $G = 10^7$ and 10^8 Pa. This can suggest that the effect of shear stiffness on soil stresses vanishes when the $G > 10^7$.

Soil Permeability

Materials that are found in nature encompass a wide range of permeabilities (k) from 10^{-10} m/s to 10^2 m/s. Among them, a porous medium of the permeability of $k \leq 10^{-6}$ m/s is classified as impervious, while a material of permeability of $k \geq 10^{-1}$ m/s is considered as pervious (see Bear, 1972). Marine sediments, however, fall within an intermediate range of permeability between 10^{-6} and 10^{-1}, and mainly cover a semi-pervious region. The permeability of common marine sediments is listed in Table 4.1. In this range, the silt, clay and other poorly-permeable sediments can provide an undrained situation within the seabed. Therefore, it is likely for the phenomenon of pore pressure accumulation to dominate the wave-induced seabed response of these soils. This subject is not covered by the present study; rather, the current research is concerned with wave-induced momentary soil responses, where no pore pressure built-up would be observed in marine sediments. The momentary seabed behaviour is expected to dominate the behaviour of seabed soils with a

permeability ranging from 10^{-1} m/s (gravel) to 10^{-4} m/s (fine sand). Therefore, values of permeability adopted for the parametric study are selected from this range.

Table 4.1. Permeability of marine sediments.

Impervious		Semi Pervious				Pervious	
	Marine Sediments						
$<10^{-6}$ m/s	10^{-6} m/s	10^{-5} m/s	10^{-4} m/s	10^{-3} m/s	10^{-2} m/s	10^{-1} m/s	$>10^{-1}$ m/s
	Clay, Silt and Very Fine Sand		Fine Sand	Sand	Coarse Sand	Gravel	

As illustrated in Figure 4.20 to Figure 4.22, the pore pressure and soil stresses vary considerably by changing k, while their distribution maintains its pattern. On one hand, the gravel and the coarse sand are found to behave almost similarly, showing small values of soil stresses and a slight attenuation of pore pressure near the pipeline. The close behaviour of gravel and coarse sand may be linked to the fact that in these highly-permeable materials, the characteristic time that the soil requires to adapt to the wave loading is quite small. Therefore, the chosen wave period becomes large compared to the soil characteristic response time. Consequently, the adopted wave loading may no longer be "quick" for those types of soil. This in turn results in the responses of these soils being less influenced by the permeability.

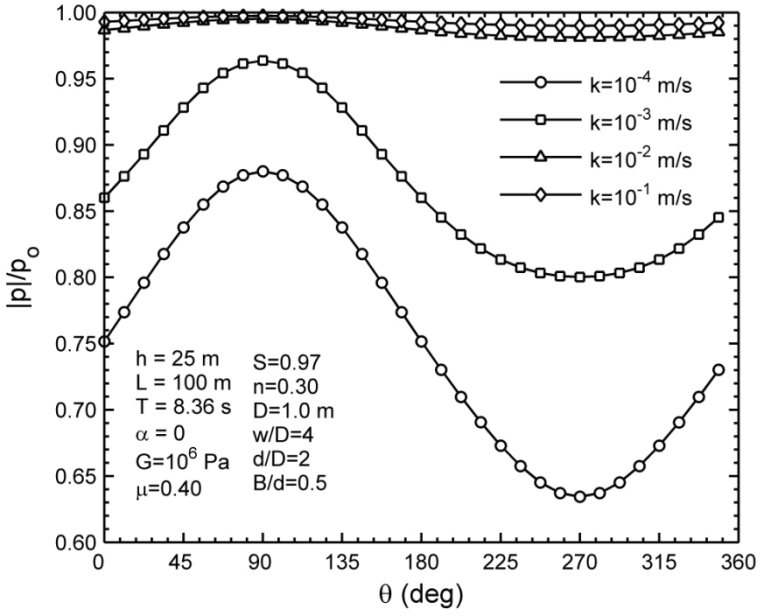

Figure 4.20. Distribution of $|p|/p_o$ around pipeline circumference for various k.

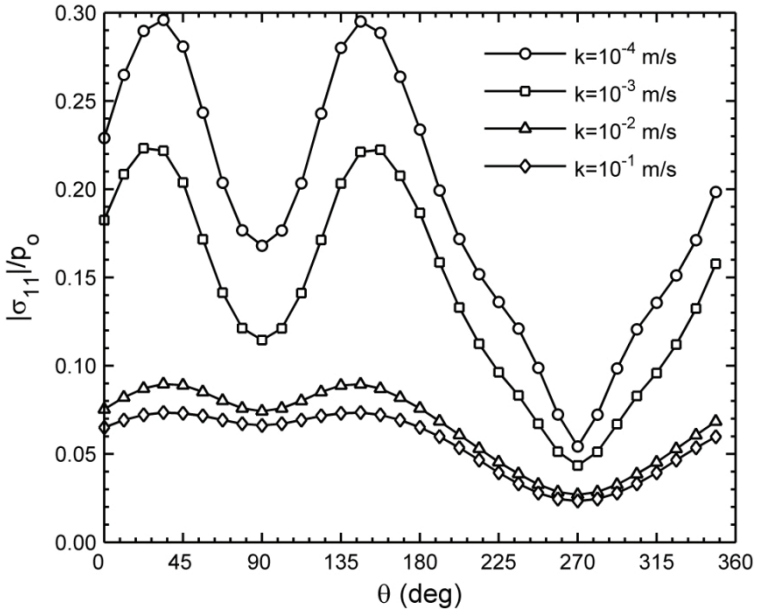

Figure 4.21. Distribution of $|\sigma_{11}|/p_o$ around pipeline circumference for various k (input data as in Figure 4.20).

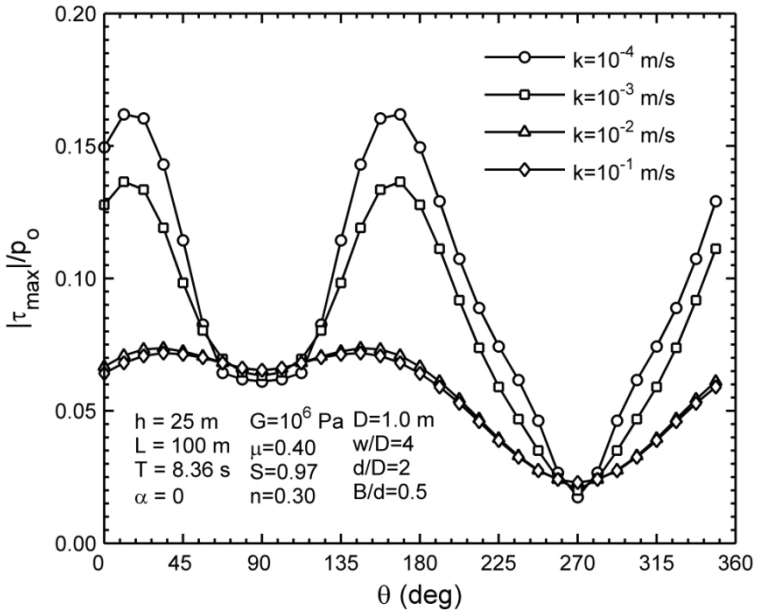

Figure 4.22. Distribution of $|\tau_{max}|/p_o$ around pipeline circumference for various k.

On the other hand, the amplitude of pore pressure is revealed to be largely attenuated when the seabed soil is constituted from sands or fine sands. At the same time, poorly-permeable soils are also exposed to larger amplitudes of shear and normal stresses, in comparison with highly-permeable seabed materials. It is worth noting that responses of highly-permeable soils are found to be more uniformly distributed around the

structure; whereas, sharp variations of response are observed over the perimeter of a pipeline buried in a low permeability medium.

The Degree of Saturation

Based on the degree of saturation, the structure of an unsaturated soil is classified into three types, which are illustrated in Figure 4.23 (Wheeler, 1988). In soils of a low degree of saturation (*S*), the gas phase is continuous but water, forming menisci at grain contacts, is discontinuous (Figure 4.23a). Both gas and water phases become continuous for intermediate degrees of saturation (Figure 4.23b). Finally, the water phase remains continuous in nearly saturated soils while the gas phase, in the form of discrete bubbles, is discontinuous (Figure 4.23c). Actual values of critical saturation degrees, delineating these three structure types, vary in different soils. However, marine sediments are mainly classified so as to fall within the third category (Jeng, 1997b), since they typically contain a few percent of air and thus a degree of saturation of in excess of 90% (Esrig and Kirby, 1977). This amount of air content is believed to the result of decomposition of organic matter and geothermal processes (Claypool and Kaplan, 1974).

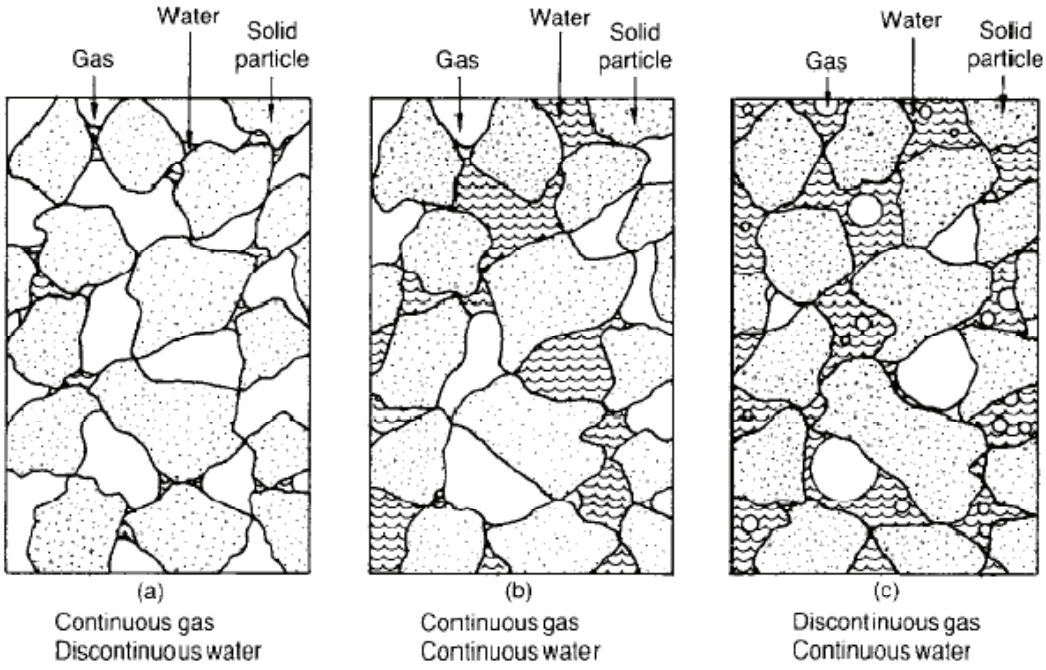

Figure 4.23. Structures of unsaturated soils (reproduced form Wheeler, 1988).

The Biot consolidation theory is used in the present study to simulate the seabed behaviour. This theory requires the introduction of a physical coefficient (β) or the compressibility of pore fluid. In nearly saturated seabeds, the third type in Figure 4.23c, it can be assumed that under the wave loading the air pressure would remain the same as the water pressure, provided that the size of discrete air bubbles are much smaller than

that of soil particles as in Figure 4.24a. Under these conditions, the air-water mixture or the so-called pore fluid behaves uniformly and can be assigned an equivalent compressibility. The bulk compressibility of pore fluid (β) is then considered to deviate from that of pure water (β_w) based on the volumetric percentage of air bubbles (1-*S*) as indicated in Verruijt (1969):

$$\beta = \beta_w + \frac{1-S}{P_{wo}} \tag{4.13}$$

where, P_{wo} is the absolute water pressure. This approach has been widely used by various researchers, who have investigated the seabed consolidation problem, among them Madsen (1978) and Hsu and Jeng (1994). Thus, it will also be followed in the present study. It should be pointed out that the relation (4.13) may not remain valid for degrees of saturation of less than 85%.

Another limitation to the application of the aforementioned approach is in gassy soils, where discrete air bubbles (voids) in a nearly saturated soil are larger than soil particles as in Figure 4.24b. Anderson *et al*. (1998) reported that most of air bubbles observed from the clear wall of their coring tube were from this type (Sandven *et al.*, 2007). The consolidation theory of gassy soils as well as its applications have been investigated in Thomas (1987), Wheeler (1988), Sills *et al*. (1991) and Wichman (1999). The seabed response near the pipeline buried in this type of unsaturated soil, however, is not covered by the present research and can be an interesting subject for future study.

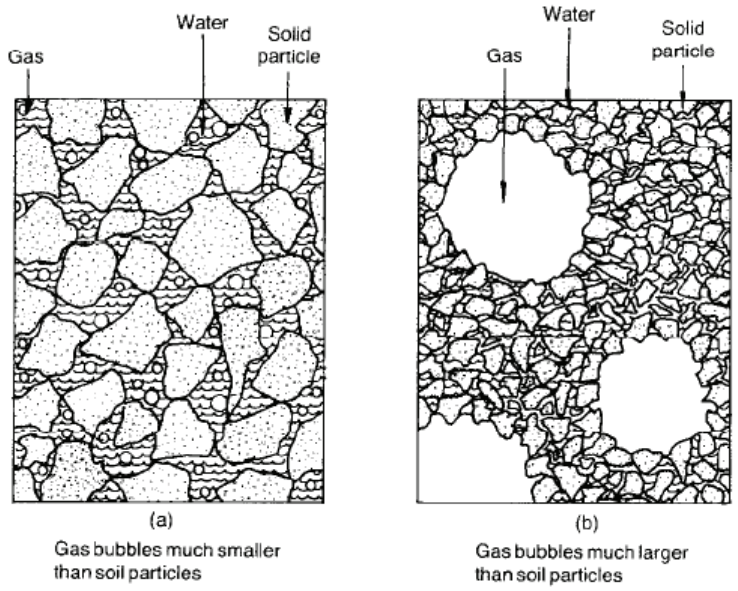

Figure 4.24. Profiles of soils containing discrete air bubbles (reproduced from Wheeler, 1988) .

It is worth noting that even a small amount of air in a seabed soil boosts the pore fluid compressibility and thus changes the seabed response drastically, as can be deduced from Equation 4.13 (Yamamoto *et al.*, 1978), Sumer and Fredsøe, 2002) and Torum, 2007). Therefore, it is beneficial to study the influence of saturation on the wave-induced seabed responses. A range of degree of saturation from 91% to 99% is selected for the purpose of the present parametric study. As shown in Figure 4.25, variations of degree of saturation do not affect the location of maximum and minimum pore pressures around pipeline circumference. Nevertheless, the pore pressure attenuation increases dramatically along with the increase of air content. That is the pore pressure is being attenuated up to around 50% for $S = 0.91$. On the other hand, less-saturated soils are under larger stresses with principal effective and shear stresses increasing while S is decreased, as shown in Figure 4.26 and Figure 4.27. It can be also observed from the illustrations that the maximum normal and shear stresses around pipeline for $S = 0.91$ are respectively 5.0 and 3.5 times greater than those for $S = 0.99$. It is evident that the seabed responses near the pipeline are highly sensitive to the degree of saturation. Therefore, it is important for design engineering purposes to accurately determine in-situ value of soil saturation before proceeding to evaluate soil responses. For this purpose, a new instrument for the accurate measurement of air content in marine sediments has been recently developed by Sandven *et al*. (2007).

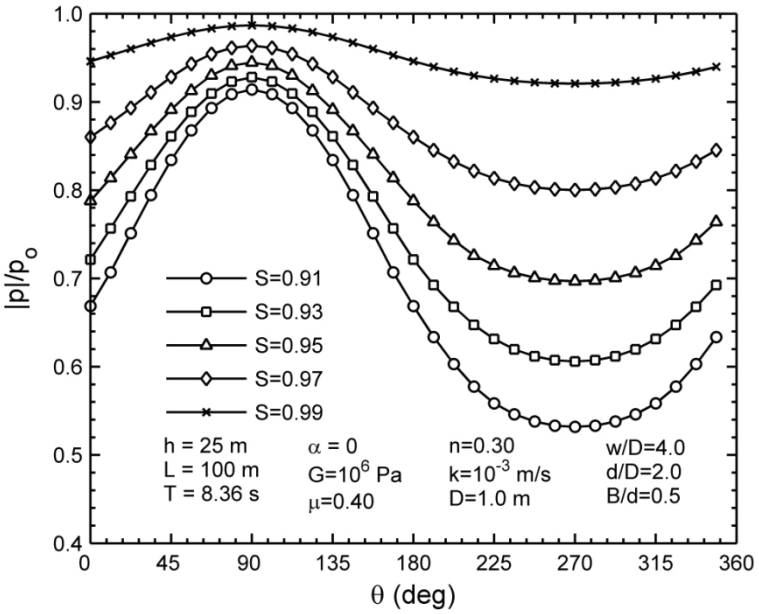

Figure 4.25. The distribution of $|p|/p_o$ around pipeline circumference for various S.

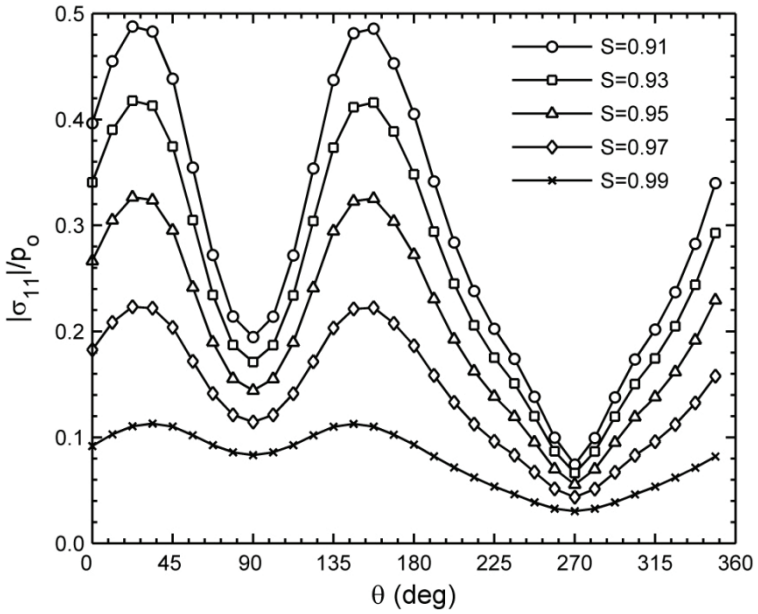

Figure 4.26. The distribution of $|\sigma_{11}|/p_o$ around pipeline for various S (input data as in Figure 4.25).

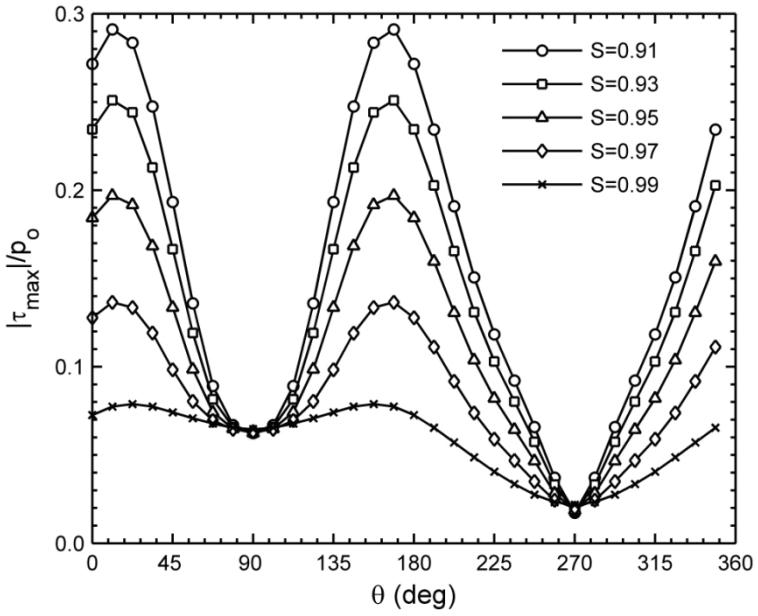

Figure 4.27. The distribution of $|\tau_{max}|/p_o$ around pipeline for various S (input data as in Figure 4.25).

4.1.1.3 Influences of Trench and Pipeline Geometries

Trench Width

The trench width (w) is an influential factor on the wave-induced soil response around a pipeline. Considering practical engineering purposes, in the present study, the trench width is normalized by the

pipeline diameter. The normalized trench width (w/*D*) is considered to vary between 1.5 and 4.0; and influences of non-dimensional trench width are discussed in this section.

The amplitude of pore pressure around a pipeline, normalized by the wave pressure at the mudline ($|p|/p_o$), decreases while widening the trench, as is shown in Figure 4.28. The effect of trench width on pore pressure, however, vanishes when the normalized trench width become larger than 3.0, since the pore pressure distribution around pipeline remains practically unchanged for $w/D \geq 3.0$. On the other hand, maximum pore pressure amplitude occurs at the pipe crest ($\theta = 90°$), whilst the pore pressure utmost attenuation is at the pipe bottom ($\theta = 270°$). These locations will remain unchanged for all trench widths.

As shown in Figure 4.29, the wave-induced major principal effective stress around the pipeline is larger in wider trenches. Nevertheless, increasing the trench width does not significantly influence the major principal stress, when $w/D \geq 3.5$. In a narrow trench ($w/D = 1.5$), the seabed soil near the pipe experiences the maximum $|\sigma_{11}|/p_o$ at $\theta = 45°$ and 135°. These locations are respectively shifted towards $\theta = 22.5°$ and 157.5° while the trench is widened to $w/D = 4.0$. The lowest major principal stress is always observed at the bottom of the pipe perimeter ($\theta = 270°$).

The distribution of maximum shear stress around the pipeline follows a similar pattern to that of major principal effective stress. Figure 4.30, however, shows that values of $|\tau_{max}|/p_o$ are smaller than those of $|\sigma_{11}|/p_o$. On the other hand, the effect of trench width on increasing shear stresses also vanishes when $w/D \geq 3.0$. The highest and lowest shear stresses respectively take place at θ=22.5°, 157.5° and θ=270° around the pipeline.

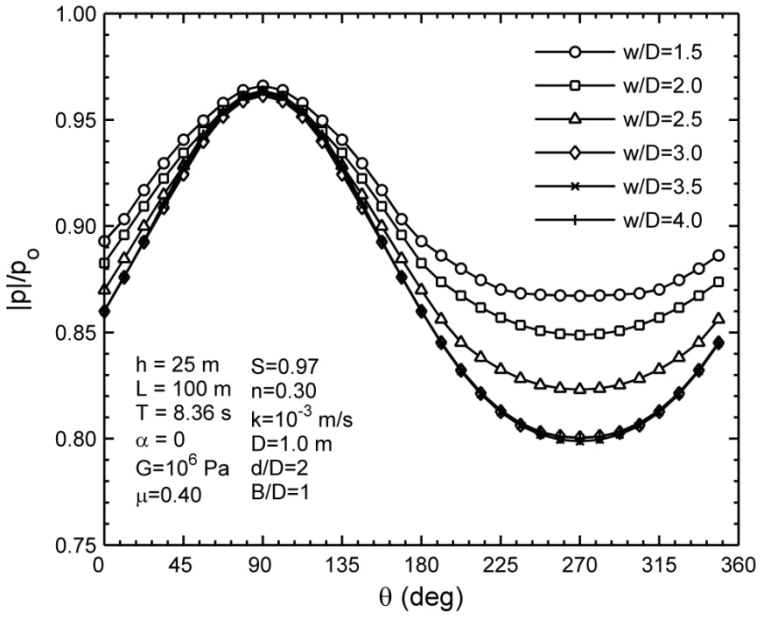

Figure 4.28. The distribution of $|p|/p_o$ around pipeline circumference for various w/D.

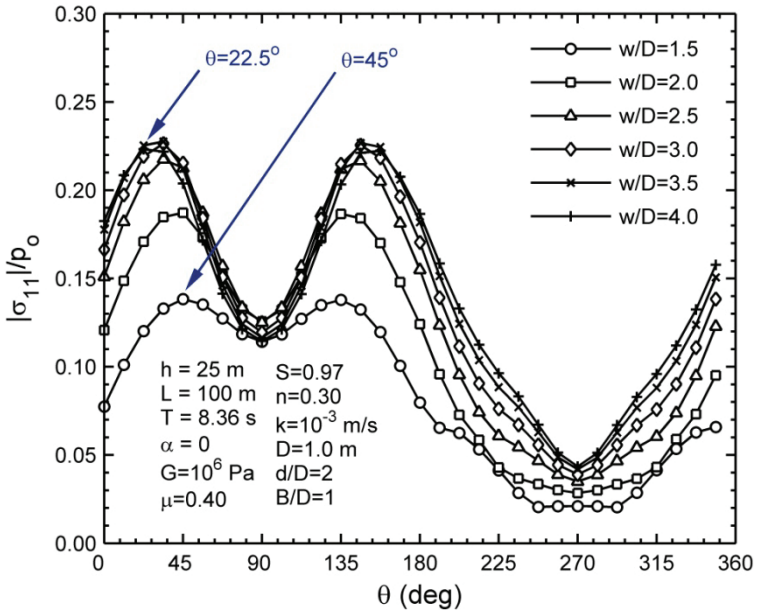

Figure 4.29. The distribution of $|\sigma_{11}|/p_o$ around pipeline circumference for various w/D.

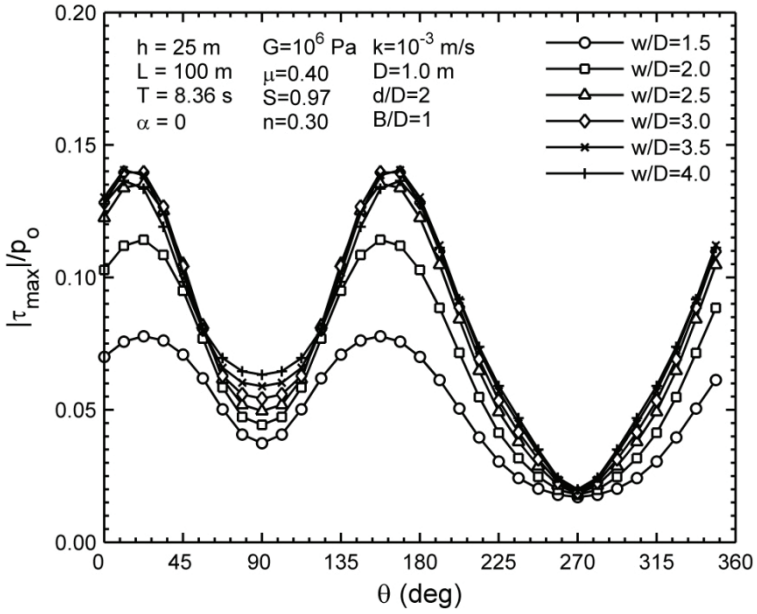

Figure 4.30. The distribution of $|\tau_{max}|/p_o$ around pipeline circumference for various w/D.

The Trench Depth

The influence of pipe burial depth (B) on the wave-induced seabed response is a critical factor in the design of a submarine pipeline. In this parametric study, the pipe is assumed to be buried halfway through the trench depth (d), i.e. $B/d = 0.5$. Therefore, effects of pipe burial and trench depth are studied simultaneously by varying the trench depth. It is, however, worthy to emphasize that the developed numerical model is capable of carrying out numerical simulations for any arbitrary geometry. The influence of normalized trench depth (d/D) on the pore pressure amplitude around a pipeline is shown in Figure 4.31. The pore pressure amplitude decreases monotonically by increasing d/D from 1.5 to 3.5. On the other hand, principal effective and shear stresses around the pipe, illustrated in Figure 4.32 and Figure 4.33, are also found to be larger in deeper trenches. However, $|\sigma_{11}|/p_o$ at the lower part of the pipeline, is not significantly affected by the variation of trench depth.

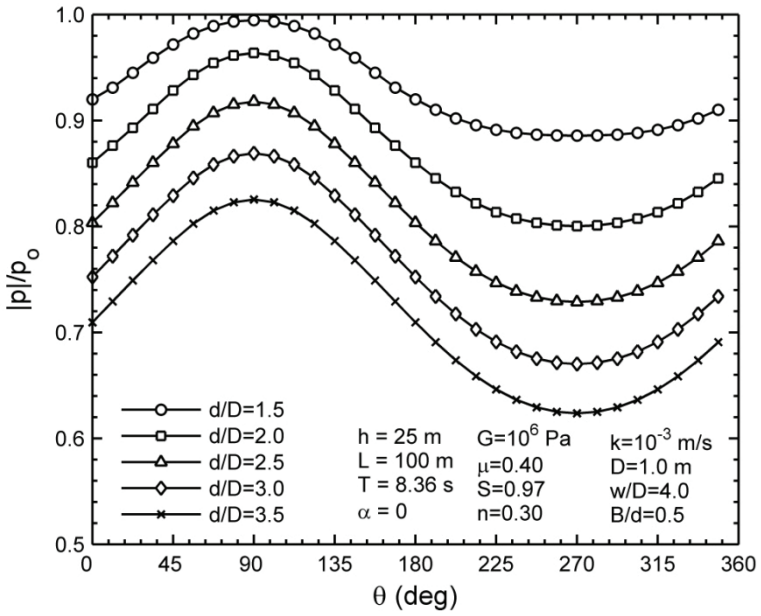

Figure 4.31. The distribution of $|p|/p_o$ around pipeline circumference for various d/D.

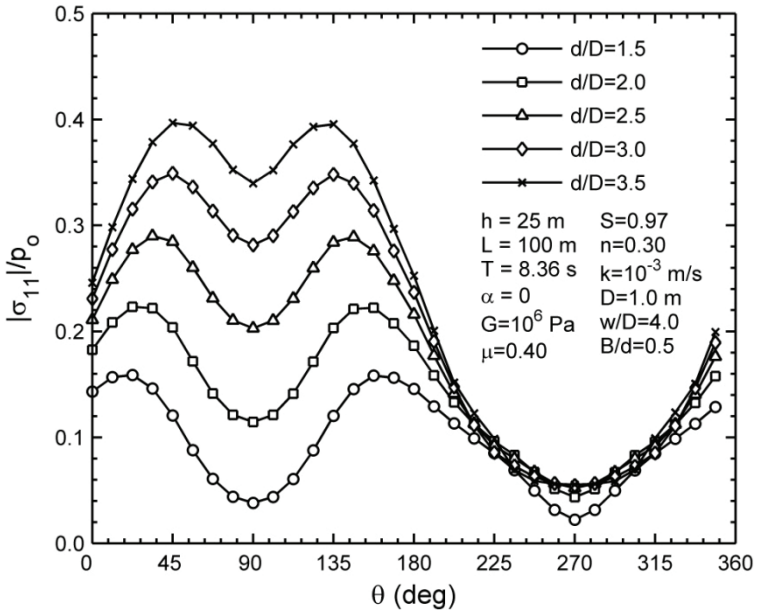

Figure 4.32. The distribution of $|\sigma_{11}|/p_o$ around pipeline circumference for various d/D.

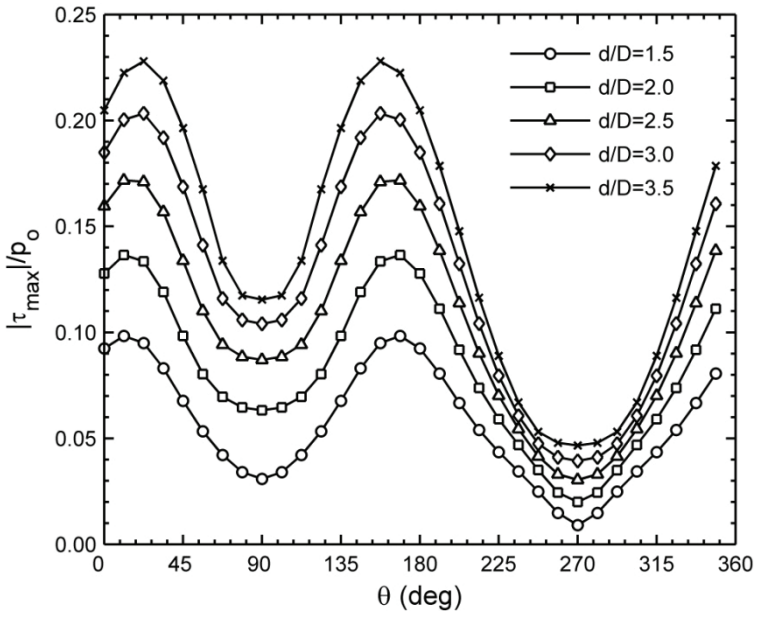

Figure 4.33. The distribution of $|\tau_{max}|/p_o$ around pipeline for various d/D (input data as in Figure 4.32)

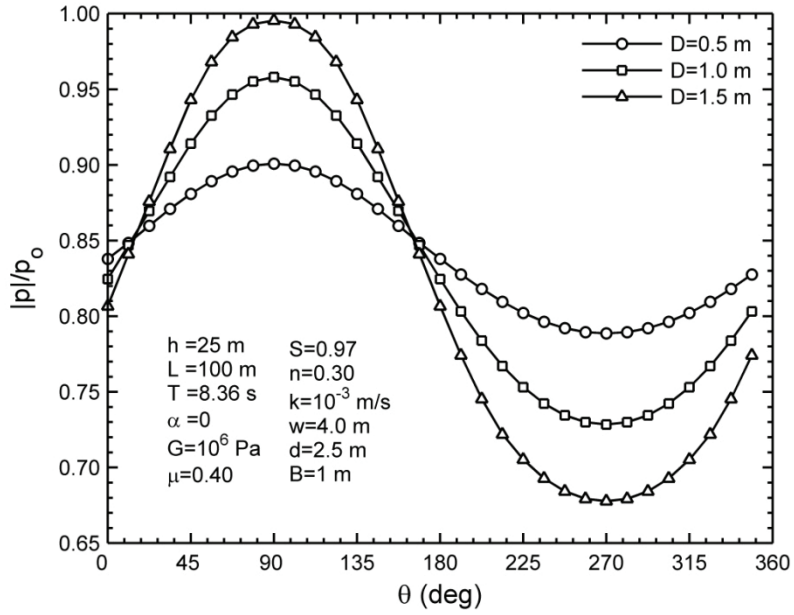

Figure 4.34. Distribution of $|p|/p_o$ around pipeline circumference for various pipe diameters.

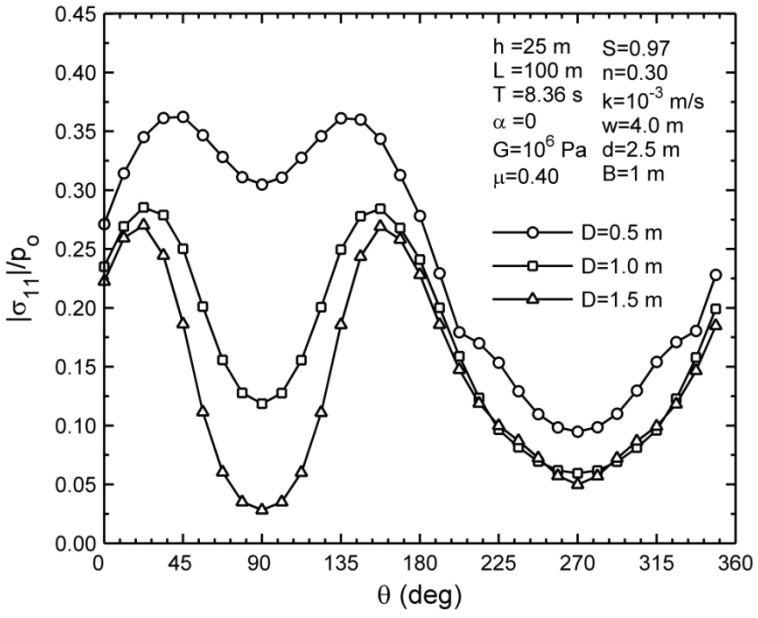

Figure 4.35. Distribution of $|\sigma_{11}|/p_o$ around pipeline circumference for various pipe diameters.

Pipeline Diameter

A pipe diameter is initially chosen in order to meet the desired fluid transport rate through the pipeline. At the same time, the interaction between the surrounding seabed soil and the pipeline is influenced by its diameter. Since such interactions, resulting forces, and seabed instabilities are key parameters in the design of pipe thickness, it is important to investigate the effect of pipe diameter on seabed responses. Varying the pipe diameter, the pore pressure amplitude responds in a different way at the lower and upper parts of pipeline, as plotted in Figure 4.34. In fact, $|p|/p_o$ decreases around the pipe crest and increases close to the pipe bottom, when a smaller pipe is used. Despite the behaviour of pore pressure, major principal and maximum shear stresses, shown in Figure 4.35 and Figure 4.36, increase monotonically while decreasing the pipe diameter. This could be attributed to large spatial gradients of soil displacements in the confined region near a small pipeline, knowing that a non-slip condition is considered on the pipe surface.

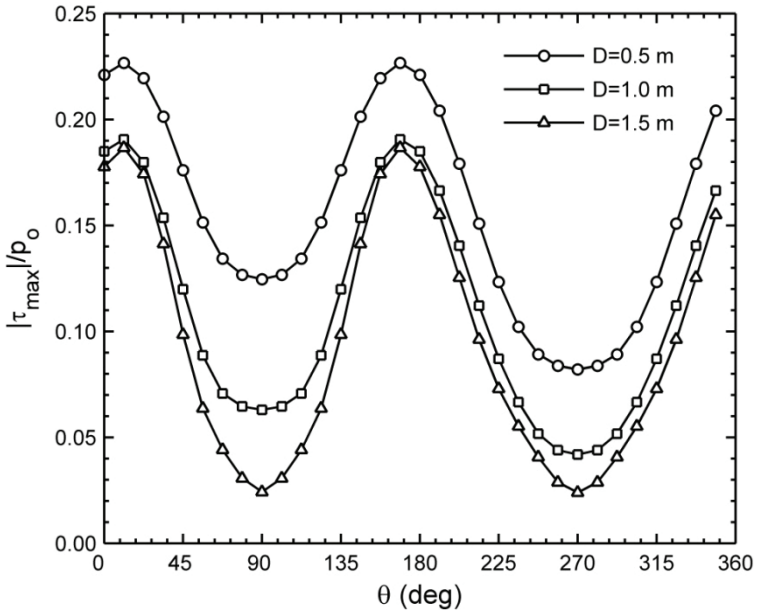

Figure 4.36. Distribution of $|\tau_{max}|/p_o$ around pipeline circumference for various pipe diameters.

4.2 Wave-Associated Seabed Instabilities

4.2.1 Soil Shear Failure

Seabed soil failure, due to shear stresses, in the region close to the pipeline has been recognised as one of main mechanisms that will lead to the pipeline instability. In fact, the shear failure is the loss of soil ability to resist against shear stresses. This phenomenon is accompanied by the sliding of soil layers on each other and thus often by large horizontal displacements in the seabed deposit. The submarine pipeline, buried in the failed soil region, consequently undergoes large deformations and internal stresses, which in turn triggers the

failure of the structure. Therefore, it is necessary to study the phenomenon of soil shear failure in the vicinity of a submarine pipeline. To date, several criteria have been proposed in the literature to justify the occurrence of soil shear failure. Among them, the Mohr-Coulomb shear failure criterion has been widely used by engineers in various geotechnical engineering applications (Craig, 1997). Thus, this criterion is adopted in the present study to investigate the soil instability as the result of excessive wave-induced shear stresses. Herein, a brief description on the Mohr-Coulomb criterion is presented.

Seabed stresses introduced and evaluated in previous sections were only due to the dynamic action of ocean wave pressure. However, the seabed soil is also under a static loading from its self-weight. It is important to note that soil instabilities are dominated by *absolute* seabed responses, which are formed by the superposition of *static* and *dynamic* (wave-induced) components of soil stresses. Therefore, it is essential to formulate absolute soil stresses before proceeding to describe the shear failure criterion. Considering a soil element located at the elevation z below the seabed surface, the state of static overburden effective stresses induced by the buoyant weight of soil column above this element is illustrated in Figure 4.37b. Soil overburden effective stresses are, therefore, as:

$$\sigma'_{ox} = \sigma'_{oy} = K_{\circ}\gamma'_s z = K_{\circ}(\gamma_s - \gamma_w)z \tag{4.14}$$

$$\sigma'_{oz} = \gamma'_s z = (\gamma_s - \gamma_w)z \tag{4.15}$$

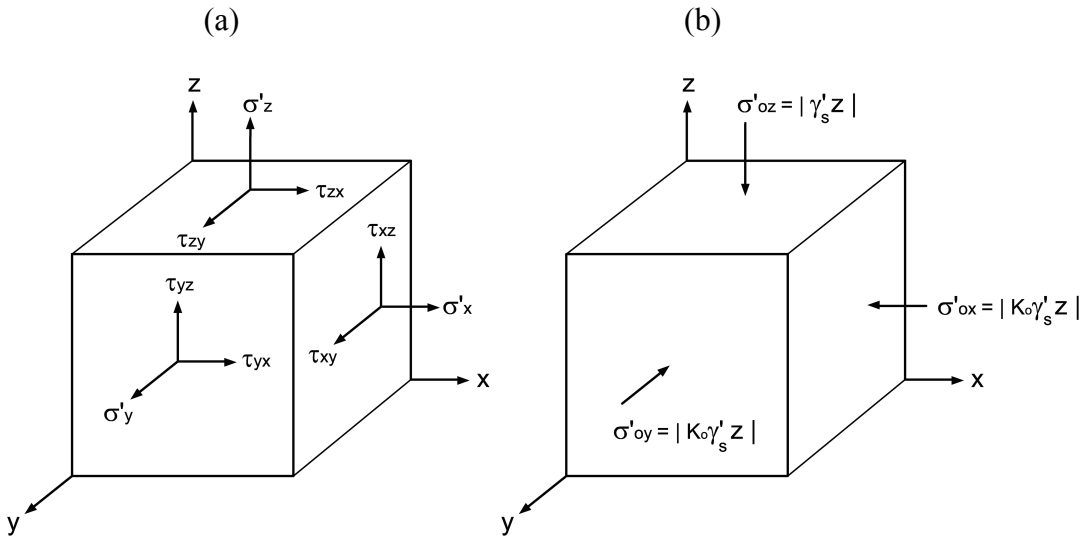

Figure 4.37. (a) Dynamic and (b) static components of seabed soil stresses.

where, σ'_{ox}, σ'_{oy} and σ'_{oz} are static normal effective stresses in the *x*-, *y*-, and *z*- directions, respectively; γ'_s is the submerged unit weight of the soil, γ_s and γ_w are unit weights of soil and water, respectively; and K_o is the coefficient of earth lateral pressure. As throughout this text, a negative value represents a compressive stress mode. It is also worthy to point out that the soil self-weight imposes no shear stresses in the *x*-, *y*-, and *z*- planes on the soil element. Finally, absolute soil stresses are:

$$\bar{\sigma}'_x = \sigma'_x + K_\circ(\gamma_s - \gamma_w)z \tag{4.16}$$

$$\bar{\sigma}'_y = \sigma'_y + K_\circ(\gamma_s - \gamma_w)z \tag{4.17}$$

$$\bar{\sigma}'_z = \sigma'_z + (\gamma_s - \gamma_w)z \tag{4.18}$$

Absolute *x*, *y*- and *z*- effective stresses can further be used to obtain absolute principal effective stresses though the same methodology as described by equations (4.2)-(4.5).

To describe the shear failure criterion, let us assume an arbitrary plane within the soil element, normal to which an absolute effective stress of $\bar{\sigma}'$ is acting in the compressive mode. At the same time, the maximum absolute shear stress that acts within this plane is assumed to be represented by $\bar{\tau}$. According to Coulomb's criterion, the shear stress that brings the soil to the state of shear failure ($\bar{\tau}_f$) is related $\bar{\sigma}'$ by:

$$\bar{\tau}_f = -\bar{\sigma}' \tan\left(\phi_f\right) \tag{4.19}$$

in which, ϕ_f is the soil internal friction angle, which is a property of seabed soil[7]. The shear failure occurs if the absolute soil shear stress exceeds $\bar{\tau}_f$. By defining the stress angle (ϕ), with analogy to the equation (4.19), as the ratio of absolute shear stress to the absolute normal effective stress, the shear failure criterion can be expressed by:

$$\phi \geq \phi_f \tag{4.20}$$

On the other hand, the state of soil stress on any arbitrary plane falls within the region confined by three-dimensional Mohr circles. Therefore, the utmost stress angle for a given state of soil stress is limited to the slope of a line that is tangent to the greatest of Mohr circles, as plotted in Figure 4.38. The stress angle is therefore:

[7] Note that the negative sign in eq. (4.19) stems in the negative sign agreement for compressive stresses. The same point should be noted also in Figure 4.38 and eq. (4.21).

$$\phi = \sin^{-1}\left(\frac{\bar{\sigma}'_{33} - \bar{\sigma}'_{11}}{\bar{\sigma}'_{11} + \bar{\sigma}'_{33}}\right) \tag{4.21}$$

where, $\bar{\sigma}'_{11}$ and $\bar{\sigma}'_{33}$ are respectively major and minor absolute principal effective stresses, as illustrated. Equations (4.20) and (4.21) can be used to justify the occurrence of shear failure in a seabed soil.

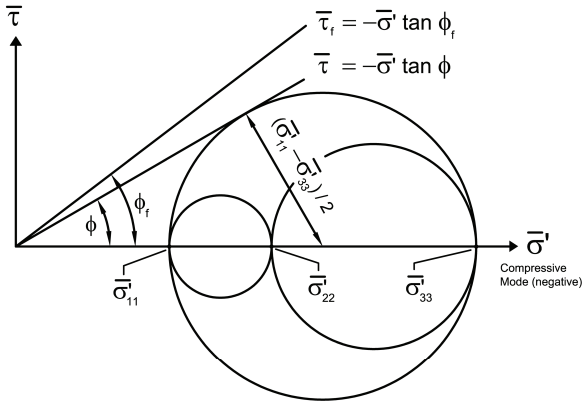

Figure 4.38. The Mohr-Coulomb shear failure criterion.

Before proceeding to the next section, it is also useful to explain to which extent static and dynamic components of seabed loading contribute to the potential of soil shear failure. For this purpose, consider a soil element within the seabed without the presence of wave dynamic loading, as in Figure 4.37b. Since, there are no shear stresses acting on surfaces of this soil element, σ'_{ox}, σ'_{oy} and σ'_{oz}, also serve as principal effective stresses under the static loading. Substituting these stresses into the equation (4.21), the at-rest stress angle corresponding to the initial geostatic state of soil stresses may be defined and simplified as:

$$\phi_\circ = \sin^{-1}\left(\frac{\sigma'_{oz} - \sigma'_{ox}}{\sigma'_{oz} + \sigma'_{ox}}\right) = \sin^{-1}\left(\frac{1 - K_\circ}{1 + K_\circ}\right) \tag{4.22}$$

On the other hand, the soil coefficient of lateral earth pressure can be related to the internal friction angle by the formula proposed by Jacky (1944):

$$K_\circ = 1 - \sin\left(\phi_f\right) \tag{4.23}$$

Substituting equation (4.23) into (4.22), one will get:

$$\sin\phi_o = \frac{\sin\phi_f}{2-\sin\phi_f} \tag{4.24}$$

Polous (1988) reported that the internal friction angle of a sandy seabed ranges from 20° to 30° (Wang *et al.*, 2007). In this range, it is possible to accurately fit a linear relation into the equation (4.24). However, let us approximate the equation (4.24) in $20°< \phi_f <30°$ by a simpler linear relation, which is of unit slope:

$$\phi_o = \phi_f - C \tag{4.25}$$

where, C is a constant that can be considered to be around 9.5° (see Figure 4.39). Inspired by the relation (4.25), it is then possible to define a wave-induced perturbation in soil stress angle such as $(\Delta\phi)_{wave}=\phi-\phi_o$. Such wave-associated perturbation is therefore able to bring the soil from the state of geostatic stresses into the shear failure, if it is as large as $C = (\Delta\phi)_{critical}= 9.5°$. This approach may be useful to gauge how significantly soil, wave and trench properties can influence the potential of seabed shear failure. In fact, a parameter may be justified as being influential, if it helps the wave-induced stress angle to change considerably towards the critical value of 9.5°. It is for the first time that the concept of wave-induced perturbation of stress angle is introduced to the literature. This concept is used as an indicative along with numerical results from the three-dimensional FEM model that are calculated directly based on equation (4.21).

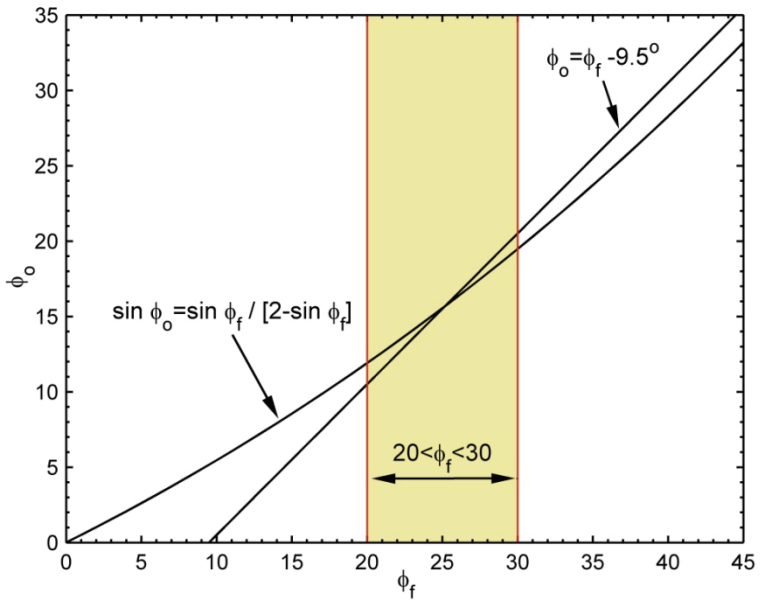

Figure 4.39. Linear approximation of relation between geostatic stress angle and internal friction angle.

It should be pointed out that, as it will be shown later, the stress angle perturbation often alters much beyond the value of 9.5 degrees as the result of a change in water wave properties. In fact, a small change in wave characteristics can be so influential in altering the sate of soil stresses from the compressive to the tensile mode. In contrary, soil properties are often found to produce much smaller effects on perturbations of stress angle. However, the influence of most soil properties is still comparable with 9.5 degrees. Therefore, both soil and wave properties will be considered in this research to carry out a parametric study on the stress angle. More details of the parametric study will be presented in coming sections.

4.2.2 Soil Liquefaction

Another important mechanism for the instability of submarine buried pipelines is the seabed liquefaction. The liquefaction, as defined in Marcuson (1978), is the transformation of a granular material from a solid to a liquefied state as a consequence of increase in pore water pressure and reduction in compressive effective stress (Youd *et al.*, 2001) and de Groot *et al.*, 2006). In fact, a wave-induced increase in pore pressure can be strong enough to cause the effective stress to vanish or even go into the tensile mode. This is triggered by the loss of grain to grain contacts in the soil matrix and further results in the soil skeleton becoming incapable of carrying any external load, apart from its self-weight. Hence, a submarine pipe will sink or float within the liquefied seabed under the action of pipe buoyant weight. Large vertical deformations and stresses that are associated with the sinking/floatation of a buried structure, finally, can lead to its failure. It is also possible for the pipeline to be dragged within the liquefied soil due to the presence of bottom currents and thus to undergo large horizontal deformations. To avoid a catastrophe resulting from the pipeline failure, it is essential to investigate the potential of soil liquefaction in the vicinity of this structure. For this purpose, a reliable liquefaction criterion has to be applied.

Among available studies, researchers have considered various criteria to justify the occurrence of seabed soil liquefaction. Generally speaking, a first group of researchers has been concerned with the "reduction in effective stresses" as the liquefaction criterion. Among those, Okusa (1985) suggested that a sandy bed becomes liquefied if the *absolute vertical effective stress* steps into the tensile (positive) phase. That is:

$$\overline{\sigma}'_z \geq 0 \tag{4.26}$$

It should be pointed out that seabed effective stresses are initially in the compressive mode under-calm sea conditions as the result of the weight of overlaying soil layers. Therefore, substituting the absolute vertical effective stress from equation (4.18), the aforementioned liquefaction criterion becomes as:

$$\sigma'_z + \left(\gamma_s - \gamma_w\right) z \geq 0 \tag{4.27}$$

Later, Tsai (1995) modified this criterion by considering the *average of absolute effective stresses*, as:

$$\frac{1}{3}\left(\bar{\sigma}'_x+\bar{\sigma}'_y+\bar{\sigma}'_z\right)=\frac{1}{3}\left(\sigma'_x+\sigma'_y+\sigma'_z\right)+\frac{1+2K_\circ}{3}\left(\gamma_s-\gamma_w\right)z\geq 0 \tag{4.28}$$

A common property of the work by Okusa (1985) and Tsai (1995) is the use of effective stresses. However, the fieldwork by Zen and Yamazaki (1991) revealed that field measurements of soil effective stresses involve significant inaccuracies, when the soil is near to the liquefaction state. Therefore, they suggested the use of a liquefaction criterion based on the excess pore pressure. In fact, Zen and Yamazaki (1990b) applied the underlying assumptions of one-dimensional consolidation theory to replace the change of vertical effective stress from the geostatic state to the absolute value (i.e. wave-associated vertical effective stress) by the *excess pore pressure*. Hence, the equation (4.27) was *approximated* by the following criterion:

$$\bar{\sigma}'_z\approx p_{excess}+\left(\gamma_s-\gamma_w\right)z\geq 0 \tag{4.29}$$

where, the excess pore pressure is:

$$p_{excess}=p-p_{bed} \tag{4.30}$$

The advantage of this method is the use of wave-induced pore pressure, which is found to be reliably measured even in nearly liquefied soils. Later, Hsu *et al*. (1995) and Jeng (1997a) extended this approximate framework to three-dimensions with an analogy to the equation (4.28). They have also shown that their liquefaction criterion, formulated in equation (4.31), reproduces field observations of Zen and Yamazaki (1991) better than other aforementioned criteria. Therefore, this criterion is adopted in the present study to justify the occurrence of seabed liquefaction in the vicinity of submarine buried pipelines.

$$p_{excess}+\frac{1}{3}\left(1+2K_\circ\right)\left(\gamma_s-\gamma_w\right)z\geq 0 \tag{4.31}$$

The adopted liquefaction criterion is shown in Figure 4.40 for the case of a naked seabed in the absence of a pipeline. As it is illustrated, the excess pore pressure becomes positive in seabed under the wave trough. This is because the wave dynamic pressure (p_{bed}) is attenuated within the porous bed and the wave-induced pore pressure (p) is, therefore, a fraction of wave pressure. Hence, under the wave trough, where the pressure is in suction (negative) mode, $p_{\text{excess}} = p - p_{\text{bed}}$ is positive. However, it should be pointed out that this illustration is an indicative idealized case. In reality, where a phase lag also exists between the pore pressure and the seabed loading, a positive excess pore pressure can be observed distant from the wave trough. In particular, such a phase lag can be extremely significant when the structure exists. The soil liquefaction occurs under stormy conditions when the excess pore pressure exceeds the compressive mean geostatic stress, which is linearly increasing over the seabed depth. Therefore, a liquefied state of soil is observed in a layer

immediately below the seabed surface, as indicated. It should be noted that the seabed surface may be always considered to be liquefied.

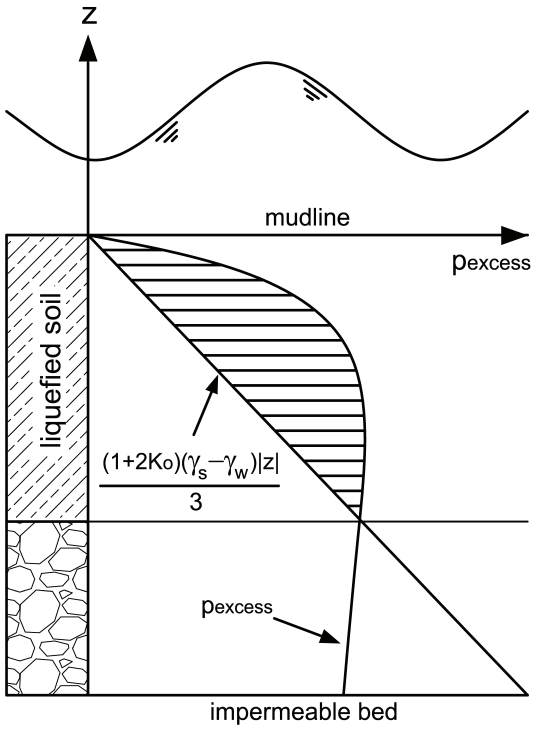

Figure 4.40. The concept of wave-induced liquefaction after Zen and Yamazaki (1990b).

4.2.3 Parametric Study

In this section, a parametric study on seabed instabilities is proposed with an analogy to the parametric study previously carried on wave-induced seabed responses. For this purpose, potentials of soil liquefaction and shear failure around a pipeline are studied. The excess pore pressure and the stress angle are respectively considered as indicators of liquefaction and shear failure potentials and successively investigated in conjunction with their critical limits that were previously introduced in relations (4.31) and (4.20). Influences of wave obliquity, soil properties, trench/pipeline geometries and water wave characteristics on the excess pore pressure and stress angle are thoroughly studied using the developed three-dimensional numerical model. It should be emphasised that a detailed study on seabed instabilities around submarine pipelines was not previously available in the literature even using two-dimensional models.

Finally, since the wave-loading is of a periodic nature both in time and space, both the stress angle and excess pressure also follow similar periodic patterns. Nevertheless, it will be shown that spatial and temporal distributions of these variables are not simply sinusoidal. Therefore, such distributions will be discussed prior

to going further into the parametric study. From that point onward, amplitudes of the stress angle and excess pore pressure will be the subject of parametric study. It is worthy of note that peak or the most critical values of these parameters over a wave period is referred to by the term *amplitude*, in this text.

4.2.3.1 Three-Dimensionalities of Ocean Waves

One of the key objectives of developing the three-dimensional finite element model is to determine the influence of wave obliquity on the potential of seabed instability near the pipeline. No study is yet available in the literature to address such effects. On the other hand, the occurrence of liquefaction and shear failure are respectively justified based on the wave-induced excess pore pressure (p_{excess}) and the stress angle (ϕ) within the seabed soil. Hence, variations of these parameters with the wave direction (α) are investigated in this section.

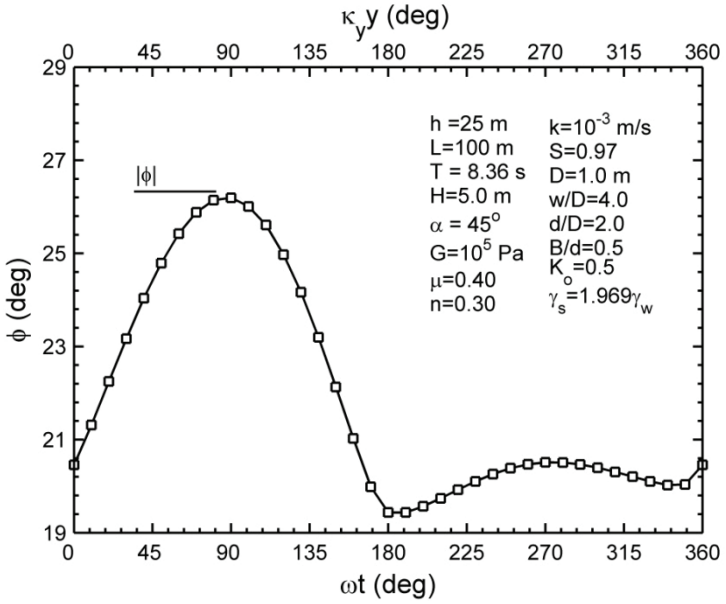

Figure 4.41. The distribution of stress angle for a point located on the pipe perimeter at θ=135° (a) over a pipeline span axis, when t=T (see the upper horizontal axis: $\kappa_y y$), (b) over a wave period, when y=0 (see the lower horizontal axis: ωt).

As discussed earlier in section 4.1.1.1, the wave obliquity affects seabed responses through the following mechanisms: (1) *three-dimensional geometry-based influences* and (2) *effects of wave direction on the amplitude of seabed responses*. The former requires variations of pore pressure and soil stresses to be periodic over spans of the length $L/\cos(\alpha)$ along the pipe longitudinal axis, as well as, over the wave period. In the same manner, key parameters to justify the potential of soil instabilities, p_{excess} and ϕ, would not be an exception. In particular for the stress angle, however, the spatial and temporal distribution, though being periodic, is not linearly sinusoidal, as illustrated in Figure 4.41. The complex distribution pattern of stress

angle, nevertheless, is of little or no importance, since it is the peak value of stress angle $|\phi|$, which is the key factor to evaluate the risk associated with the shear failure. This peak value is referred to as the *amplitude* of stress angle, throughout this text.

On the other hand, it is vital to coastal geotechnical engineers to determine influences of wave direction on the so-called amplitude of stress angle $|\phi|$ and excess pore pressure $|p_{excess}|$. Figure 4.42 shows the distribution of $|\phi|$ around the pipeline circumference for various wave obliquities. It is evident that sheltered and naked sides of a pipeline behave symmetrically when ocean waves are propagating parallel with the pipeline (α=0°). That is θ = 90° and 270° serve as axes of symmetry for the illustrated distribution pattern (see filled circles). The symmetric behaviour, however, is not applicable when the pipe is exposed to an oblique wave. The obliquity-induced asymmetry is more significant at the lower half of the pipe perimeter (180° < θ < 360°). In the presented example, the amplitude of the stress angle is found to vary mainly monotonically with α, in each of the circumferential spans formed between the six illustrated *inversion nodes/regions*. The direction of this monotonic trend reveres among adjacent circumferential spans.

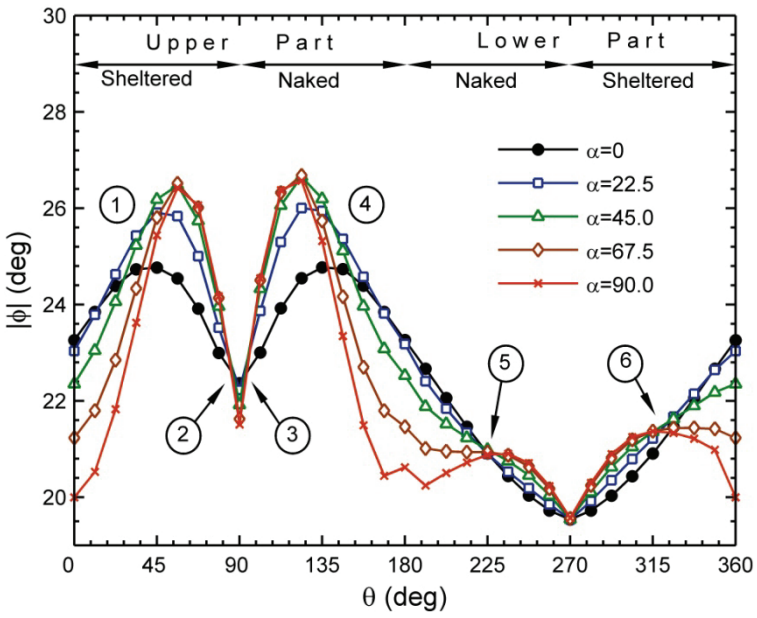

Figure 4.42. The distribution of stress angle amplitude ($|\phi|$) around pipe circumference for various wave directions (soil, wave and pipe properties are as in Figure 4.41).

A wide range of wave, soil and trench properties has been investigated in this study and numerical results have shown that the obliquity-induced asymmetry of stress angle remains a characteristic feature for all cases. However, monotonic variations of stress angle with the wave direction have been observed exclusively in highly permeable, very loose, and highly saturated soils. Due to this complex behaviour, a possible way to justify how significant influences of wave obliquity are, is to consider the largest stress angle

that could be ever experienced around a pipeline. This is because it is important for pipeline engineers to avoid the occurrence of shear failure at any point over the pipe circumference. In this regard, Table 4.2 presents the maximum value of stress angle over the pipeline perimeter (ϕ_{max}), for several simulated cases. In this table, the value of ϕ_{max} corresponding to waves propagating parallel with and normal to the pipeline are respectively shown by ϕ_{max}^{0} and ϕ_{max}^{90}; meanwhile ϕ_{max}^{cr} stands for the most critical value of stress angle that a wave of an arbitrary direction can generate; finally, α_{cr} is the wave direction, for which ϕ_{max}^{cr} is observed. It should be noted that for some cases ϕ_{max}^{cr} can be more than 30° larger than ϕ_{max}^{90}, which represents a two-dimensional case (see last row of table). At the same time, although other cases show much smaller difference, it should be still remembered from the previous section that the soil will fail if the waves could increase the stress angle only about 9.5 degrees. Therefore, any three-dimensional effect that can boost up the stress angle even a few degrees can still be considered as being significant. On the other hand, an inspection into values of α_{cr} in the table shows that the two limiting cases of α = 0° or 90° are not always responsible for the most critical situation.

Table 4.2. The maximum of stress angle (ϕ_{max}) experienced around pipeline for a variety of soil and wave properties (unless explicitly expressed within the table, soil, wave and pipe properties are as h=25 m, T=8.36 s, L=100 m, G=10^6 Pa, μ=0.4, n=0.3, k=10^{-3} m/s, S=0.97, D=1.0 m, w/D=4.0, d/D=2.0, B/d=0.5, K_o=0.5, γ_s=1.969γ_w and H=5.0 m).

The Soil / Wave Property	ϕ_{max}^{0} (deg)	ϕ_{max}^{90} (deg)	ϕ_{max}^{cr} (deg)	α_{cr} (deg)
G=10^5 Pa	24.8	26.6	26.7	67.5
G=10^8 Pa	32.2	32.7	32.8	45.5
k=10^{-4} m/s	28.4	29.0	29.0	90.0
k=10^{-1} m/s	24.8	26.7	26.8	67.0
S=91 %	40.1	41.2	41.2	90.0
S=99 %	25.4	27.2	27.2	90.0
T=12 s, L=125 m, h=12.5 m	59.6	53.4	60.1	22.5
T=10 s, L=100 m, h=12.1 m	72.6	57.4	90.0	22.5

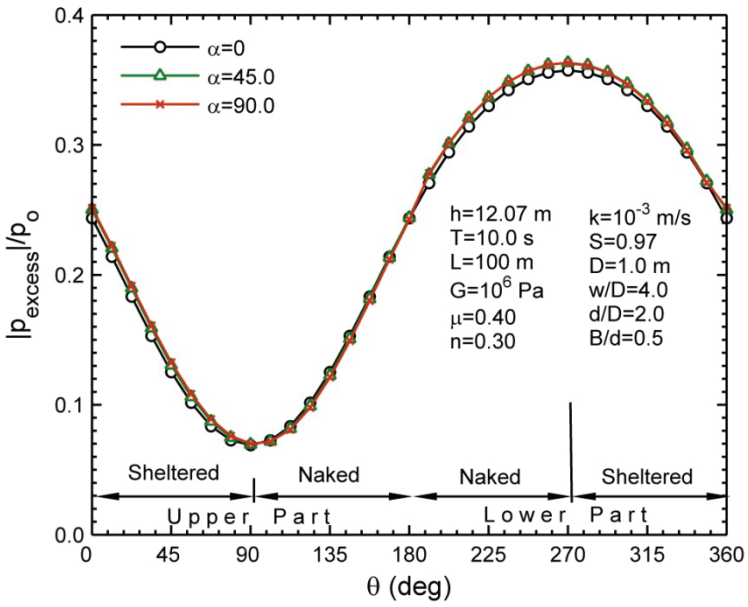

Figure 4.43. The distribution of amplitude of wave-induced excess pore pressure ($|p_{excess}|/p_o$) around pipe circumference for various wave directions.

Figure 4.43 illustrates that the influence of wave direction on the amplitude of excess pore pressure is not significant. Consequently, the potential of complete liquefaction is likely to remain unchanged even when the waves are approaching the pipeline from an oblique angle. Therefore, unlike the potential of shear failure, a two-dimensional model is sufficient to justify the occurrence of complete liquefaction around the pipeline. However, the amplitude of p_{excess}, which can be obtained from a 2-D simulation, should be considered along with the three-dimensional geometry-based influences of wave obliquity on the spatial distribution of soil responses, as previously discussed 4.1.1.1.

4.2.3.2 Influences of Seabed Soil Properties

Modulus of Soil Shear Stiffness

The influence of soil shear stiffness on the pore pressure and soil stresses has been studied earlier in this chapter. In fact, the shear modulus was found to have significant effects on the wave-associated momentary seabed behaviour. Therefore, it is essential to also examine the influence of this parameter on the potential of seabed soil instabilities. As is plotted in Figure 4.44 and Figure 4.45, amplitudes of both excess pore pressure and stress angle increase when the seabed material is stiffer. Therefore, a stiff porous bed is more vulnerable to both complete liquefaction and shear failure.

To determine the critical value of excess pore pressure, corresponding to the onset of soil liquefaction, it is possible to normalize the relation (4.31) by the amplitude of mudline pressure. Hence, the seabed will be liquefied if the non-dimensional excess pore pressure exceeds the critical value:

$$\frac{p_{\mathrm{cr}}}{p_{\circ}} = \frac{-\left(1+2K_{\circ}\right)\left(\gamma_s - \gamma_w\right)}{3p_{\circ}} z = -\eta z \tag{4.32}$$

where, η is a coefficient which is a function of lateral earth pressure coefficient, soil and water unit weights and the amplitude of mudline pressure.

The normalized critical excess pore pressure varies over the pipeline circumference, since so does the vertical coordinate z. It should be pointed out that in the evaluation of critical excess pore pressure, the pipe cross-section is assumed to be of an equivalent unit weight similar to that of porous bed. In fact, this assumption is reasonable for the typical range of materials and diameters used for the construction of underwater pipelines, as well as, for fluids usually being transported though a submarine pipe. In this parametric study, the coefficient of lateral earth pressure of $K_o = 0.5$, and soil unit weight of $\gamma_s = 1.969\ \gamma_w$ are often used to evaluate the critical excess pore pressure. This unit weight is the same as that observed in field measurements of Zen and Yamazaki (1991). A wave height of about $H = 5$ m is also often used, which may be considered as a stormy condition for the range of shallow water depths, in which the pipe burial is necessary. However, a non-breaking condition for water waves is still ensured. Although a variety of wave characteristics, i.e. wave length and wave period, could be chosen, for most cases the wave regime is deliberately chosen so the soil initially remains well away from liquefaction. This will allow us to show a picture of soil/trench/pipe parameters that may be significant enough to cause a shift from this stable situation to a liquefied state of soil.

In contrast to Figure 4.44, where the excess pressure is still far below the critical value corresponding to $\eta = 0.60$ (H =5.35 m), the stress angle in Figure 4.45 is found to go beyond the soil internal friction angle. In fact, prior to exerting the wave loading, the stress lays at the value of ϕ_o indicated on the graph. Considering the action of waves on a soil of $G = 10^6$ Pa, the stress angle still falls between its initial geostatic value and the soil internal friction angle. However, by increasing the soil stiffness to $G \geq 10^7$ Pa the soil will undergo shear failure. Under these circumstances, the seabed at the lateral sides of pipeline, in $0° < \theta < 45°$, $135° < \theta < 225°$, and $315° < \theta < 360°$, will fail. It should be pointed out that by using higher wave heights in numerical simulations, the unstable soil region around structure could even merge to cover the pipe crest as well. It is interesting to note that patterns of distributions of both excess pore pressure and stress angle remain alike for all examined soil shear moduli.

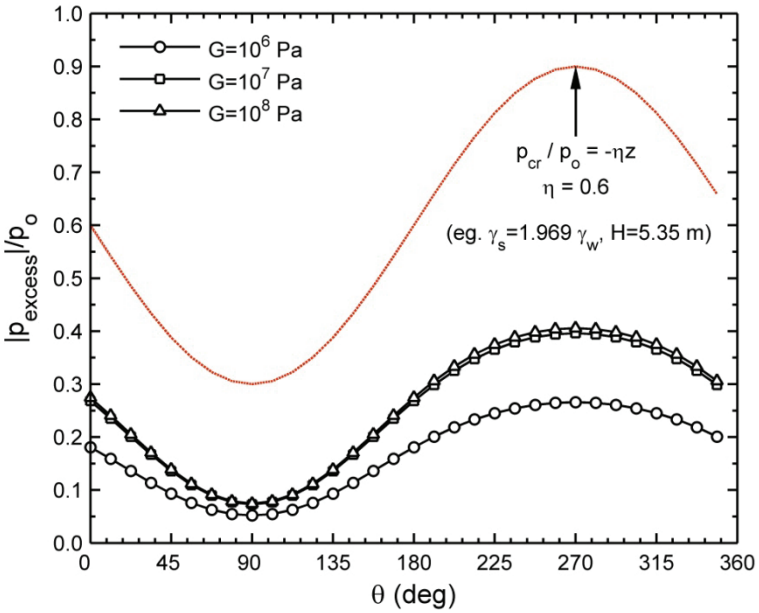

Figure 4.44. The distribution of $|p_{excess}|/p_o$ around pipe perimeter for various G (input data as in Figure 4.17).

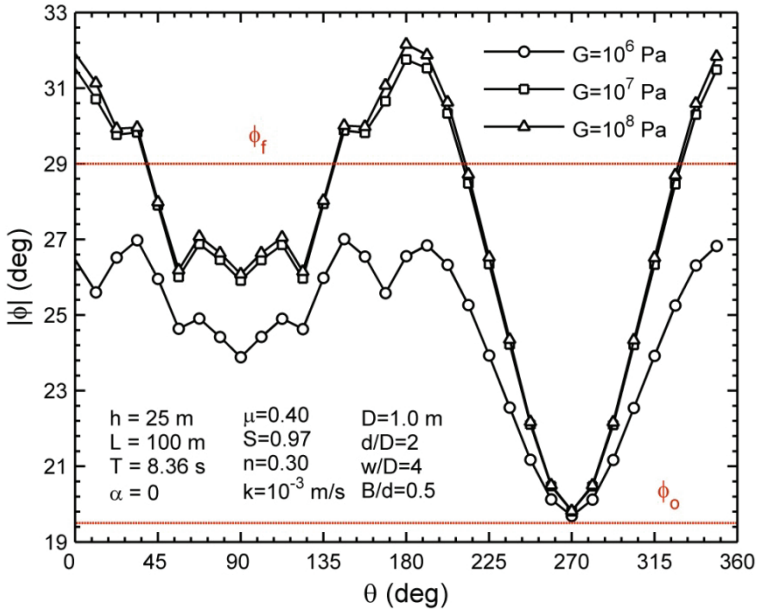

Figure 4.45. The distribution of $|\phi|$ around pipe circumference for various G (K_o=0.5, γ_s=1.969γ_w, H=5.0 m).

Soil Permeability

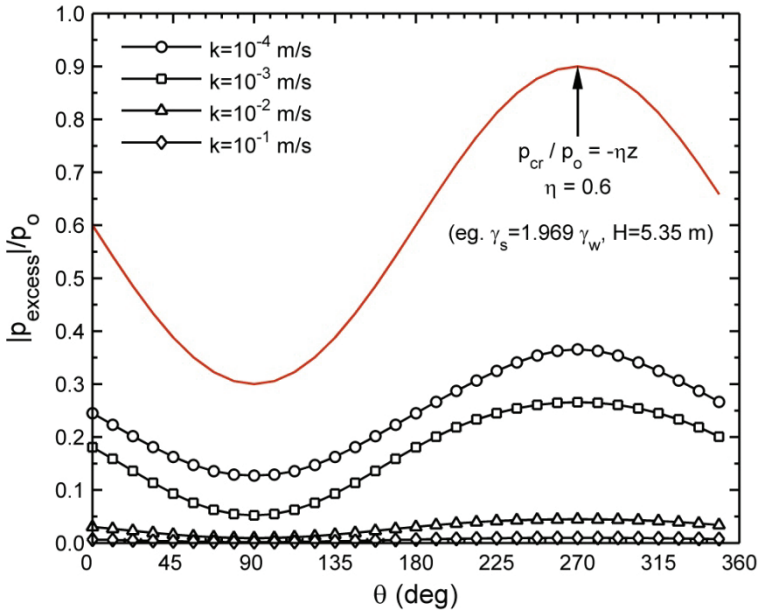

Figure 4.46. The distribution of $|p_{excess}|/p_o$ around pipe perimeter for various k (input data are as Figure 4.20).

The range of permeability, often observed in marine sediments, was introduced in Section 4.1.1.2. Several types of seabed material, with their permeabilities varying from $k = 10^{-4}$ m/s (fine sand) to $k = 10^{-1}$ m/s (gravel), have been considered as in Table 4.1. Simulation results on the potential of soil liquefaction of different soil types, as plotted in Figure 4.46, reveal that the amplitude of wave-induced excess pore pressure and thus the risk of soil liquefaction is considerably greater for fine marine sediments ($k = 10^{-3}$-10^{-4} m/s). This phenomenon is directly associated with the excessive damping of mudline dynamic pressure inside a poorly-permeable bed, as demonstrated in Figure 4.20. The risk associated with the liquefaction of gravel and other coarse sands is small and can be safely neglected under a typical storm. Similarly, finer materials also impose a higher potential of soil shear failure, as they are linked with larger stress angles such in Figure 4.47. It should be noticed that although for the lowest permeability used herein the soil is not liquefied yet, the stress angle in similar conditions has already reached near to the shear failure limit.

On the other hand, the distribution pattern of excess pore pressure is found to remain the same for all cases. However, rather different behaviour patterns have been observed for stress angle in fine and coarse materials. In fact, maximum values of stress angle are located at the lower lateral sides of the pipeline, θ=190° and 350° for fine sediments, while points of high risk of shear failure are at the upper half of the pipe, θ=45° and 135°, in gravel and coarse sands.

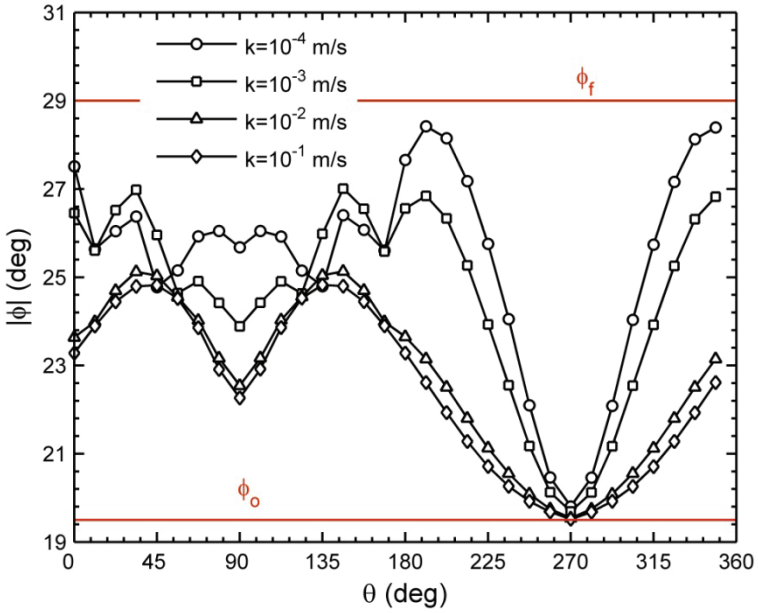

Figure 4.47. The distribution of $|\phi|$ around pipeline perimeter for various k

(Soil, wave and trench properties are as in Figure 4.20 and K_o=0.5, γ_s=1.969γ_w and H=5.0 m).

The Degree of Saturation

It is common for most marine sediments to contain a small percentage of air, and thus showing a degree of saturation between 0.90 and 1.00. However, even small amounts of air significantly reduce the compressibility of pore fluid and consequently influence seabed responses. Therefore, it is important to examine the effects of soil saturation on the instability of seabed soil, in the vicinity of a submarine buried pipeline. For this purpose a range of nearly saturated soils has been adopted to carry out the parametric study. Figure 4.48 demonstrates how significantly an increase in the soil air content will change the wave-associated excess pore pressure and the risk of complete liquefaction, compared with other soil characteristics previously studied. In addition to the critical value of excess pore pressure corresponding to a wave height of 5m, p_{cr} corresponding to an exaggerated wave height of 8 m (η = 0.4) is also plotted in the figure. It can be seen that for S=91%, the excess pore pressure coincides with this critical value and thus the seabed liquefies.

As shown in Figure 4.49, the soil stress angle also shifts up in less-saturated soils, with the 95% saturated sand being the first to show shear failure near the pipeline lateral sides. The failure region extends by further increasing the air content. This continues so that for a 91% saturated soil, the stress angle at every point apart from the region below the pipeline, goes beyond the soil internal friction angle. It should be pointed out that, generally speaking, the seabed soil in the vicinity of the pipeline base at θ = 270° is often in the most stable situation, with the stress angle always remaining almost unchanged due the action of waves.

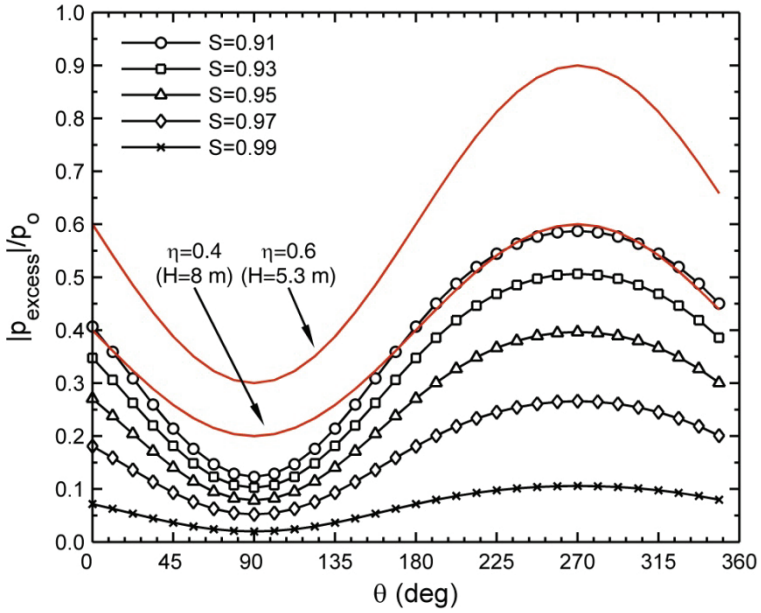

Figure 4.48. Variations of $|p_{excess}|/p_o$ with soil saturation (input data as in Figure 4.25 and K_o=0.5, γ_s=1.969γ_w)

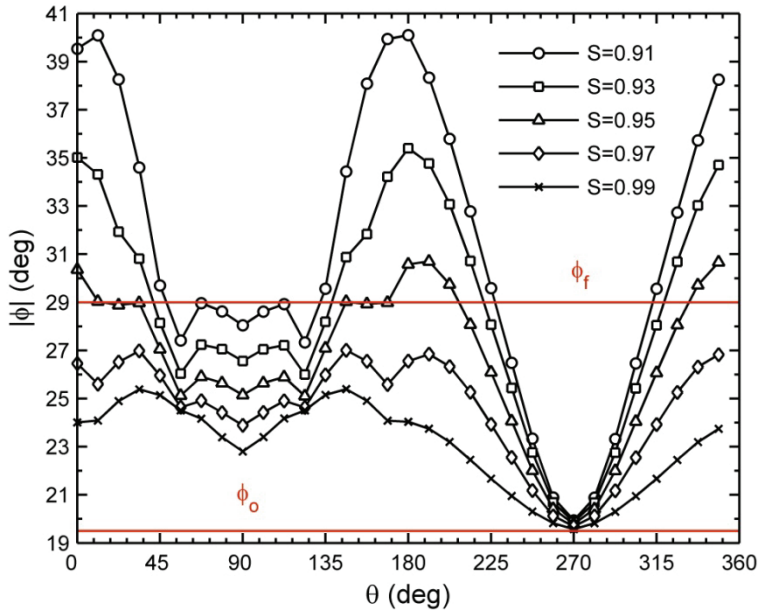

Figure 4.49. Variations of $|\phi|$ with soil saturation (input data as in Figure 4.25, K_o=0.5, γ_s=1.969γ_w, H=5.0 m)

4.2.3.3 Influences of Trench and Pipeline Geometries

Trench Depth

Although the present numerical model is capable of simulating any arbitrary trench geometry and pipe burial depth, in the present parametric study the pipeline is assumed to be buried halfway through the trench depth.

Therefore, by varying the trench depth, influences of both trench depth and pipe burial depth are studied simultaneously. Such an assumption is suitable for practical engineering purposes, since due to the high cost of an underwater excavation, the seabed will be trenched only as deep as to just comply with the desired pipe burial depth. As illustrated in Figure 4.50, the amplitude of wave-associated excess pore pressure dramatically increases in deeper trenches. This is because the mudline pressure is much attenuated in a deep trench, as discussed in section 4.1.1.3. However, in contrary to all previously presented cases, an increase in the pore pressure may not be immediately interpreted as a higher potential of complete liquefaction. This seemingly surprising statement stems back to the fact that while the pipeline is buried deeper within the trench, geostatic overburden stresses around it and thus the critical excess pore pressure will also increase. These stresses are in fact a measure for the weight of the soil column above the pipeline and their action is to resist against soil liquefaction as discussed while introducing the liquefaction criterion. Under these circumstances, one way to study the potential of seabed liquefaction is to normalize the excess pore pressure by its critical value.

A wave height and soil unit weight have been chosen so that $\eta = 0.50$ is used herein to evaluate the critical excess pore pressure and to produce the plot of Figure 4.54. Interesting features can be interpreted from the presented results. That is, moving from shallow burial depths (and trench depths) to deep burial depths, the geostatic static stress gradually become sufficient enough to overcome the increasing trend of excess pore pressure. Hence, graphs of p_{excess}/p_{cr} gradually get closer to each other when increasing the burial depth. This continues until $d/D = 3.0$, after which p_{excess}/p_{cr} even drops down by further increasing the burial depth. This feature implies that despite the traditional belief, increasing the pipe burial depth does not always lead to a more secure protection against soil liquefaction. Instead, there exists a critical burial depth, after which an increase in pipeline stability may be observed. However, a significant difficulty associated with this behaviour is that further increasing the burial depth seems no longer economical, considering that even for $d/D = 3.5$ the potential of liquefaction is still much more than that for $d/D = 1.50$. Therefore, it may be beneficial to seek other protection methods such as using a cover layer to protect the pipeline against soil liquefaction, rather than excessively increasing the burial depth.

Another important feature of the results presented is that the most critical values of p_{excess}/p_{cr} are always observed in the lower half of the pipeline. This means that in the case of an occurrence of soil instability, it is the soil at the lower half of pipeline that liquefies in the first place. However, the excess pore pressure for the presented cases still merely reaches 35% of its critical value at the lower half of the pipeline. The lower half of the pipeline being vulnerable to the liquefaction is directly the result of the attenuation of pore pressure amplitude being the highest at this region as it was repeatedly observed and discussed throughout Section 4.1.1. At the same time, one should also consider the nature of phase lag between wave-induced pore pressure and the wave dynamic pressure, which also contributes to the excess pore pressure. On the other

hand, the upper half of structure seems to be securely stable against liquefaction, especially when a trench is shallow. The significant difference between the potential of liquefaction at lower and upper parts of the pipe gradually vanishes in deeper trenches.

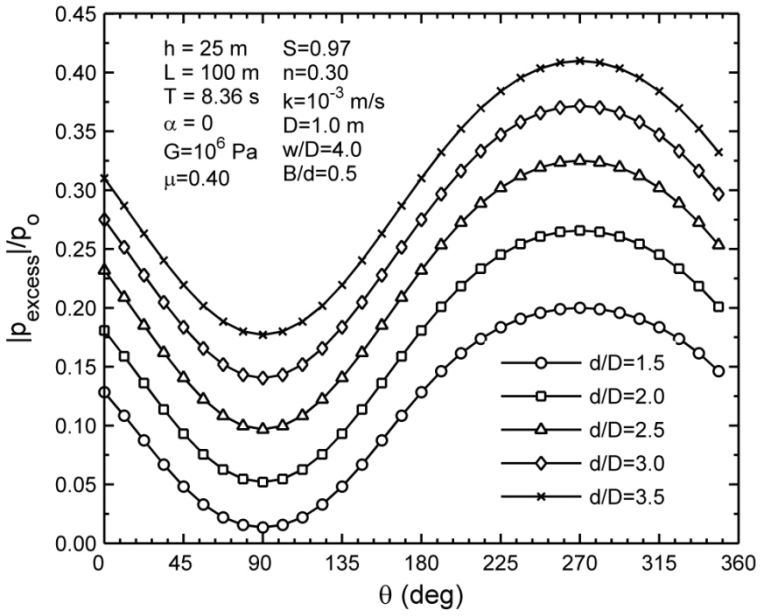

Figure 4.50. The distribution of $|p_{excess}|/p_o$ around pipeline circumference for various d/D.

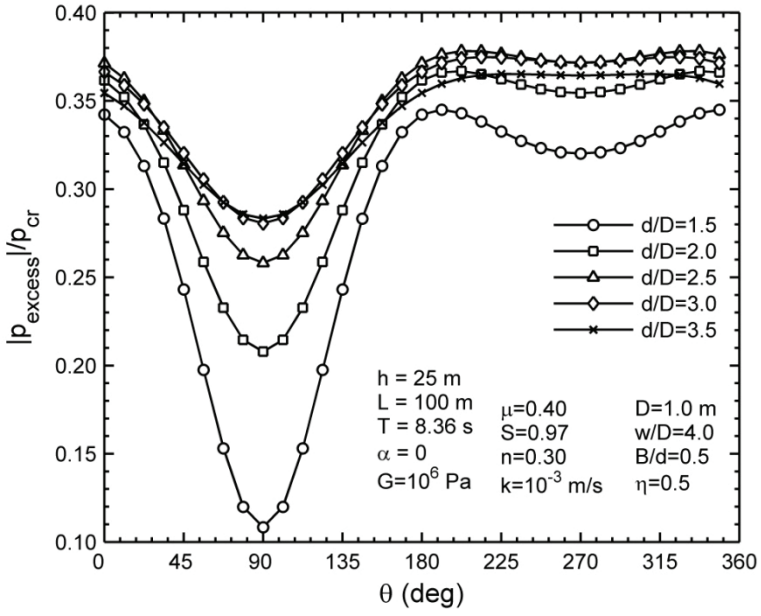

Figure 4.51. The potential of soil liquefaction around pipeline circumference for various d/D.

Despite the behaviour of liquefaction potential, the submarine pipeline is found to be more likely protected against shear failure, when buried in a deeper trench. This is the result of stress angle decreasing almost everywhere around a pipeline when *B* and *d* are increased, as shown in Figure 4.52. However, a more complicated relation between *d* and ϕ is observed near the pipe crest (θ = 90).

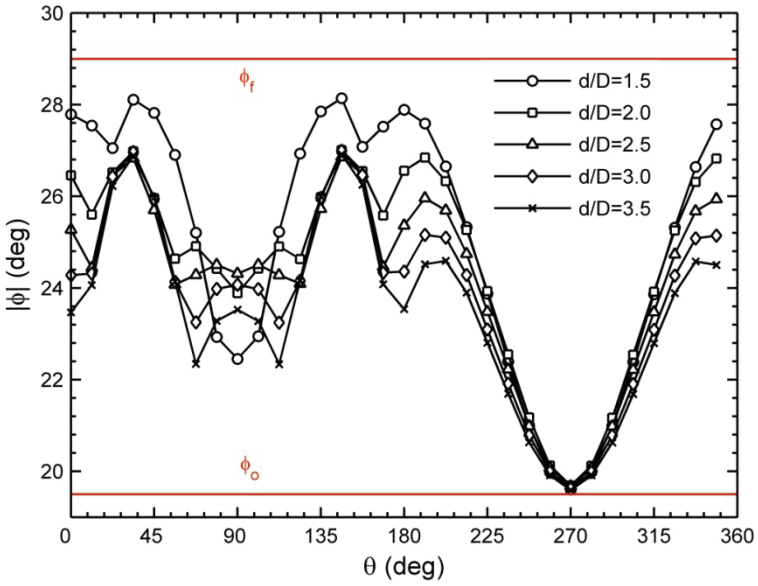

Figure 4.52. The distribution of |ϕ| around pipeline circumference for various *d*/*D*

(Soil, wave, trench and pipe properties are as in Figure 4.50, $K_o = 0.5$, $\gamma_s = 1.969\gamma_w$ and $H = 5.0$ m)

Trench Width

A trench width ranging from 1.5 to 4.0 times of the pipeline diameter is investigated in this study. Amplitudes of wave-associated excess pore pressure are plotted in Figure 4.53. The illustration shows that values of non-dimensional excess pore pressure decline by widening the trench geometry. The influence of trench width slowly vanishes in wider trenches, where graphs of excess pore pressure gradually merge on each other. However, the effect of trench breadth does not completely diminish in the range of examined trench widths.

Figure 4.54 illustrates the distribution of stress angle around the pipeline. The stress angle at the pipe bottom (θ = 270°) is merely more than the static value, imposed by the soil submerged weight. On the other hand, the risk of shear failure is highest around θ = 35° and 145°, where the stress angle is just below the soil internal friction angle of seabed soil. Furthermore, widening the trench significantly increases the stress angle almost everywhere else around the pipeline. However, a more complicated behaviour is observed near the potential shear failure regions, marked by A and B in Figure 4.54, as the stress angle is the highest for *w*/*D*= 2.5.

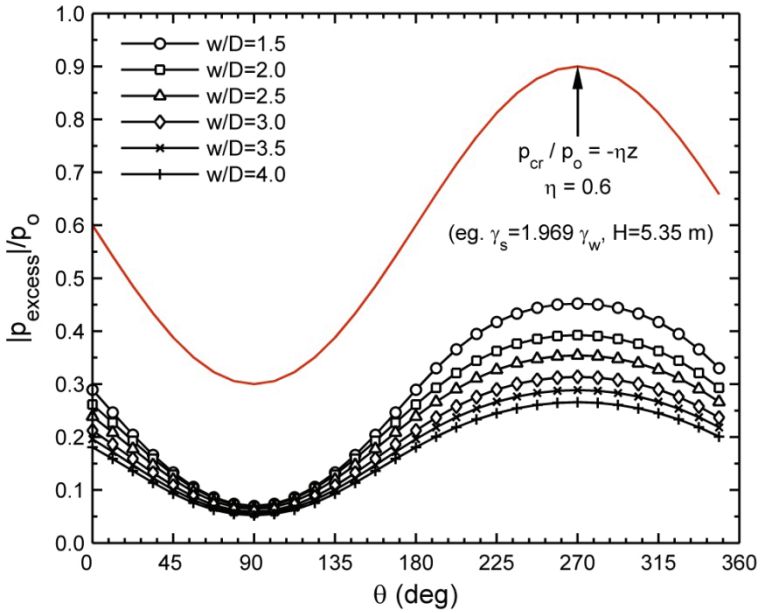

Figure 4.53. The distribution of $|p_{excess}|/p_o$ around pipe perimeter for various w/D (input data as in Figure 4.30)

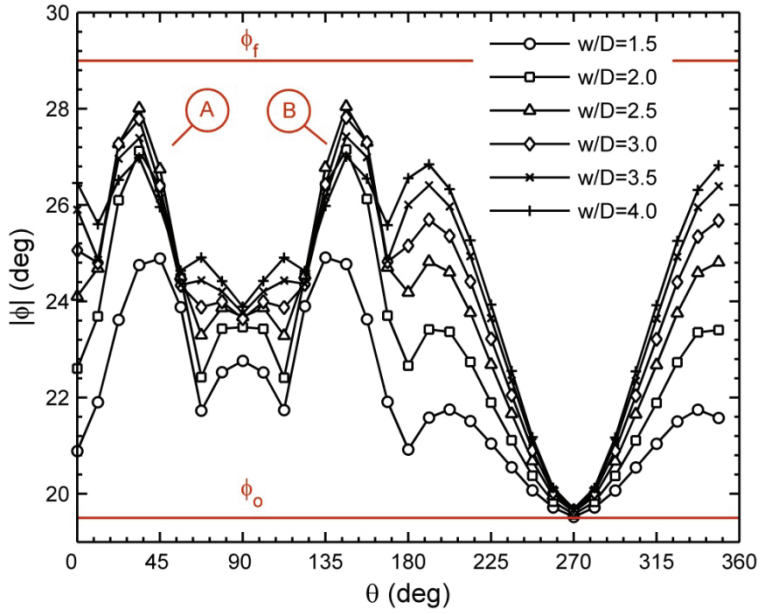

Figure 4.54. The distribution of $|\phi|$ around pipeline circumference for various w/D

(Soil, wave, trench and pipeline properties are as in Figure 4.30, $K_o = 0.5$, $\gamma_s = 1.969\gamma_w$ and $H = 5.0$ m)

Pipeline Diameter

The potential and pattern of soil liquefaction are expected to be different between pipelines of small and large diameters. To demonstrate this, Figure 4.55 shows the distribution of excess pore pressure around a pipeline perimeter for various pipe diameters. In this regard, the upper and lower halves of the pipeline are found to behave in a different way. In fact, close to the crest of the structure, $|p_{excess}|/p_o$ drops down by increasing the pipe diameter; while, an opposite trend is in the vicinity of the pipeline bottom. However, these results are not sufficient to justify how the potential of soil liquefaction varies with the pipe diameter. This is because by enlarging D, geostatic overburden stresses will also drop at the upper half of the structure, while they will increase at its lower. Therefore, it is essential to examine the ratio between the excess pore pressure and its critical value. The distribution pattern of $|p_{excess}|/p_{cr}$ around the pipeline is plotted in Figure 4.56. Expectedly, $|p_{excess}|/p_{cr}$ is found to have a similar behaviour as $|p_{excess}|/p_o$. This behaviour was in fact expected, since generally speaking the pipeline is a slender structure. Hence, a change in its diameter may not impose a significant effect on "z" coordinates and thus "$p_{cr} = \eta z$" of points located on its circumference.

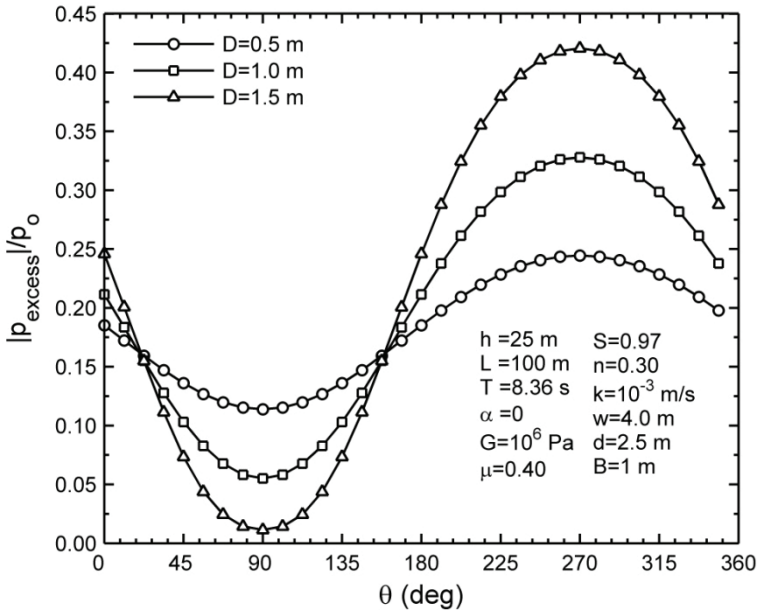

Figure 4.55. The distribution of $|p_{excess}|/p_o$ around pipeline circumference for various pipe diameters.

Another feature of the potential of soil liquefaction near the structure is that as the diameter decreases, a more uniform distribution of $|p_{excess}|/p_{cr}$ around the pipe perimeter is observed. Therefore, in the event of soil instability, it is likely for a slender pipeline to be completely surrounded by liquefied soil. Consequently, a slender pipeline could sink or float within the bed, depending on the magnitude of seepage force and pipeline weight. However, the significant difference between $|p_{excess}|/p_{cr}$ at the lower and upper parts of a large-diameter pipe requires extremely steep waves (i.e. a large η) to liquefy the seabed at the pipe crest, while the

pipe bottom is capable of being liquefied much earlier. This uneven liquefaction pattern allows the structure only to sink within the bed, since the soil in the upper half of the structure may not be liquefied in most cases. However, strict knowledge of all acting and reacting forces on the structure is necessary to draw a strong conclusion. Further, the excess pore pressure in the presented case is still far beyond the critical liquefaction limit (p_{cr}) for a storm of H = 5.35 m (η = 0.6), which was assumed to plot the Figure 4.56.

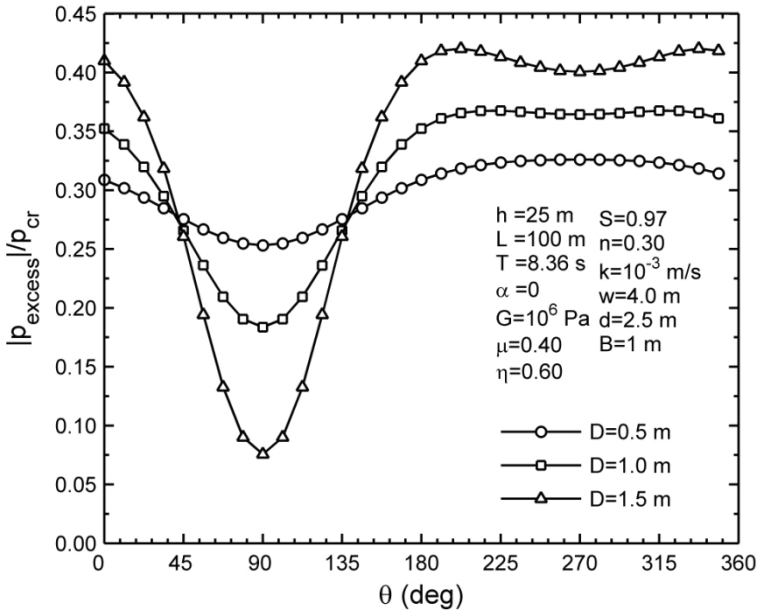

Figure 4.56. The potential of soil liquefaction around pipeline for various pipeline diameters.

4.2.3.4 Influences of Ocean Wave Properties

Wave Period

It has been previously shown in the Section 4.1.1.1 that an increase in the wave period (T) forcefully shifts up the normalized wave-associated normal and shear stresses within the seabed soil. This effect has been attributed to the characteristic time required by the influence of mudline loading to penetrate into the seabed, in comparison with the period (frequency) of such a loading. It is important to examine the existence of a similar behaviour in the distribution of excess pore pressure around a pipeline. Therefore, several wave events of the same wave length (L = 100 m) but of variable frequency have been considered herein. These frequencies correspond to wave periods of 8.36 s to 14 s, which are common in the ocean environment. It is worth being reminded that the wave dispersion equation requires wave events of longer periods to take place in shallower water depths. According to linear wave theory, therefore, the amplitude of mudline pressure (p_o) is larger under these circumstances. However, this effect is excluded from the parametric study on the excess pore pressure, when it is normalized by the amplitude of wave pressure at the mudline. Figure 4.57 indicates that this normalized amplitude of excess pore pressure increases as does the wave period. The effect of T,

however, gradually fades away, as the excess pore pressure ratio goes beyond T = 12 s to 14 s. This phenomenon implies that loadings of period of more than 12 s can no longer be considered as "quick" compared with the characteristic time that soil around the pipeline requires to adapt with the wave loading.

Once again, the occurrence of complete liquefaction around a pipeline, nevertheless, should be justified against non-dimensional geostatic overburden stresses. However, since p_{cr}/p_o varies as the wave period changes, it is appropriate to examine p_{excess}/p_{cr} to study the potential of soil liquefaction. This issue is addressed in Figure 4.58. As illustrated, the lower part of the pipeline ($180° < \theta < 360°$) falls within the liquefied region for the wave period of 14 s and wave height of 5.0 m, since the excess pore pressure goes beyond its critical value (p_{cr}). The increased potential of liquefaction in longer wave periods is mainly because of the fact that low frequency waves are associated with excessively larger values of mudline loading.

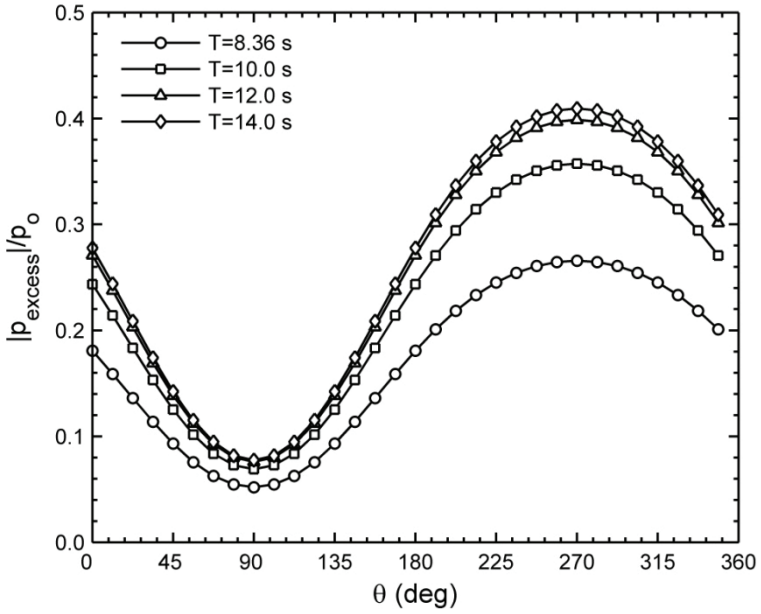

Figure 4.57. The distribution of $|p_{excess}|/p_o$ around pipe perimeter for various T (input data as in Figure 4.11)

Unlike the potential of liquefaction, soil shear failure occurs around the pipeline even for much shorter wave periods. Referring to Figure 4.59, a 5.0 m wave height triggers the soil shear failure in the upper part of the pipeline as well as most of its lower part, in wave periods of equal or greater than 10 seconds. Nonetheless, the seabed soil under the pipe base ($\theta = 270°$) interestingly remains strongly stable against shear failure, in all examined cases. It is important to note that a stress angle (ϕ) between 0° and 90° portrays a Mohr circle with normal stresses completely being in a compressive phase. Meanwhile as ϕ increases by increasing T, the Mohr circle shifts towards the tensile phase. A Mohr circle with a tensile mode of stress on any plane is indicated by ϕ=90° in the present illustration. Knowing that sandy beds, which are non-cohesive,

may not resist against a tensile stress, such a kind of instable situation is observed for T = 12 s and 14 s, as plotted.

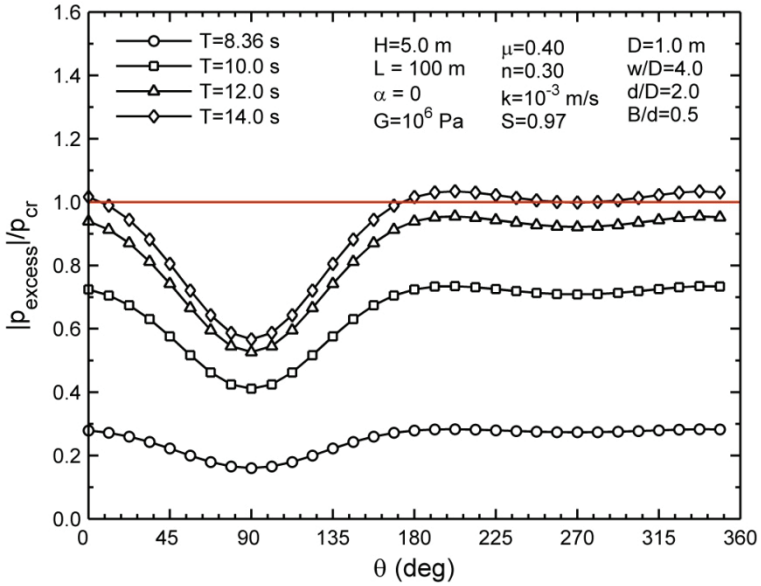

Figure 4.58. The potential of soil liquefaction around pipe perimeter for various T. (K_o = 0.5 and γ_s = 1.969γ_w).

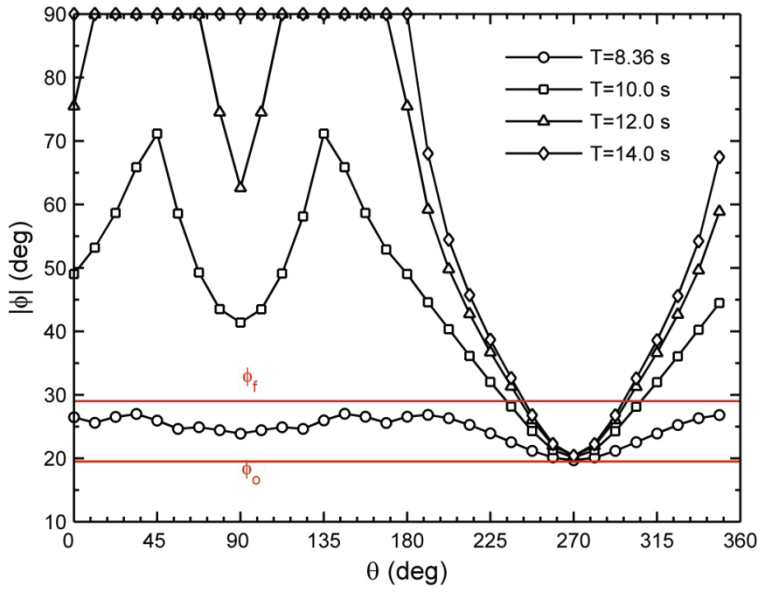

Figure 4.59. The distribution of |ϕ| around pipeline circumference for various wave periods

(Soil, wave, trench and pipeline properties are as in Figure 4.11, K_o = 0.5, γ_s = 1.969γ_w and H = 5.0 m)

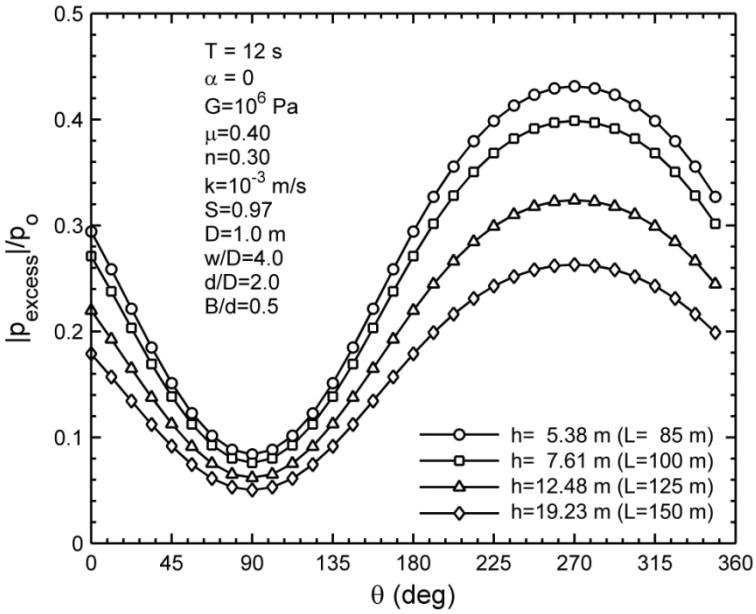

Figure 4.60. The distribution of $|p_{excess}|/p_o$ around pipeline circumference for various water depths.

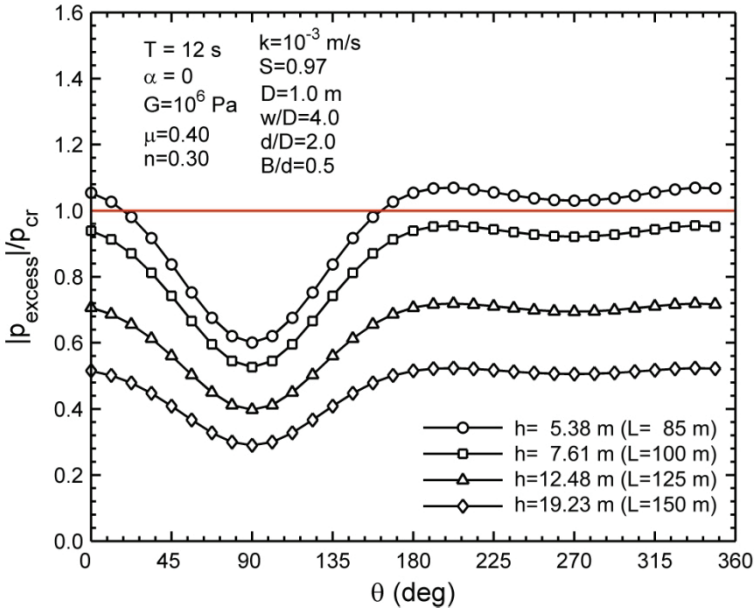

Figure 4.61. The potential of soil liquefaction around pipe perimeter for various h ($K_o = 0.5$ and $\gamma_s = 1.969\gamma_w$).

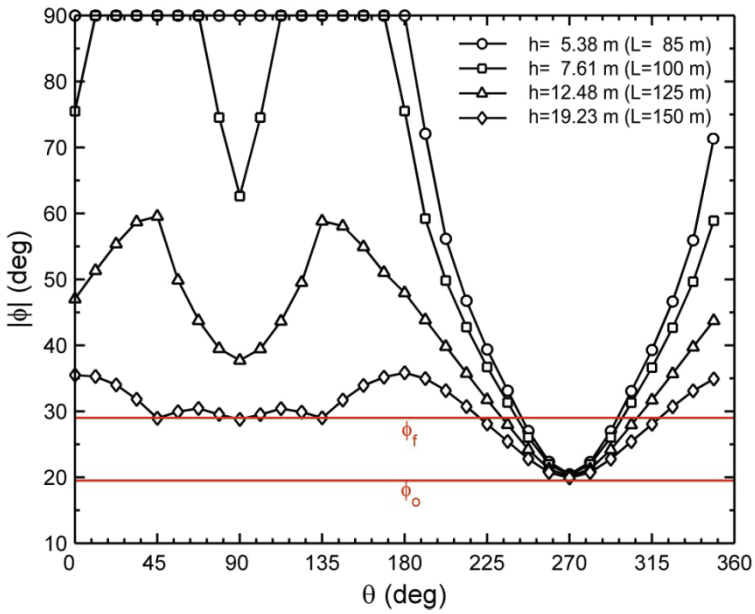

Figure 4.62. The distribution of $|\phi|$ around pipeline for various water depths (input data as in Figure 4.61)

Water Depth

Figure 4.60 illustrates the influence of water depth on normalized amplitudes of wave-induced excess pore pressure. It should be pointed out that a decrease in water depth is associated with an increase in the amplitude of the mudline wave pressure (p_o). However, since the excess pore pressure, herein, is normalized by the amplitude of mudline pressure, this effect is not included in results presented in Figure 4.60. Instead, as discussed earlier in this chapter, as the wave enters shallower water depths, its wave length decreases. Thus, the geometry of wave loading on the seabed alters and thus the normalized excess pore pressure will be influenced. As illustrated, the normalized excess pore pressure ($|p_{excess}|/p_o$) will increase as shallower water depths are chosen. Meanwhile, the unfortunate combination of increases in both $|p_{excess}|/p_o$ and p_o for shallow water depths, results in the pipeline being extremely vulnerable to the soil liquefaction in shallow waters, as can be deduced from Figure 4.61. It is observed that for h = 5.38 m and H = 5 m, the $|p_{excess}|$ exceeds the mean static overburden stress (p_{cr}) everywhere in the lower half of pipeline. Therefore, it is predicted that the soil in the vicinity of the lower part of the structure will be completely liquefied under this wave regime. At the same time, the threat for soil shear failure is even more substantial, since the stress angle in the upper half of the pipeline goes beyond the soil internal friction angle for all examined water depths, as depicted in Figure 4.62. It should be pointed out that Mohr's circles will shift into the tensile zone for both h = 5.38 m h = 7.61 m, as the stress angle reaches 90°. This is due to the mudline dynamic loading that becomes excessively large in shallow waters.

4.3 Summary

The foregoing chapter was devoted to an investigation of the momentary seabed behaviour in the vicinity of a submarine pipeline. The study was conducted under two main headings. In the first section, a parametric study on wave-associated seabed responses, i.e. the pore pressure and soil stresses, was carried out. The numerical results importantly revealed that the wave obliquity significantly influences the wave-induced principal and shear stresses. However, the pore pressure was found not to be considerably affected by the three-dimensional nature of wave loading. Further, it was also found that the symmetry in the distribution of seabed responses around a pipe circumference, which was the characteristic feature of cases with waves propagating parallel with the pipeline, would not hold under oblique wave loading. This behaviour led to the phenomenon of observation of "inversion nodes". The parametric study was then further continued to discuss effects of other wave properties, soil characteristics and the trench geometry on soil responses.

Under the second main heading, potentials of seabed instabilities in the vicinity of structure were investigated. It should be pointed that among mechanisms of seabed instability, the soil liquefaction is associated with the wave-induced excess pore pressure, while the soil shear failure is linked to the stress angle. To discuss the seabed shear failure, the concept of wave-induced perturbation of stress angle was introduced for the first time in the present study; where it was found that the seabed soil undergoes a shear failure if the stress angle shifts up by as much 9.5 degrees, from its geostatic value, due to the action of waves. Further, with an analogy to the first section, a parametric study on the excess pore pressure and the stress angle was also carried out using the developed three-dimensional FEM model. Simulations showed that the wave obliquity notably contributes to the soil stress angle. Therefore, it was concluded that three-dimensional effects might not be always neglected without the commitment of serious errors to the prediction of soil shear failure. On the other hand, a two-dimensional model, nevertheless, was still found adequate to estimate the excess pore pressure and thus the risk of soil liquefaction near the pipeline. Influences of wave, soil, trench and pipeline properties on potentials of seabed instabilities were also studied in detail.

Chapter 5

CONCLUSIONS AND FUTURE RESEARCH DIRECTIONS

5.1 Conclusions

The phenomenon of three-dimensional interaction between water waves, seabed soil and a submarine buried pipeline is a multifactorial problem, in which behaviours of involved mediums are interdependently coupled with each other. This provides an extremely complex system to investigate. On the other hand, the evidence of complicated soil patterns, such as variable soil permeability, variable soil stiffness, soil hydraulic and structural anisotropies, etc. would also add to this complexity, if not making a general investigation impossible. As such, no analytical solution is yet available even to the most simplified case of two-dimensional response of a uniform isotropic seabed in the vicinity of a submarine pipeline. However, numerical modelling can provide a flexible yet powerful tool to overcome deficiencies of an analytical approach. To date, several studies have been concerned with the problem of two-dimensional wave-soil-pipe interaction from various prospects. Nevertheless, no study is available in the literature to address this problem from a three-dimensional point of view.

As such, the primary objective of this research is to determine whether seabed responses near underwater buried pipelines are influenced by three-dimensional effects. For this purpose, assumptions have been made that a fixed rigid pipeline is buried within a trench with impervious rigid backfilled with an isotropic homogenous soil, which undergoes loading from an ocean wave propagating obliquely with respect to the orientation of structure. A finite element model was then developed to solve the three-dimensional seabed consolidation equations with the assumption of linear elastic soil behaviour, where soil strains are considered to be small. In this model, a non-slip boundary condition between soil and pipeline was considered. Finally, the momentary seabed responses including pore pressure, effective and shear stresses have been investigated in the region close to the structure. The following conclusions may be drawn from the numerical results presented in this study:

1. A fully 3-D Finite Element Model, namely *WSPI-3D*, has been developed in this study. The numerical model has been comprehensively validated against an analytical solution for the

simplified case of the response of a finite seabed in the absence of a structure, wave tank experimental data in the presence of a buried pipeline, as well as, a previously developed two-dimensional model. Excellent agreement has been achieved between simulation results and both analytical solutions and experimental data. In addition, the present model has been found to outperform the aforementioned two-dimensional model.

2. At any point within the seabed domain, wave-induced responses vary periodically over the wave period. However, despite the behaviour of pore pressure and normal effective stresses in the *x*-, *y*- and *z*- planes, such a periodic distribution for soil principal effective stresses does not simply follow a linear sinusoidal pattern.

3. The obliquity of ocean waves with respect to the orientation of a pipeline significantly influences wave-associated responses of the seabed soil. These influences can be explained through the following two mechanisms: (*i*) three-dimensional geometry-based effects, and (*ii*) changes in amplitudes of soil responses due to three-dimensionalities. The former is associated with the formation of pipeline spans of the length of $L/\cos(\alpha)$, over which soil responses show a periodical distribution. The term *geometry-based* refers to the fact that such periodic behaviour can be readily deduced from the three-dimensional geometry of wave loading without performing a numerical simulation. On the other hand, the amplitudes of pore pressure and soil stresses are also found to vary monotonically by wave obliquity. This behaviour is accompanied with the formations of multiple regions around the pipe circumference, separated by so-called *inversion nodes*. The direction of such monotonic behaviour alters between neighbouring regions around the pipeline. Finally, it is worthy of mentioning that although the amplitudes of soil maximum shear and major principal effective stresses will be considerably affected by the three-dimensionalities of the problem, it is found sufficient to use a two-dimensional model to evaluate the amplitude of pore pressure around the pipeline perimeter.

4. The mechanical properties of a wave, such as wave period and wave length, play an important role in accordance with the wave-induced soil responses in the vicinity of the structure. In fact, high- frequency and long waves are associated with less attenuated mudline pressures inside the seabed and also smaller soil stresses. The dependency of seabed responses to wave frequency, especially for shorter wave periods, is linked to the so-called phenomenon of "quick" loading in comparison with a characteristic time required by the soil the adapt to surface pressure variations. On the other hand, an increase in the horizontal pressure (loading) gradient between wave crest and wave trough in shorter waves is used to explain the dependency of soil responses on the wave length.

5. Marine sediments fall within a wide range of semi-pervious materials with the permeability ranging from 10^{-6} to 10^{-1} m/s. Over this range, the mudline pressure merely damps in highly-permeable soils such as gravel and coarse sand, due to the relatively easy transmission of pore fluid within the porous bed. Soil stresses are also found to be considerably smaller in these types of seabed soils. On the contrary, relatively poor-permeablity materials such as sand and fine sand are associated with excessive pore pressure attenuations and large soil effective and shear stresses. This behaviour is likely to be motivated by the fact that a soil element in a poor-permeability material requires a longer time, when compared with the wave period, to respond to surface pressure fluctuations.

6. The compressibility of pore fluid is mainly dependent on its degree of saturation. It is reported that a few percent of air bubbles increases the compressibility of pore fluid to a great extent. As such, poorly-saturated soils trigger large pore fluid pressure attenuations and soil stresses around the submarine buried pipeline.

7. The most critical state for soil stresses occurs wider and deeper trenches as well as more slender pipelines. Nevertheless, the influence of trench width on soil responses is found to vanish when the trench is widened to more than 3.0-3.5 times of the pipe diameter. On the other hand, the diameter of a pipeline induces different influences on pore pressures of lower and upper halves of pipeline. That is the upper half showing an increase in pore-pressure when the pipe diameter is larger, while the lower half behaves in contrary.

It has been reported in the literature that the failure of many submarine pipelines is caused by seabed instabilities, rather than construction deficiencies. Therefore, it is beneficial to apply the present three-dimensional model to investigating the potential of known mechanisms of soil instability in the vicinity of a pipeline. This includes wave-induced soil liquefaction and soil shear failure. It is worthy to note that no systematic study is yet available even in two-dimensions to address these issues. Therefore, a parametric study has been systematically carried out in the present research to investigate the influences of wave obliquity, soil, wave and geometrical properties on the potentials of momentary seabed liquefaction and shear failure. The proposed analysis was carried out based on the assumption that the coefficient of lateral earth pressure (K_o) remains constant[8]. The following main conclusions can be drawn:

8. The concept of wave-induced perturbation of soil stress angle has been introduced for the first time in this study. It was found that the seabed undergoes shear failure when the soil stress angle increases 9.5 degrees from its geostatic value, due to the action of water waves.

[8] The assumption of a constant coefficient of lateral earth pressure, in fact, simplifies the problem by neglecting the effect of the pipeline installation on the potential of seabed instabilities.

9. The wave obliquity influences the amplitudes of excess pore pressure and soil stresses in the same fashion as it acts on wave-induced pore pressure and principal stresses. The asymmetric distribution of potentials of seabed instabilities around a pipeline is the characteristic of an oblique wave system. However, the amplitudes of these potentials undergo a monotonic variation with wave obliquity only in highly-permeable, very loose and highly-saturated soils. As well, the stress angle around a submarine pipeline exposed to an oblique wave is observed to be up to 30 degrees larger than that in a two-dimensional system with waves approaching perpendicular to the pipeline orientation. On the contrary, it is found sufficient to justify the potential for complete liquefaction near the structure by using a two-dimensional model, as the excess pore pressure is found not to be significantly affected by the wave direction.

10. Generally speaking, an ordinary ocean storm may trigger a seabed shear failure, while the complete liquefaction of a soil is often observed only if ocean waves are too steep. On the other hand, the shear failure is often found to initiate on the upper lateral sides of the pipe circumference, at $\theta \approx 35°$ and 145°. The pipeline base is the most stable location against the shear failure with no significant perturbation in the stress angle due to the action of waves. On the contrary, complete liquefaction is likely to be started at the lower half of a pipeline, while the upper half remains safe for most ordinary wave heights.

11. Among various types of marine sediments, stiff, poorly-permeable, and soils with a low degree of saturation are most vulnerable to both types of seabed instabilities: shear failure and soil liquefaction. The degree of saturation is found to play the most influential role among other factors. This is due to the significant sensitivity of pore fluid compressibility to the amount of air bubbles in a seabed soil.

12. The soil stress angle and so the risk of shear failure is higher in a wide and shallow trench. On the contrary, the wave-induced excess pore pressure is revealed to be considerably larger in a deep and narrow trench. In deep trenches, the behaviour of excess pore pressure, however, does not necessarily pose a higher potential of liquefaction. This is because the critical value of excess pore pressure corresponding to liquefaction near the pipeline will also increase as the structure is buried deeper. As a result, it has been observed that liquefaction potential increases as the trench is deepened up to 3.0 times the pipe diameter, after which geostatic stresses become sufficient enough to decrease the potential of soil liquefaction. Nevertheless, it may not be economical to excavate a trench with a depth of more than three times the pipe diameter. Therefore, it may be beneficial to bury the pipeline in a shallow wide trench for protection against shear failure, while using other methods such as a cover layer on the seabed surface for pipeline protection against complete liquefaction.

13. The most influential parameter on seabed instabilities are water wave properties, i.e. wave period, wave length and water depth. Any change in these parameters will cause a change in the mudline dynamic pressure, which is directly proportional to the instability of the seabed soil.

5.2 Future Research Directions

The centre of attention in the present study is on three-dimensional aspects of interaction between ocean waves, marine sediments and a buried pipeline. In this regard, a numerical approach has been applied to investigate influences of wave obliquity on seabed responses in the vicinity of a pipeline. Numerical results reveal that such effects play an influential role on evaluating potentials of seabed instabilities. Therefore, they might not be neglected without the commitment of serious errors. Future research, however, is still necessary via improvements of simplifying assumptions that underlie the current study or via applications of alternative approaches. Consequently, the following topics are recommended as being possible future research directions:

1. Due to complexities involved in this problem and a large number of influential parameters, it is beneficial for practical engineering purposes to develop an analytical solution to wave-induced seabed responses in the presence of a pipeline. Such a solution, using two-dimensional soil consolidation theory, has been attempted by Matsui (1982), where a seabed of infinite thickness was considered. He applied a domain decomposition technique to derive a semi-analytical solution. However, a closed-form solution has not been achieved due to mathematical complexities. A similar approach may be used to also address cases of finite seabed depth as well as the three-dimensional wave-soil-pipe interaction.

2. The current study considers a *Quasi-Static* soil consolidation model to express the seabed soil behaviour. Thus, the accelerations due to the pore fluid motion and soil deformations are neglected. Recently, Luan *et al*. (2008) developed a two-dimensional numerical model for a similar problem based on the assumption of a *u-p* model dominating the soil behaviour. This model considers the dynamic response of the solid phase, but neglects the inertia terms in the pore fluid motion. Therefore, it may be useful to propose a *fully-dynamic* model for the wave-soil-pipe interaction problem to examine the influence of fluid inertia terms.

3. An underlying assumption in the present research is that the seabed soil is a linear elastic medium. This approach, therefore, might have resulted in some inaccuracies over the prediction of real soil behaviour near the pipeline. Thus, it is beneficial to also use a non-linear plastic theory to study wave-associated soil responses and seabed instabilities.

4. In this study, only the momentary seabed responses have been concerned. However, it is reported in the literature that the seabed soil also becomes unstable as the result of pore pressure built-up due to the progressive nature of ocean waves. In two-dimensions, several investigations are available to study the phenomenon of pore-pressure build-up in the presence of a submarine pipeline. However, no study is yet available to address this problem from a three-dimensional point of view. Recently, Jeng *et al.* (2007) used a three-dimensional approach to address this issue in the absence of a structure. A similar methodology may be implemented as a routine in the present numerical model to study the 3-D problem of residual response of seabed soil near underwater pipelines.

REFERENCES

Anderson, A. L., Abegg, F., Hawkins, J. A., Duncan, M. E. and Lyons, A. P. (1998). *Bubble populations and acoustic interaction with the gassy floor of Eckernförde Bay*. Continental Shelf Research 18(14), 1807-1838.

ASCE preliminary research on pipeline flotation: Report of the Pipeline Flotation Research Council. (1966). Journal of the Pipeline Division 92(1), 27-74.

Bathe, K. J. (2004). *ADINA user's manual version 8.2.2*, ADINA R&D Inc.

Bear, J. (1972). *Dynamics of fluids in porous media*, 764 pp., American Elsevier, New York.

Biot, M. A. (1941). *General Theory of Three-Dimensional Consolidation*. Journal of Applied Physics 12(2), 155-164.

Biot, M. A. (1962). *Generalized Theory of Acoustic Propagation in Porous Dissipative Media*. The Journal of the Acoustical Society of America 34(9A), 1254-1264.

Bobby, W., Arockiasamy, M., Haldar, A. K. and Reddy, D. V. (1979). *Finite element analysis of pipe-soil-wave interaction*. Proceedings of 2nd International Conference on Behaviour of Off-Shore Structures (BOSS '79), pp. 503-506, London, England, 28-31 August 1979.

Bonar, A. J. and Ghazzaly, O. I. (1973). *Research on Pipeline Floatation*. Transportation Engineering Journal, ASCE 99(TE2), 211-233.

Brinkman, H. C. (1947). *On the permeability of media consisting of closely packed porous particles*. Applied Science Research A1, 81-86.

Brown, R. J. (1957). *Soil mechanics important in marine pipeline construction*. Oil and Gas Journal 55, 151-155.

Chan, A. H. C. (1995). *User manual for DIANA-SWANDYNE II*, Department of Civil Engineering, University of Birmingham, Birmingham.

Chen, T. N., Cai, K. F. and Lin, Y. S. (2005). *Three-dimensional finite element modeling for wave-seabed pipeline interaction*. Proceedings of MTS/IEEE OCEANS 2005, pp. 778-784, Washington D.C., 17-23 Sep. 2005.

Cheng, A. H. D. and Liu, P. L. F. (1986). *Seepage force on a pipeline buried in a poroelastic seabed under wave loadings*. Applied Ocean Research 8(1), 22-32.

Christian, J. T., Taylor, P. K., Yen, J. K. C. and Erali, D. R. (1974). *Large diameter underwater pipeline for nuclear power plant designed against soil liquefaction*. Proceedings of 6th Annual Offshore Technology Conference, pp. 597–606, Houston, Texas, 6-8 May.

Claypool, G. E. and Kaplan, I. R. (1974). *The origin and distribution of methane in marine sediments*. In: Natural gases in marine sediments. Kaplan, I. R. (ed), chapter, pp. 99-139, Plenum Press, New York and London.

COMSOL (2006). *Comsol Multiphysics Version 3.3 User's Guide*

Craig, R. F. (1997). *Soil mechanics*, 6th ed., 485 pp., E & FN Spon, London, UK.

Dawson, T. H. (1978). *Wave propagation over a deformable sea floor*. Ocean Engineering 5(4), 227-234.

de Groot, M. B., Bolton, M. D., Foray, P., Meijers, P., Palmer, A. C., Sandven, R., Sawicki, A. and Teh, T. C. (2006). *Physics of Liquefaction Phenomena around Marine Structures*. Journal of Waterway, Port, Coastal, and Ocean Engineering 132(4), 227-243.

Dean, R. G. and Dalrymple, R. A. (1984). *Water wave mechanics for engineers and scientists*, 353 pp., World Scientific, Singapore.

Dunn, S. L., Vun, P. L., Chan, A. H. C. and Damgaard, J. S. (2006). *Numerical Modeling of Wave-Induced Liquefaction around Pipelines*. Journal of Waterway, Port, Coastal, and Ocean Engineering 132(4), 276-288.

Esrig, M. I. and Kirby, R. C. (1977). *Implications of gas content for predicting the stability of submarine slopes*. Marine Geotechnology 2, 81-100.

Gao, F.-P. and Wu, Y.-X. (2006). *Non-linear wave-induced transient response of soil around a trenched pipeline*. Ocean Engineering 33(3-4), 311-330.

Gao, F. P., Jeng, D. S. and Sekiguchi, H. (2003). *Numerical study on the interaction between non-linear wave, buried pipeline and non-homogenous porous seabed*. Computers and Geotechnics 30(6), 535-547.

Gatmiri, B. (1990). *A simplified finite element analysis of wave-induced effective stresses and pore pressures in permeable sea beds*. Géotechnique 40(1), 15-30.

Gatmiri, B. (1992). *Response of a cross-anisotropic seabed to ocean waves*. Journal of Geotech. Eng. Div., ASCE 118(9), 1295-1314.

Herbich, J. B. (1977). *Wave-induced scour around offshore pipelines*. Proceedings of Offshore Technology Conference, pp. 79-90, Houston, Texas, May 1977.

Hittori, A., Sakai, T. and Hatanaka, K. (1992). *Wave-induced pore water pressure and seabed stability*. Proceedings of 23rd International Conference on Coastal Engineering, ASCE, pp. 2095-2107.

Hsu, J. R. C., Tsuchiya, Y. and Silvester, H. (1979). *Third-order approximation to short-crested waves*. Journal of Fluid Mechanics 90, 179-196.

Hsu, J. R. C. and Jeng, D. S. (1994). *Wave-induced soil response in an unsaturated anisotropic seabed of finite thickness*. International Journal for Numerical and Analytical Methods in Geomechanics 18(11), 785-807.

Hsu, J. R. C., Jeng, D. S. and Lee, C. P. (1995). *Oscillatory soil response and liquefaction in an unsaturated layered seabed*. International Journal for Numerical and Analytical Methods in Geomechanics 19(12), 825-849.

Hunt, J. N. (1959). *On the damping of gravity waves propagated over a permeable surface*. Journal of Geophys. Res. 64, 437-442.

Inoue, R. (1975). *Propagation of pore water pressure in sand layer of high degree of saturation*. Proceedings of the JSCE 236, 81-92.

Jacky, J. (1944). *The coefficient of earth pressure at rest*. Journal for Society of Hungarian Architects and Engineers, 355-358.

Jeng, D.-S. and Hsu, J. R. C. (1996). *Wave-induced soil response in a nearly saturated sea-bed of finite thickness*. Géotechnique 46(3), 427-440.

Jeng, D.-S. (1997a). *Wave-induced seabed instability in front of a breakwater*. Ocean Engineering 24(10), 887-917.

Jeng, D.-S. (1997b). *Wave-induced seabed response in front of a breakwater*, University of Western Australia, Perth, Australia.

Jeng, D.-S. (1997c). *Soil response in cross-anisotropic seabed due to standing waves*. Journal of Geotechnical and Geoenvironmental Engineering 123(1), 9-19.

Jeng, D.-S. and Seymour, B. R. (1997). *Response in seabed of finite depth with variable permeability*. Journal of Geotechnical and Geoenvironmental Engineering 123(10), 902-911.

Jeng, D.-S. and Lin, Y. S. (1999a). *Wave-induced pore pressure around a buried pipeline in Gibson soil: finite element analysis*. International Journal for Numerical and Analytical Methods in Geomechanics 23(13), 1559-1578.

Jeng, D.-S. and Lin, Y. S. (1999b). *Pore pressure on a submarine pipeline in a cross-anisotropic nonhomogeneous seabed under water-wave loading*. Can. Geotech. J. 36(3), 563-572

Jeng, D.-S. and Cheng, L. (2000). *Wave-induced seabed instability around a buried pipeline in a poro-elastic seabed*. Ocean Engineering 27(2), 127-146.

Jeng, D.-S. and Lin, Y. S. (2000). *Response of Inhomogeneous Seabed around Buried Pipeline under Ocean Waves*. Journal of Engineering Mechanics 126(4), 321-332.

Jeng, D.-S. (2001). *Numerical modelling for wave-seabed-pipe interaction in a nonhomogeneous porous seabed*. Soil Dynamics and Earthquake Engineering 21(8), 699-712.

Jeng, D.-S. and Postma, P. F. (2001a). *Internal Stresses of a buried concrete pipe under wave loading*. Proceedings of The Australian Structural Engineering Conference, pp. 45-51, Gold Coast, Australia.

Jeng, D.-S. and Postma, P. F. (2001b). *Finite Element Analysis of an Offshore Pipeline Buried in a Porous Seabed: Effects of Cover Layer*. Proceedings of 8th International Conference on Civil and Structural Engineering Computing, Stirling, Scotland.

Jeng, D.-S., Postma, P. F. and Lin, Y. S. (2001). *Stresses and Deformation of Buried Pipeline under Wave Loading*. Journal of Transportation Engineering 127(5), 398-407.

Jeng, D.-S. (2003a). *Wave-induced sea floor dynamics*. Applied Mechanics Reviews 56(4), 407-429.

Jeng, D.-S. (2003b). *Discussion of ''Simplified solution of wave-induced seabed response in anisotropic seabed'' by Yuhi and Ishida*. Journal of Waterway, Port, Coastal, and Ocean Engineering 129(3), 151–153.

Jeng, D.-S. and Cha, D. H. (2003). *Effects of dynamic soil behavior and wave non-linearity on the wave-induced pore pressure and effective stresses in porous seabed*. Ocean Engineering 30, 2065-2089.

Jeng, D.-S., Seymour, B. R. and Li, J. (2007). *A new approximation for pore pressure accumulation in marine sediment due to water waves*. International Journal for Numerical and Analytical Methods in Geomechanics 31(1), 53–69.

Jeng, D.-S. (2008). *Random wave-induced pore pressure and effective stresses in marine sediments*. In: Ocean Engineering Research Advances. Prescott, A. I. (ed), chapter 5, pp. 113-166, Nova Science Publishers Inc.

Kitano, T. and Mase, H. (2001). *Wave-induced pore water pressure in a seabed with inhomogeneous permeability*. Ocean Engineering 28(3), 279-296.

Lai, N. W., Dominguez, R. F. and Dunlap, W. A. (1974). *Numerical solutions for determining wave-induced pressure distributions around buried pipelines*, Department of Civil Engineering, Texas A&M University, Texas.

Lennon, G. P. (1983). *Wave-induced forces on buried pipelines*. Proceedings of Coastal Structures '83, pp. 505-518, Arlington, VA, March 9-11, 1983.

Lennon, G. P. (1985). *Wave-induced forces on buried pipelines*. Journal of Waterway, Port, Coastal, and Ocean Engineering 111(3), 511-524.

Lin, Y. S. and Jeng, D. S. (1997). *The Effects of Variable Permeability on the Wave-induced Seabed Response*. Ocean Engineering 24(7), 623-643.

Lin, Y. S. and Jeng, D. S. (2000). *Effects of variable shear modulus on wave-induced seabed response*. Journal of Chinese Institute of Engineers 24(1), 109-115.

Liu, H. and Jeng, D.-S. (2007). *A semi-analytical solution for random wave-induced soil response and seabed liquefaction in marine sediments*. Ocean Engineering 34(8-9), 1211-1224.

Liu, P. L. F. (1973). *Damping of water waves over porous bed*. Journal of Hydraulics Division ASCE 99(12), 2263-2271.

Liu, P. L. F. (1977). *On gravity waves propagated over a layered permeable bed*. Coastal Engineering 1, 135-148.

Liu, P. L. F. and O'Donnell, T. P. (1979). *Wave-induced forces on buried pipelines in permeable seabeds*. Proceedings of Civil Engineering in the Oceans IV, pp. 111–121, September 1979.

Luan, M., Qu, P., Jeng, D. S., Guo, Y. and Yang, Q. (2008). *Dynamic response of a porous seabed-pipeline interaction under wave loading: Soil-pipeline contact effects and inertial effects*. Computers and Geotechnics 35(2), 173-186.

MacPherson, H. (1978). *Wave forces on pipelines buried in permeable seabed*. Journal of the Waterway, Port, Coastal and Ocean Division, ASCE 104(4), 407-419.

Madsen, O. S. (1978). *Wave-induced pore pressure and effective stresses in a porous bed*. Géotechnique 28(4), 377-393.

Maeno, Y. and Hasegawa, T. (1985). *Evaluation of wave-induced pore pressure in sand layer by wave steepness*. Coastal Engineering in Japan 28, 31-44.

Magda, W. (1996). *Wave-induced uplift force acting on a submarine buried pipeline: Finite element formulation and verification of computations*. Computers and Geotechnics 19(1), 47-73.

Magda, W. (1997). *Wave-induced uplift force on a submarine pipeline buried in a compressible seabed*. Ocean Engineering 24(6), 551-576.

Magda, W. (2000). *Wave-induced cyclic pore-pressure perturbation effects in hydrodynamic uplift force acting on submarine pipeline buried in seabed sediments*. Coastal Engineering 39, 243-272.

Mallaid, W. W. and Dalrymple, R. A. (1977). *Water waves propagating over a deformable bottom*. Proceedings of 9th Offshore Technology Conference (OTC), pp. 141-145, Houston, Texas, USA.

Mantovani, P. F. (1983). *An image theory approach to wave-induced seepage effects on buried offshore pipelines*, The University of Wisconsin at Madison, Wisconsin.

Marcuson, W. F. (1978). *Definition of terms related to liquefaction*. Journal of Geotech. Eng. Div., ASCE 104(9), 1197-1200.

Matsui, K. (1982). *Pressure and stress distribution around a pipeline buried in a poro-elastic seabed*. Dissertation, The University of Houston, Houston, Texas.

Maurray, J. D. (1965). *Viscous damping of gravity waves over a permeable bed*. Journal of Geophys. Res. 70, 2325-2331.

McClain, C. R., Huang, N. E. and Pietrafesa, L. J. (1977). *Application of a "radiation-type" boundary condition to the wave, porous bed problem*. Journal of Physical Oceanography 7(6), 823-835.

McDougal, W. G., Davidson, S. H., Monkmeyer, P. L. and Sollitt, C. K. (1988). *Wave-induced forces on buried pipelines*. Journal of Waterway, Port, Coastal, and Ocean Engineering 114(2), 220-263.

Mei, C. C. and Foda, M. A. (1981). *Wave-induced responses in a fluid filled poro-elastic solid with a free surface - a boundary layer theory*. Geophys. J. Royal Astro. Soc. 66, 597- 631.

Monkmeyer, P. L., Mantovani, P. and Vincent, H. (1983). *Wave-induced seepage effects on a buried pipeline*. Proceedings of Coastal Structures '83, pp. 519-531, Arlington, VA, March 9-11, 1983.

Moshagen, H. and Tørum, A. (1975). *Wave-induced pressures in permeable seabeds*. Journal of the Waterways, Harbours, and Coastal Engineering Division ASCE 101(1), 49-57.

Nago, H., Maeno, S., Matsumoto, T., Hachiman, Y. (1993). *Liquefaction and densification of loosely deposited sand bed under water pressure variation*. Proceedings of the 3rd International Offshore and Polar Engineering Conference, pp. 578-584, Singapore.

Nakamura, H., Onishi, R. and Minamide, H. (1973). *On the seepage in the seabed due to waves*. Proceedings of 20th Coastal Engineering Conference, JSCE, pp. 421-428.

Okusa, S., Nakamura, T. and Fukue, M. (1984). *Measurements of wave-induced pore pressure and coefficient of permeability of submarine sediments during reversing flow*. In: Seabed mechanics : edited proceedings of IUTAM / IUGG Symposium, 5-9 September 1983. Denness, B. (ed), chapter, pp. 113-122, Graham & Trotman, London.

Okusa, S. (1985). *Wave-induced stresses in unsaturated submarine sediments*. Géotechnique 35(4), 517-532.

Polous, H. G. (1988). *Marine geotechnics*, 473 pp., Unwin Hyman, London; Boston.

Postma, P. F. and Jeng, D.-S. (2001). *Effects of a cover layer on the seabed response around a submarine pipeline*. Proceedings of Computer Methods and Advances in Geomechanics, pp. 1117–1120, AA Balkema.

Prevost, J. H., Eide, O. and Anderson, K. H. (1975). *Discussion on "wave-induced pressures in permeable seabeds" by Moshagen and Tørum*. Journal of the Waterways, Harbors, and Coastal Engineering Division ASCE 101(1), 464-465.

Putnam, J. A. (1949). *Loss of wave energy due to percolation in a permeable see bottom*. Transaction, American Geophysical Union 30(3), 349-356.

Reid, R. O. and Kajiura, K. (1957). *On the damping of gravity waves over a permeable sea bed*. Transaction, American Geophysical Union 38, 662-666.

Sakai, T., Hittori, A. and Hatanaka, K. (1991). *Wave-induced transient pore water pressure and seabed instability in surf zone*. Proceedings of International Conference on Geotechnical Engineering for Coastal Development - Theory and Practice on Soft Ground (Geo-Coastal 91), pp. 627-632.

Sandven, R., Husby, E., Husby, J. E., Jonland, J., Roksvg, K. O., Staehli, F. and Tellugen, R. (2007). *Development of a Sampler for Measurement of Gas Content in Soils*. Journal of Waterway, Port, Coastal, and Ocean Engineering 133(1), 3-13.

Shabani, B. and Jeng, D.-S. (2007a). *3-D model for wave-induced seabed response around submarine buried pipelines*. Presented at Coasts and Ports 2007, Melbourne, Australia, 18-20 July 2007.

Shabani, B. and Jeng, D.-S. (2007b). *Three-dimensional analysis of momentary liquefaction near submarine pipelines*. Presented at 16th Australasian Fluid Mechanics Conference, Gold Coast, Australia, 3-7 December 2007.

Sills, G. C., Wheeler, S. J., Thomas, S. D. and Gardner, T. N. (1991). *Behaviour of offshore soils containing gas bubbles*. Géotechnique 41(2), 227-241.

Sleath, J. F. A. (1970). *Wave-induced pressures in beds of sand*. Journal of Hydraulics Division ASCE 96(2), 367-378.

Solecki, R. and Conant, R. J. (2003). *Advanced mechanics of materials / Roman Solecki, R. Jay Conant*, Oxford University Press, New York ; Oxford :.

Spierenburg, S. E. J. (1986). *Wave-induced pore pressures around submarine pipelines*. Coastal Engineering 10(1), 33-48.

Sudhan, C. M., Sundar, V. and Rao, S. N. (2002). *Wave induced forces around buried pipelines*. Ocean Engineering 29(5), 533-544.

Sumer, B. M., Fredsøe, J., Christensen, S. and Lind, M. T. (1999). *Sinking/floatation of pipelines and other objects in liquefied soil under waves*. Coastal Engineering 38(2), 53-90.

Sumer, B. M. and Fredsøe, J. (2002). *The mechanics of scour in the marine environment*, 554 pp., World Scientific, Singapore

Sumer, B. M. (2006). *Special issue on liquefaction around marine structures*. Journal of Waterway, Port, Coastal, and Ocean Engineering 132(4), 225-226.

Sumer, B. M., Hatipoglu, F., Fredsøe, J. and Hansen, N.-E. O. (2006a). *Critical Flotation Density of Pipelines in Soils Liquefied by Waves and Density of Liquefied Soils*. Journal of Waterway, Port, Coastal, and Ocean Engineering 132(4), 252-265.

Sumer, B. M., Truelsen, C. and Fredsøe, J. (2006b). *Liquefaction around Pipelines under Waves*. Journal of Waterway, Port, Coastal, and Ocean Engineering 132(4), 266-275.

Sumer, B. M. (2007). *Special issue on liquefaction around marine structures. Miscellaneous*. Journal of Waterway, Port, Coastal, and Ocean Engineering 133(1), 1-2.

Teh, T. C. (2003). *Stability of marine pipelines on unstable and liquefied seabed*. Dissertation, University of Cambridge.

Terzaghi, K. (1925). *Erdbaumechanik auf bodenphysikalischer grundlage*, 399 pp., Franz Deuticke, Leipzig und Wien (Leipzig and Vienna).

Thomas, S. D. (1987). *The consolidation behaviour of gassy soil*, The University of Oxford.

Thomas, S. D. (1989). *A finite element model for the analysis of wave induced stresses, displacements and pore pressures in an unsaturated seabed I: theory*. Computers and Geotechnics 8(1), 1-38.

Thomas, S. D. (1995). *A finite element model for the analysis of wave induced stresses, displacements and pore pressures in an unsaturated seabed II: Model verification*. Computers and Geotechnics 17(1), 107-132.

Torum, A. (2007). *Wave-Induced Pore Pressures---Air/Gas Content*. Journal of Waterway, Port, Coastal, and Ocean Engineering 133(1), 83-86.

Tsai, C. P. (1995). *Wave-induced liquefaction potential in a porous seabed in front of a breakwater*. Ocean Engineering 22(1), 1-18.

Tsui, Y. and Helfrich, S. C. (1983). *Wave-induced pore pressures in submerged sand layer*. Journal of the Geotechnical Engineering Division, ASCE 109(GT4), 608-618.

Turcotte, B. R., Liu, P. L.-F. and Kulhawy, F. H. (1984). *Laboratory evaluation of wave tank parameters for wave-sediment interaction*, School of Civil and Environmental Engineering, Cornell University, Ithaca, New York.

Verruijt, A. (1969). *Elastic storage of aquifers*. In: Flow through porous media. De Wiest, R. J. M. (ed), chapter, pp. 331-376, Academic Press, New York.

Vun, P. L., Chan, A. H. C. and Dunn, S. L. (2005). *Numerical analysis of wave-induced liquefaction around buried pipeline*. Proceedings of 13th UK National Conference of ACME, pp. 111-114, University of Sheffield, UK, 21-22 March 2005

Wang, J. G., Karim, M. R. and Lin, P. Z. (2007). *Analysis of seabed instability using element free Galerkin method*. Ocean Engineering 34(2), 247-260.

Wang, X., Jeng, D. S. and Lin, Y. S. (2000). *Effects of a cover layer on wave-induced pore pressure around a buried pipe in an anisotropic seabed*. Ocean Engineering 27(8), 823-839.

Wheeler, S. J. (1988). *A conceptual model for soils containing large gas bubbles*. Géotechnique 38(3), 389-397.

Wichman, B. G. H. M. (1999). *Consolidation behaviour of gassy mud: theory and experimental validation*, Delft University of Technology.

Yamamoto, T. (1977). *Wave induced instability in seabeds*. Proceedings of Fifth Symposium of the Waterway, Port, Coastal and Ocean Division of ASCE: Coastal Sediments '77, pp. 898-913, Charleston, SC, USA, Nov. 2-4, 1977.

Yamamoto, T., Koning, H. L., Sellmeijer, H. and Hijum, E. V. (1978). *On the response of a poro-elastic bed to water waves*. Journal of Fluid Mechanics Digital Archive 87(1), 193-206.

Yamamoto, T. (1981). *Wave-induced pore pressures and effective stresses in inhomogeneous seabed foundations*. Ocean Engineering 8(1), 1-16.

Youd, T. L., Idriss, I. M., Ronald, D. A., Ignacio, A., Gonzalo, C., John, T. C., Richardo, D., Finn, W. D. L., Leslie, F. H., Jr., Mary Ellen, H., Kenji, I., Joseph, P. K., Sam, S. C. L., William, F. M., III, Geoffrey, R. M., James, K. M., Yoshiharu, M., Maurice, S. P., Peter, K. R., Raymond, B. S. and

Kenneth, H. S., II (2001). *Liquefaction Resistance of Soils: Summary Report from the 1996 NCEER and 1998 NCEER/NSF Workshops on Evaluation of Liquefaction Resistance of Soils*, pp. 817-833, ASCE.

Yuhi, M. and Ishida, H. (2002). *Simplified Solutions for Wave-Induced Response of Anisotropic Seabed*. Journal of Waterway, Port, Coastal, and Ocean Engineering 128(1), 46-50.

Zen, K. and Yamazaki, H. (1990a). *Oscillatory pore pressure and liquefaction in seabed induced by ocean waves*. Soils and Foundations 30(4), 147-161.

Zen, K. and Yamazaki, H. (1990b). *Mechanism of wave-induced liquefaction and densification in seabed*. Soils and Foundations 30(4), 90-104.

Zen, K. and Yamazaki, H. (1991). *Field observation and analysis of wave-induced liquefaction in seabed*. Soils and Foundations 31(4), 161-179.

Zienkiewicz, O. C., Chang, C. T. and Bettess, P. (1980). *Drained, undrained, consolidating and dynamic behaviour assumptions in soils*. Géotechnique 30(4), 385-395.